Submitted to Annual Review
of Nuclear Science

LBL-7527
Preprint

ADVANCES IN MUON SPIN ROTATION

J. H. Brewer and K. M. Crowe

July 1978

Prepared for the U. S. Department of Energy
under Contract W-7405-ENG-48

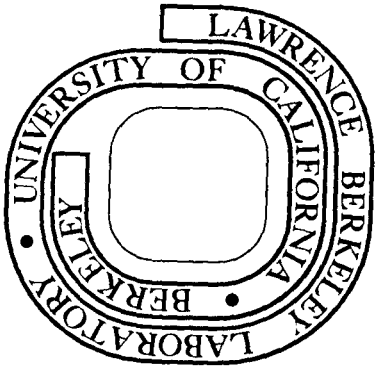

DISCLAIMER

Ann. Rev. Nucl. Part. Sci. 1978. 28:239–326

ADVANCES IN MUON SPIN ROTATION[1]

J. H. Brewer

Department of Physics, University of British Columbia, Vancouver, British Columbia, Canada

K. M. Crowe

Department of Physics, University of California, Berkeley, California 94720

CONTENTS

1 INTRODUCTION

1.1 *Muon Spin Rotation*

The parity-violating asymmetric decay of the positive muon was first observed in 1957 by two different experimental techniques (1, 2). The first involved precession of the muon magnetic moment in an applied magnetic field, and was the percursor of the μSR (muon spin rotation) techniques used today. The original apparatus of Garwin et al (1) is pictured in Figure 1. The essential features of the technique are evident: a "μ stop" timing pulse is generated by a muon entering the target through counters 1 and 2; when the muon decays, if the positron is emitted in the direction of counters 3 and 4, a "decay e" trigger is generated. Such triggers are more likely to occur at times when the muon spin has rotated in a magnetic field in such a way that it points toward the positron telescope. In the original experiment the relative probability of a decay e trigger during a gate from 0.75 to 2.0 μsec after

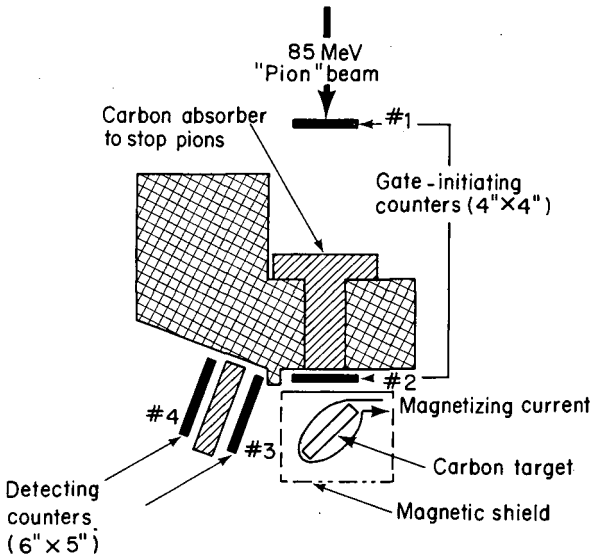

Figure 1 Experimental arrangement. The magnetizing coil was closely wound directly on the carbon to provide a uniform vertical field of 79 gauss per ampere (1).

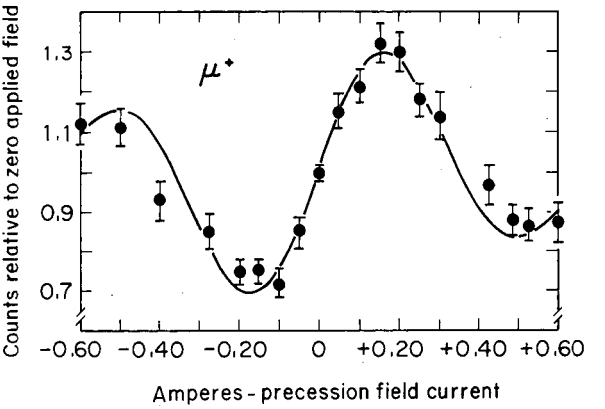

Figure 2 Variation of gated 3–4 counting rate with magnetizing current. The solid curve is computed from an assumed electron angular distribution $1-\frac{1}{3}\cos\theta$, with counter and gate-width resolution folded in.

the μ stop was measured as a function of the magnetic field applied to the muon. The results are shown in Figure 2.

A μSR arrangement typical of those currently in use is represented in Figure 3; the main difference is that the magnetic field is fixed and the positron detection probability is measured as a function of the time the muon spends in the target. The magnetic field is produced by an electromagnet or Helmholtz coil, and timing pulses, μ stop, and decay e are

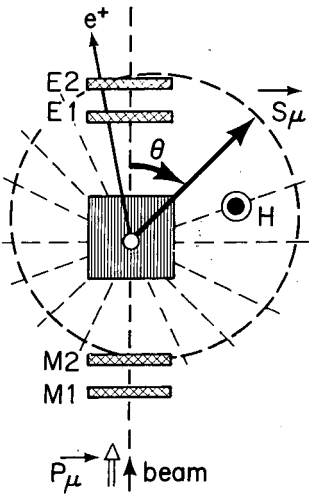

Figure 3 Schematic experimental arrangement in a transverse field. The asymmetric decay pattern is rotating past the counters.

generated as in the Garwin experiment. The time interval between these two pulses is histogrammed to produce a spectrum like that shown in Figure 4*a*, which represents the time distribution of the probability of detecting the positron in a fixed direction. This distribution reflects the exponential decay of the muon, but more importantly (in this context) the superimposed oscillations reflect the preference of the positrons to be emitted along the spin of the muon. The spin precesses in the local field at its Larmor frequency, $\omega_\mu = \gamma_\mu B$, where

$$\gamma_\mu = 8.514 \times 10^4 \text{ rad s}^{-1}\text{G}^{-1} \ (\gamma_\mu = 0.01355 \text{ MHz per gauss}). \quad 1.$$

The fact that the muon precesses in the local field is dramatized by the spectrum in Figure 4*b*, which represents μ^+ precession in a single crystal of Co at 320°C in zero applied field. The local field is entirely provided by the microscopic magnetization of cobalt.

Such a spectrum is fitted to the functional form

$$dN(t)/dt = N_0 \{B + \exp(-t/\tau_\mu)[1 - A_0 P(t)]\}, \quad 2.$$

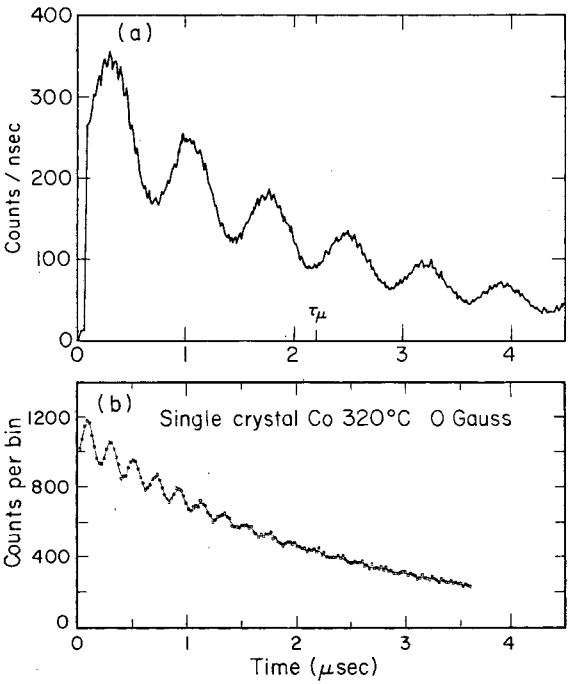

Figure 4 Typical experimental histogram. In (*a*), the positive muons stop in a target of CCl_4 in a magnetic field of 100 gauss. In (*b*), the stopping target is cobalt in zero external field. The mean muon decay lifetime $\tau = 2.20$ μsec is seen.

where B is a constant accidental background, τ_μ is the μ^+ lifetime (2.20 μsec), A_0 is the empirical maximum asymmetry (typically between 0.25 and 0.4), and $P(t)$ is the projection of the time-dependent polarization of the muon spin ensemble along the direction of the positron counter telescope. For simple one-frequency examples like that shown in Figure 4, $P(t)$ has the form

$$P(t) = P_0 f(t) \cos(\omega_\mu t + \phi), \qquad 3.$$

where P_0 is the apparent initial muon polarization, $f(t)$ is the (time-dependent) amplitude of the oscillations, and ϕ is the apparent initial phase of the precession. For the majority of cases, $f(t)$ is an exponential decay, $f(t) = \exp(-t/T_2)$, where the transverse relaxation time T_2 is a measure of local field fluctuations and other dynamics of the coupling of the muon spin to the medium. Often, however, $f(t)$ may be a gaussian relaxation term or even more complicated time dependence.

In many cases the "μSR signal," $P(t)$, exhibits more than one precession frequency, in which case the simple description Equation 3 must be replaced by a sum of similar terms for each frequency. Whether constraints are imposed upon the extra parameters depends upon the theory of the multifrequency precession. In general the physics is contained in $P(t)$, both experimentally and theoretically. Usually these more complicated spectra yield their information most easily to a Fourier transform.

The above description obviously reflects a bias toward positive muon spin rotation (μ^+SR) as opposed to negative (μ^-SR). This does not mean that we consider μ^-SR unimportant. On the contrary, while the μ^-SR technique is more difficult because of small muon polarizations in the final state and the dominance of muon capture over decay for high Z, it may soon provide very important information complementary to that discussed here (3–5). However, the overwhelming majority of μSR work is still being done with positive muons, and this review reflects that fact. The treatment of μ^-SR spectra follows the above description, except that one is usually obliged to introduce several distinct components of the form of Equation 2, each characterized by a different muon lifetime for negative muons captured by different elements.

The source of the asymmetry in muon decay, the characteristics of the basic effect, formal descriptions of the parameterization of the time distribution $dN(t)/dt$, and the elements of basic μSR techniques are well documented in Reference 11; we do not duplicate the basics here, except to raise conceptual points and describe improvements to the technique.

1.2 *Muon Depolarization*

In the first experiments on asymmetric muon decay (e.g. 12), there was evidence of the effects of the stopping medium upon the muon polarization. Most metals left the μ^+ polarization essentially undisturbed, but other solids showed a wide variation in the "residual" μ^+ polarization, designated P_{res}. In liquids, P_{res} was a strong function of the chemical properties of the solution. From the outset, it was realized (2) that variations in P_{res} were mainly due to the temporary formation of muonium (μ^+e^-) atoms, in which the hyperfine coupling of the muon and electron spins caused a reversal of the muon spin within a fraction of a nanosecond. However, it was essential that muonium (or Mu) atoms be short-lived, since not all the polarization was lost, and since the observed precession was at the frequency of a free muon, rather than that of the triplet state of Mu (103 times faster). After some initial confusion, it was recognized that this effect probably involved chemical reactions of the hydrogen-like Mu atom, which afforded an opportunity for study of its chemistry (7). However, all of the early models were either incorrect or incomplete, and for several years progress along these lines was hampered by inability to make quantitative predictions. At the same time, however, another application of μSR techniques was developed in a quite different field of physics.

1.3 *Muonium and Quantum Electrodynamics*

The development of advanced μSR technology was largely the result of a program of measurements of the muon magnetic moment (8), its anomalous magnetic moment $(g-2)$ (9), and the hyperfine splitting of the muonium atom (10), which has provided the most stringent test of quantum electrodynamics (QED) to date, and which continues today (13). The hyperfine splitting of Mu due to the Fermi contact interaction coupling muon and electron spins is perfectly analogous to that of the H atom, except that in this purely leptonic atom there are no complications caused by strong-interaction-induced anomalous magnetic moments. We remark only briefly on the form and consequences of this interaction, leaving the interested reader to consult one of the many fine reviews of this topic (9, 13).

The Hamiltonian acting on the spins in the Mu atom, including an external field **B** and the contact interaction, is

$$\mathcal{H} = \tfrac{1}{2}\hbar\,(\gamma_\mu \boldsymbol{\sigma}_\mu - \gamma_e \boldsymbol{\sigma}_e)\cdot \mathbf{B} + \tfrac{1}{4}\hbar\,\omega_0(\boldsymbol{\sigma}_\mu \cdot \boldsymbol{\sigma}_e), \qquad 4.$$

where $\boldsymbol{\sigma}_\mu$ and $\boldsymbol{\sigma}_e$ are the muon and electron spin Pauli operators, $\gamma_\mu/2\pi = 0.01355$ MHz per gauss and $\gamma_e = (m_\mu/m_e)\gamma_\mu = 206.77\,\gamma_\mu$ are the

muon and electron gyromagnetic ratios, and ω_0 is the hyperfine frequency (13),

$$\omega_0 = 2.804 \times 10^{10} \text{ rad per sec } (\omega_0/2\pi = 4463 \text{ MHz}). \quad 5.$$

This Hamiltonian has energy eigenstates and eigenvalues

$$|1\rangle = |++\rangle, E_1/\hbar = \frac{\omega_0}{4} + \omega_- \quad 6a.$$

$$|2\rangle = s|+-\rangle + c|-+\rangle, E_2/\hbar = -\frac{\omega_0}{4} + \left(\frac{\omega_0^2}{4} + \omega_+^2\right)^{\frac{1}{2}} \quad 6b.$$

$$|3\rangle = |--\rangle, E_3/\hbar = \frac{\omega_0}{4} - \omega_- \quad 6c.$$

$$|4\rangle = s|-+\rangle - c|+-\rangle, E_4/\hbar = -\frac{\omega_0}{4} - \left(\frac{\omega_0^2}{4} + \omega_+^2\right)^{\frac{1}{2}}, \quad 6d.$$

where $$c = \frac{1}{\sqrt{2}}\left(1 + \frac{x}{(1+x^2)^{\frac{1}{2}}}\right)^{\frac{1}{2}}, \quad 7a.$$

$$s = \frac{1}{\sqrt{2}}\left(1 - \frac{x}{(1+x^2)^{\frac{1}{2}}}\right)^{\frac{1}{2}}, \quad 7b.$$

and $$\omega_\pm = \tfrac{1}{2}(|\omega^e| \pm |\omega^\mu|). \quad 7c.$$

Here "+/−" refers to $m = +$ or $-\frac{1}{2}$ along the external field direction for the muon (first sign) and electron (second sign) spins. These energy levels are plotted as a function of external field in Figure 5, a typical Breit-Rabi diagram. In this figure, an unphysical value of the muon mass (and therefore the muon magnetic moment) is used to exhibit the curvature at low field at the same time as the asymptotic behavior at high field. The field is given in units of the dimensionless "specific field,"

$$x = 2\omega_+/\omega_0 = (g_e\mu_0^e - g_\mu\mu_0^\mu)|B|/\hbar\omega_0 = B/B_0, \quad B_0 = 1585 \text{ G}. \quad 8.$$

Also shown in Figure 5 are the observable transition frequencies $\nu_{ij} = \nu_i - \nu_j$ corresponding to allowed ($\Delta m = \pm 1$) electromagnetic transitions. These are the frequencies actually measured by resonant Mu depolarization in a rf field in the QED tests. They are also observable in muonium spin rotation (MSR) experiments as precession frequencies in a transverse field (14) and are referred to again later. We give here the formula for the time dependence $\hat{P}(t)$ of the muon polarization in free muonium in a transverse magnetic field, using the complex convention in which the real part of $\hat{P}(t)$ is the muon polarization along its initial (x) direction, and the imaginary part is the muon polarization

along the y direction, which makes a right-handed coordinate system with the magnetic field (z) direction (11):

$$\hat{P}(t) = \tfrac{1}{2}[c^2(e^{i\omega_{12}t} + e^{-i\omega_{34}t}) + S^2(e^{i\omega_{23}t} + e^{i\omega_{14}t})], \quad 9.$$

where $\omega_{ij} \equiv 2\pi\nu_{ij}$. This can be reduced to the form

$$\hat{P}(t) = e^{i\omega_- t}\cos(\tfrac{1}{2}\omega_0 t)[\cos(\tfrac{1}{2}\omega_0 + \Omega)t - i(c^2 - s^2)\sin(\tfrac{1}{2}\omega_0 + \Omega)t] \quad 10.$$

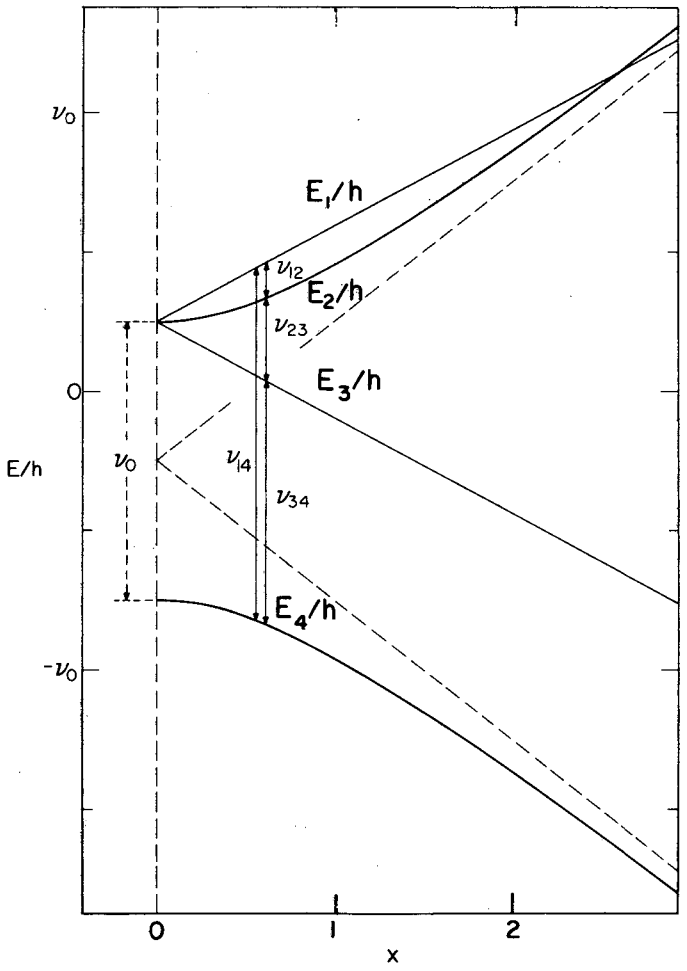

Figure 5 Energy eigenstates of $l = 0$ muonium in an external magnetic field, as a function of the dimensionless "specific field," which is given in Equation 8. A nonphysical value of the muon magnetic moment is used to display clearly the qualitative features.

where $\omega_- = \frac{1}{2}(\omega_{12}+\omega_{23})$ is the mean precession frequency of triplet muonium and Ω is the splitting frequency of triplet muonium precession,

$$\Omega = \tfrac{1}{2}(\omega_{23}-\omega_{12}) = \tfrac{1}{2}\omega_0\,[(1+X^2)^{\frac{1}{2}}-1]. \qquad 11.$$

In low field, Ω is well approximated by $\Omega = \omega_-^2/\omega_0$ and $\hat{P}(t)$ has the form (averaged over the hyperfine oscillations, which are too fast to observe)

$$\langle \hat{P}(t)\rangle_{\omega_0} = \tfrac{1}{2}e^{i\omega_- t}\cos \Omega t. \qquad 12.$$

That is, "two-frequency" triplet muonium precession is seen.

Measurement of the hyperfine splitting in muonium required the development of methods of producing and observing stable Mu atoms in inert gases, which in turn led to the first studies of chemical reactions of Mu in gases (15). Similarly, the experimental basis of modern μSR techniques was developed to measure the muon's magnetic moment via its precession frequency in an external field (8). Because of the effects of diamagnetic shielding (16), interpretation of the results of that experiment depended upon a sure knowledge of the muon's final environment. This in turn led to an investigation of the chemical behavior of Mu in liquids (17, 18).

1.4 *μSR in Chemistry and Solid State Physics*

From 1957 to around 1970, the possible uses of parity-violating muon decay in materials sciences received little attention from the scientific community. However, a few groups performed important "seed" experiments (7, 12, 15, 19–22) that gave such ideas a vital experimental base; and a series of Soviet theoretical papers (23–26) pointed the way toward a quantitative understanding of the depolarization of positive muons in matter in terms of the formation, disruption, and reaction of Mu atoms. Thus in the early 1970s the field began to gel. The following section of this review describes the main lines of progress in those formative years.

Since about 1975 the volume of experimental and theoretical activity in this field has grown almost exponentially, producing a great variety of new information and clarifications of old questions. In Figure 6 we indicate schematically the current breadth of μSR research in materials science, with apologies to the omitted topics certain to have been developed during the preparation of this review. Obviously we cannot attempt a comprehensive review of such a collection of research topics, so we have selected what seem now to be centrally important subjects that represent breakthroughs in qualitative understanding and that will be of benefit to many of the subfields shown in Figure 6. These highlights of recent progress in μSR are the subject of the third section of this review.

2 THE FORMATIVE PERIOD: 1957–1975

2.1 *Depolarization and Muonium Chemistry*

2.1.1 FAST DEPOLARIZATION AND THE RESIDUAL POLARIZATION As mentioned in the introduction, the effects of the chemical properties of the stopping medium upon the muon's residual polarization were noticed in the very first experiments verifying the asymmetric decay of the muon. Those experiments, like most that followed for the next decade, were performed in the condensed phase—most often liquids—because of the difficulty of stopping muon beams in low density gas targets; the experimental observable was in most cases the quasifree precession amplitude of muons in diamagnetic environments. Thus the first theoretical studies of the behavior of muons in matter were oriented toward explaining the varying degrees of depolarization in terms of the

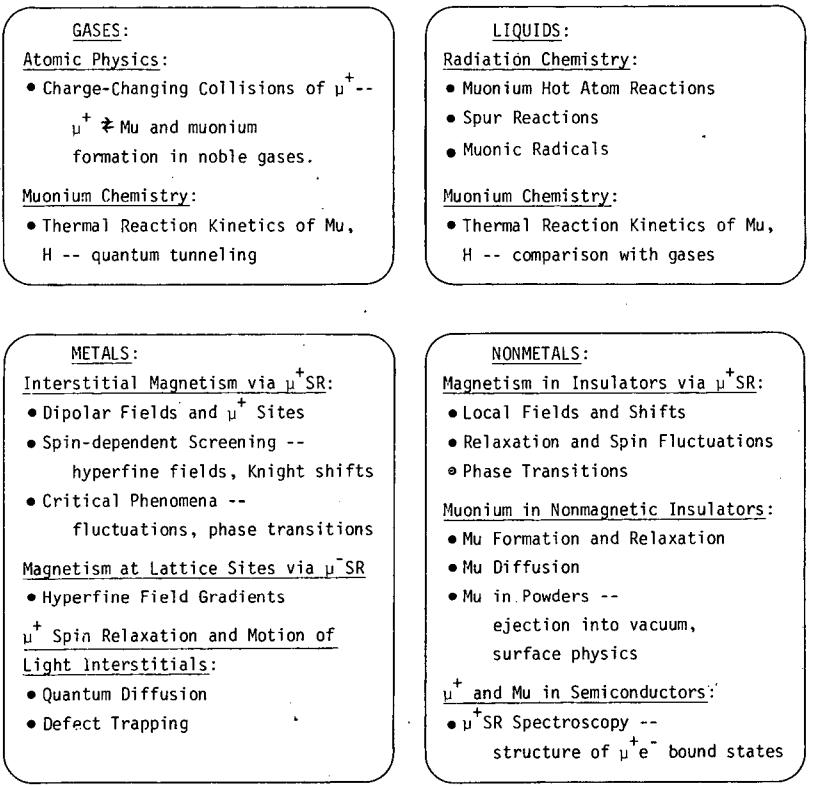

Figure 6 The major active fields of μSR research as of 1977.

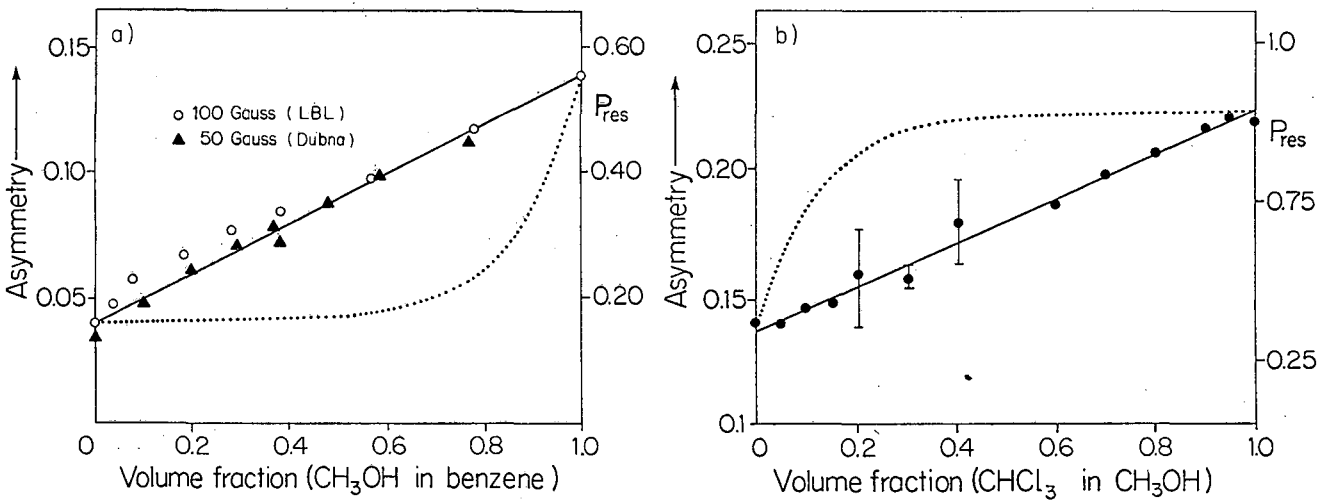

Figure 7 (*left*) Measured asymmetry of μ^+ precession and corresponding residual polarization P_{res} as a function of the volume fraction of CH_3OH in C_6H_6 in two transverse magnetic fields. Circles represent data from LBL at 100 G; triangles represent data from JINR at 50 G. The dotted line indicates how the asymmetry would be expected to change if benzene gave "sponge-like" protection to CH_3OH. (*right*) Similar data from LBL on $CH_3OH/CHCl_4$ mixtures in 100 G fields. The dotted line here indicates how the asymmetry is expected to vary if selective reaction by $CHCl_3$ were possible, or if spur scavenging by $CHCl_3$ occurred.

properties of the medium. It was immediately realized that the Mu atom was responsible, with its hyperfine interaction and rapid precession; but there was uncertainty about why this depolarizing effect was not always complete. In 1963 Nosov & Yakovleva (23) introduced a density matrix formalism describing the evolution of muon and electron spins in muonium, allowing for "spin-flipping" of the electron by outside influences; in 1969 Ivanter & Smilga (25) pointed out that fast chemical reaction of the Mu atoms placed the muons in diamagnetic molecules, which would quench the depolarizing effect of Mu formation, and offered an elegant quantitative model for the residual polarization.

The implication that depolarization studies could provide information about the chemistry of muonium atoms had already been recognized by Firsov & Byakov (7). However, their first attempts at such an application (22) were limited by an incorrect model. Data from that study are shown in Figure 7 along with more recent results exhibiting the dependence of P_{res} upon the volume fraction of mixtures of benzene, methanol, and chloroform. In 1971, it was demonstrated that the purely thermal reaction scheme of Ivanter & Smilga could not account for the observed effects, unless a high probability of epithermal reaction was included (27). That is, a significant fraction of muons destined for depolarization are saved from that fate "on the way in" by higher energy (up to a few

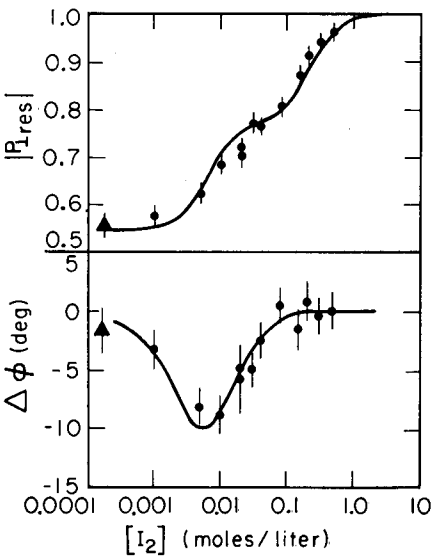

Figure 8 Magnitude $|P_{res}|$ and apparent initial phase $\Delta\phi$ of the residual μ^+ polarization in methanol solutions at 100 G, as a function of the concentration of dissolved iodine.

tens of eV) chemical reactions leaving the muons in diamagnetic molecules. Thus μSR experimenters were introduced to the field of "hot atom" chemistry. The behavior shown in Figure 7, which was attributed to thermal reactions of Mu by Babaev et al (22), is now interpreted in terms of hot atom reactions alone. At the same time, the 1971 experiment (27) verified the important role played by thermal reactions (in that case, $Mu + I_2 \rightarrow MuI + I$) in the de- or repolarization scheme. Figure 8 shows data taken later (18) on the same reaction in methanol solvent. Clearly evident is the variation of the apparent initial phase of the muon precession due to short-lived, high frequency precession of Mu atoms—a distinctive feature of the depolarization mechanism.

By 1972 the role of radicals in the general depolarization mechanism had been recognized as well (17), and it appeared that a correct qualitative description of the depolarization process had been achieved (18). Figure 9 shows data from that experiment, which demonstrates that the simpler theory excluding radicals (dashed line) was unable to explain the repolarization of muons in benzene by the addition of bromine reagent. Unfortunately, the additional parameters required in the more elaborate reaction scheme made the fitted values less unambiguous, and it became apparent that accessible parameters would have to be measured as precisely as possible before the general model could be used to measure rate constants for the various chemical reactions involved (18a).

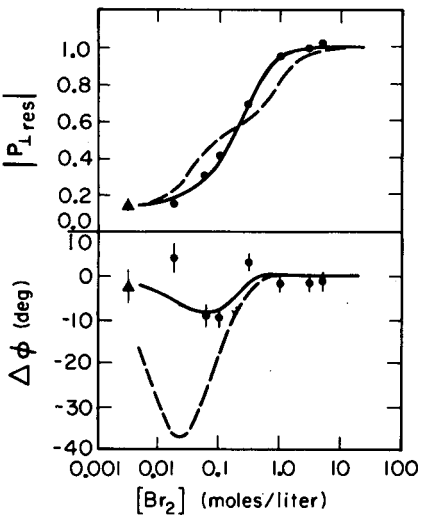

Figure 9 Residual muon polarization in benzene as a function of the concentration of dissolved bromine. Uncertainties of $|P_{res}|$ data are smaller than the dimensions of the points.

2.1.2 SLOW RELAXATION IN PARAMAGNETIC SOLUTIONS Residual polarization studies rely upon measurements of the amplitude and apparent initial phase of muon precession; these quantities vary because of the fast depolarization of the muons by short-lived muonium formation. Once the Mu atoms have reacted, placing the muons in diamagnetic compounds with some residual polarization, the muons can still be depolarized gradually by random local magnetic fields or spin-lattice relaxation phenomena. The rate of this slow depolarization is characterized by the transverse relaxation time T_2 in $f(t)$ of Equation 3 (12, 18b); early studies of this parameter (28) gave μ^+SR experimenters access to several new topics, one of which was the structure of liquids (29).

In aqueous solutions of $MnCl_2$, the residual muon polarization was found to be independent of concentration, which indicated a lack of any fast thermal reactions with the solute, and suggested that the observable muon precession signal came from MuOH molecules formed epithermally (11). Like H_2O, these "muonic water" molecules spend part of their time in $Mu(H_2O)$ complexes, where the muons (like protons) are relaxed by interactions with the paramagnetic ions. Figure 10 shows the observed

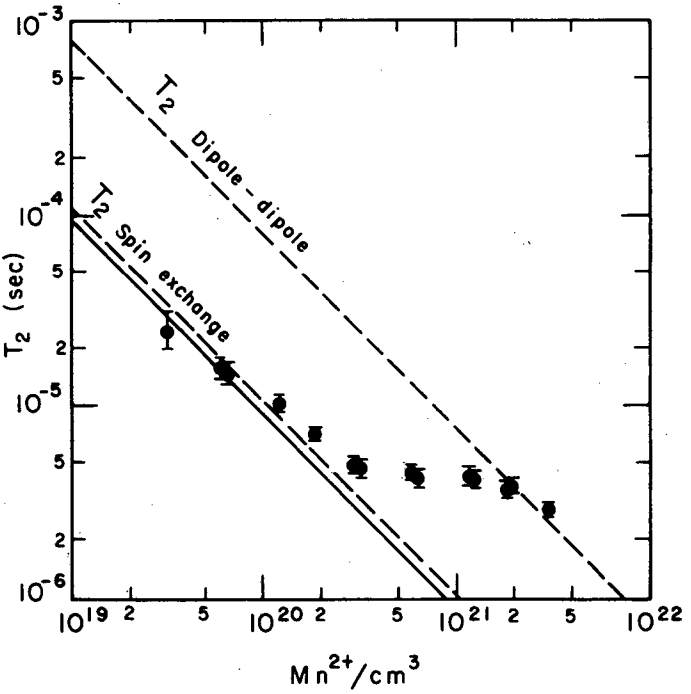

Figure 10 Transverse muon relaxation times in $MnCl_2$ solutions.

dependence of the μ^+ relaxation time on the concentration of Mn^{++}. The muon lifetime sets practical limits of about 20 nsec to about 20 μsec on conveniently measurable values of T_2, although in principle both these limits can be transcended by high statistics. In this case (29) the lower limit was set by the solubility of $MnCl_2$ in water. The relaxation at low concentrations follows the dependence predicted for spin-exchange interactions between the paramagnetic ion and the normally diamagnetic MuOH molecule, but at high concentrations this mechanism is broken and the slower relaxation of the muon by the dipolar field of the ion takes over. This is thought to be due to mutual interactions of neighboring Mn^{++} ions, and thus provides a measure of local structure and correlation times in the liquid. The muon offers certain advantages over proton NMR in these studies, since the region of fast relaxation where NMR has difficulties is just where μSR works best. However, this promising line of investigation has remained virtually untouched since 1972.

2.2 μ^+ *Site in Solids*

The sensitivity of μSR to local magnetic fields (through the muon precession frequency) and their dispersion (through the relaxation rate) make the muon a different probe of the solid state, analogous to nuclear magnetic resonance (NMR) or electron paramagnetic resonance (EPR); this was recognized as soon as the asymmetric decay was discovered. Furthermore, unlike NMR, μSR is free of complications associated with rf fields and the necessity for macroscopic populations of the resonant species; μSR is a purely passive technique using no more than one muon at a time in the sample. Thus it was expected (correctly) that μSR would furnish new information about local fields in crystals, thus contributing to the microscopic theory of magnetism, among other topics in solid state physics.

However, knowing the local fields "seen" by the muon is not of great value until we have some idea where the muon is in the crystal lattice. This places great emphasis upon the determination of muon locations, a topic still of high priority today.

2.2.1 μ^+ SITE IN GYPSUM

The first μ^+ site determination was performed (21) in a single crystal of gypsum ($CaSO_4 \cdot 2H_2O$), for which the NMR of protons was well known (30). As indicated in Figure 11, the fixed location of the protons in gypsum leads to a unique contribution to the net magnetic field seen by one proton because of the dipolar field of an adjacent proton. Since the proton has spin $\frac{1}{2}$, this field either adds or subtracts from the applied external field, producing two discrete values of the net field "seen" by a given proton. The magnitude of this splitting depends on the

orientation of the crystal in the external field, and in some cases a double splitting (four discrete frequencies) is observed, owing to the influence of two different proton-proton orientations (30). The analogous μ^+SR experiment led to a test of the μ^+ location in gypsum. If the μ^+ were interstitial or mobile in the crystal, the dipolar fields of the protons would simply cause relaxation of the muon spin. However, if the muons replaced protons at the appropriate lattice sites, the μSR results would show exactly the same behavior as the proton NMR had. The experiment (21) showed the split-frequency muon precession expected for muons occupying proton sites, and thus gave the first positive identification of the μ^+ site in a crystal.

2.2.2 μ^+ LOCATION IN METALS In simple metals, there is no ion site where the μ^+ will be electrically equivalent, and thus the muon must be either interstitial or trapped at vacancies, dislocations, or other defect centers. The question of which of these possibilities is preferred is crucial to interpretations of local field and relaxation measurements with muons. Recently there has been considerable progress along these lines, again relying upon the local dipolar field contributions (see Section 3.3.1), but

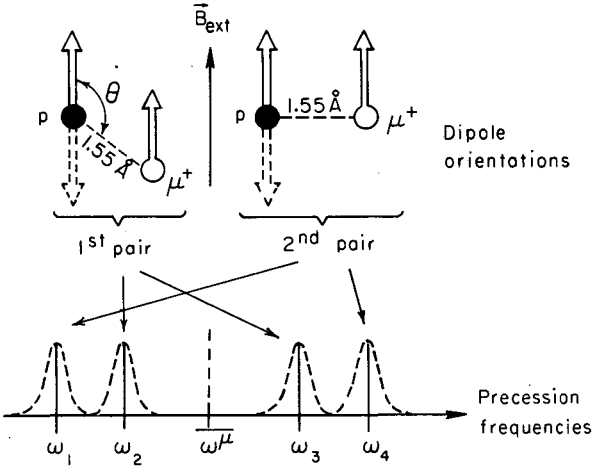

Figure 11 Muon-proton dipole-dipole interaction in a single crystal of gypsum: schematic representation of the effect of the muon-proton situation relative to the magnetic field direction on the μ^+ spin precession. $\overline{\omega^\mu}$ corresponds to the precession frequency unperturbed by dipole-dipole interactions; it is split by that interaction into two symmetrically shifted frequencies (one per proton spin orientation for each μ^+-p pair. The line broadening produced by the magnetic dipoles farther away is indicated by the dashed curves.

for many years this question was obscured by the tendency of the muon to diffuse rapidly in metals—a phenomenon of intrinsic interest independent of the site determination.

2.3 μ^+ *Motion in Metals*

A muon held immobile at a well-defined interstitial position in a non-magnetic metal whose nuclei have magnetic moments should experience a gaussian relaxation $f(t) = \exp(-\sigma^2 t^2)$, where σ^2 characterizes the averaged strength and orientation of dipolar fields from neighboring nuclear moments (30). Such behavior was observed by Gurevich et al (31) for μSR in copper at 77°K, indicating that the muons were not diffusing significantly at that temperature.

However, at higher temperatures the μ^+ relaxation became slower and more exponential, which indicated a "motional narrowing" effect of the μ^+ diffusion upon the relaxation rate of the muon (analogous to the linewidth in NMR). The origin of this effect is simple. As the μ^+ moves more rapidly between sites with different fields, it begins to see the average field, and the "dephasing" effects of different fields at different sites disappear (32). Figure 12 shows the temperature dependence of the relaxation rate of muons in Cu (31). At temperatures above about 120°K the data are described by a motional-narrowing model in which muon diffusion is governed by a thermally activated "hopping" between potential wells.

The results of that experiment were perplexing: The activation energy

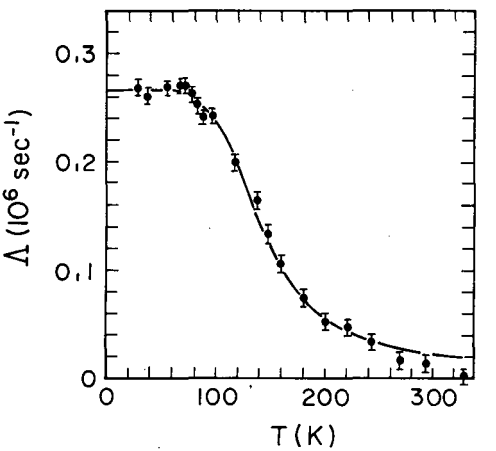

Figure 12 The μ^+ relaxation rate in Cu as a function of temperature.

extracted for the μ^+ hopping process was small compared with the values for hydrogen, and the preexponential factor (characteristic of the vibrational frequency of the muon in the potential well) was lower by a factor of a million. As it now turns out, the case of Cu studied by Gurevich et al (31) was one of the few examples of relaxation/diffusion μSR studies that exhibit the simple behavior shown in Figure 12. Other nonmagnetic metals have considerable structure in the temperature dependence of the depolarization rate (see Section 3.4).

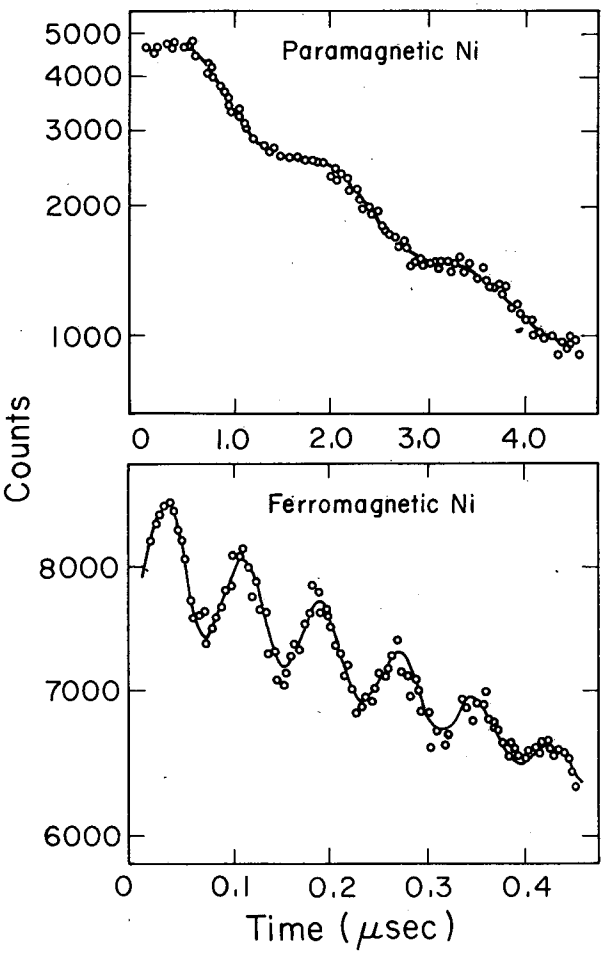

Figure 13 The μ^+ SR time spectra in paramagnetic nickel at about 670°K and ferromagnetic nickel at 551°K. The data shown are semilog plots of the number of decay positrons detected in a fixed direction as a function of time after a muon stop. Note that the time scales differ by a factor of ten.

2.4 *The Muon as a Magnetic Probe*

2.4.1 μ^+ IN FERROMAGNETS Since the muon was effective as a detector of small local fields, it was suspected that it might also be used to probe the internal fields in magnetic metals; however, early survey experiments failed to reveal any μSR signals from magnetic samples. This was largely because of inadequate purity in the samples initially used; the problem was first solved by raising the temperature of the samples until the muons diffused rapidly enough to quench any depolarization. Figure 13 shows the μ^+SR time spectra from that first study by Foy et al (33). The temperature dependence of the local field in nickel follows a Brillouin function approximately the same as the temperature dependence of the saturation magnetization.

The average local field at the muon, $\mathbf{B}_\mu$, has several contributions:

$$\mathbf{B}_\mu = \mathbf{B}_{ext} + \mathbf{B}_{DM} + \mathbf{B}_L + \mathbf{B}_{dip} + \mathbf{B}_{hf}, \qquad 13.$$

where $\mathbf{B}_{ext}$ is the external applied field, $\mathbf{B}_{DM}$ is the sample-geometry-dependent demagnetization field, $\mathbf{B}_L$ is the "Lorentz field" of magnetic

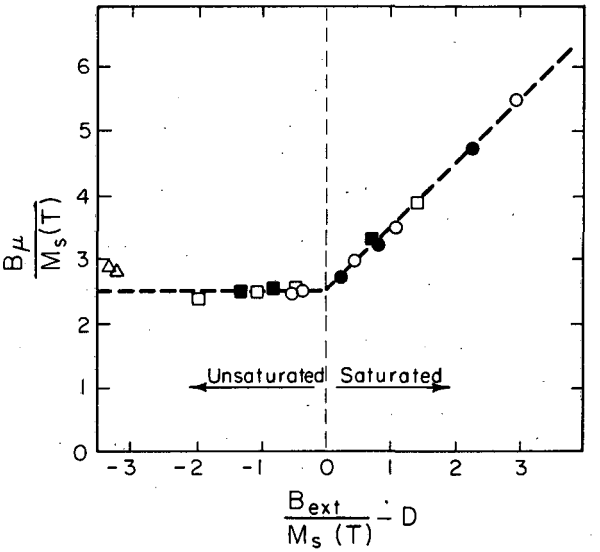

Figure 14 Local field $\mathbf{B}_\mu$ at the muon site in nickel vs $\mathbf{B}_{ext}$, the external field measured with target out. D is the sample demagnetizing factor. The points denoted by triangles are from data on an approximately spherical single crystal with [111] axis parallel to $\mathbf{B}_{ext}$ at 300 and 77°K. Other points are from data on a polycrystalline ellipsoid (4.5 × 2 × 0.5 in.). Solid and open circles refer to the 4.5-in. axis parallel to $\mathbf{B}_{ext}$ ($D = 0.69$) at 523 and 573°K respectively. Solid and open squares refer to the 2-in. axis parallel to $\mathbf{B}_{ext}$ ($D = 2.24$) at 523 and 573°K.

charge on the inner surface of an imaginary sphere centered on the muon, $\mathbf{B}_{dip}$ is the field due to dipole moments within that sphere, and $\mathbf{B}_{hf}$ is the effective field due to local interaction with polarized electrons. For high permeability material below saturation, $\mathbf{B}_{DM}$ cancels $\mathbf{B}_{ext}$, as can be seen from Figure 14, showing the dependence of $\mathbf{B}_{\mu}$ on $\mathbf{B}_{ext}$ in Ni (11).

All the terms in Equation 13 are easily calculable except $\mathbf{B}_{dip}$ and $\mathbf{B}_{hf}$. For Ni, the interstitial site has cubic symmetry and thus $\mathbf{B}_{dip}$ averages to zero, and for Fe there are two otherwise equivalent interstitial sites, one with a dipolar field of about 10 kG and the other (only half as numerous) with $\mathbf{B}_{dip}$ of about -20 kG. Thus in either case, as long as the μ^+ diffuses rapidly between sites, the time-averaged dipolar field is zero. (This argument applies equally well for the interstitial sites with octahedrally or tetrahedrally positioned ion neighbors.) At lower temperatures the different fields at different sites in Fe cause a dramatic relaxation of the muon, which has been the subject of several recent studies (see Section 3.3.3).

Thus the early results of Kossler et al (33) and others (34, 35) were reducible to measurements of temperature dependence of $\mathbf{B}_{hf}$ in Ni and Fe. Subsequent work has followed similar patterns. The theoretical value of a measurement of $\mathbf{B}_{hf}$ at the positive muon depends upon the eventual clarification of: (*a*) the site occupied by the muon most of the time; (*b*) the vibrational motion of the muon in that site; (*c*) the distortion of the lattice by the presence of the muon; (*d*) the screening of the muon by conduction electrons; and (*e*) the spin dependence of that screening, since it is largely the same polarized conduction electrons that deliver the effective contact field to the muon. Early treatments helped to explain the qualitative behavior of (*d*) and (*e*) (36), but these theoretical problems are still with us today.

2.4.2 KNIGHT SHIFTS In nonmagnetic metals the conduction electrons are slightly polarized by the external field, and though the resulting contact field at the muon is normally small (a few gauss), the mechanism is analogous to that producing $\mathbf{B}_{hf}$ in ferromagnetic metals. Thus the theoretical problems described above apply equally to the interpretation of Knight shifts in nonmagnetic metals.

As early as 1963, muonic Knight shifts were measured with 10-ppm accuracy in various metals as part of a determination of the muon magnetic moment (20). The results of that study are shown in Table 1; the large shifts in carbon and calcium are still not understood. Recent experiments have uncovered other, even larger, anomalous Knight shifts of positive muons (see Section 3.5).

Hutchinson et al (20) also measured the magnetic moment of the

Table 1 μ^+ and μ^- Knight shifts

Target substance	μ^+ Asymmetry coefficient	μ^+ Frequency shift[a] (ppm)	μ^- Frequency shift[b] (ppm)	NMR Knight shift (ppm)
Carbon	—	+380	+ 70± 32	—
Silicon	—	—	+287±110	+ 180
Magnesium	0.12	+ 87	+334± 75	+1400
Copper	0.12	+ 81	—	+2320
Lead	0.09	+132	—	+1200
Calcium	0.09	+420	—	+3100
Lithium	0.12	+ 11	—	+ 249
Potassium	0.13	+ 88	—	+2900
Sodium	0.13	+ 79	—	+1130
Reference samples				
CH_2I_2	0.15	− 25	—	—
$CHBr_3$	0.14	− 14	—	—
H_2O	0.09	0	+540± 80[c]	—
Sulfur	—	—	+ 96±170	—

[a] The diamagnetic shielding of muons in water (~25.6 ppm) has not been included.
[b] Relativistic effects, and diamagnetic shielding, nuclear polarization, and coulomb radiative corrections have been applied. Reference: Ford, K. W., Hughes, V. W., Wills, J. G. 1963. *Phys. Rev.* 129:194.
[c] The μ^- is transferred to the oxygen. Reference: Bingham, G. 1963. *Nuovo Cimento* 27:1352; also Reference 20.

negative muon, and in the process studied the Knight shifts at the μ^- in various media. Their results are also included in Table 1. Here the interpretation is completely different: the μ^- is bound to a lattice nucleus and is so close that it effectively forms a $Z-1$ substitutional nucleus, which behaves accordingly in the lattice. If the original nucleus has a magnetic moment, the $\mu^- Z$ pseudonucleus can have several spin states, and the muon motion often becomes complicated (39). When the μ^- captures on a spinless nucleus, it precesses in the local field as if free, except for relativistic corrections (high Z only) (3). Those muons that decay instead of capturing on a proton exhibit the same asymmetric decay observed in μ^+SR, except that the μ^- polarization is usually only about 15% in the final state. The field seen by the μ^-, then, is different from that seen by a $Z-1$ substitutional impurity only if the local field has such a large spatial gradient that it is significantly different at the mean radius of the muon's orbit from the value averaged over the nucleus (3).

2.4.3 μ^-SR IN MAGNETIC CRYSTALS Since Knight shifts are small in the first place and the difference between those seen by $\mu^- Z$ and $Z-1$ substitutional nuclei are expected to be subtle, it may prove difficult to extract

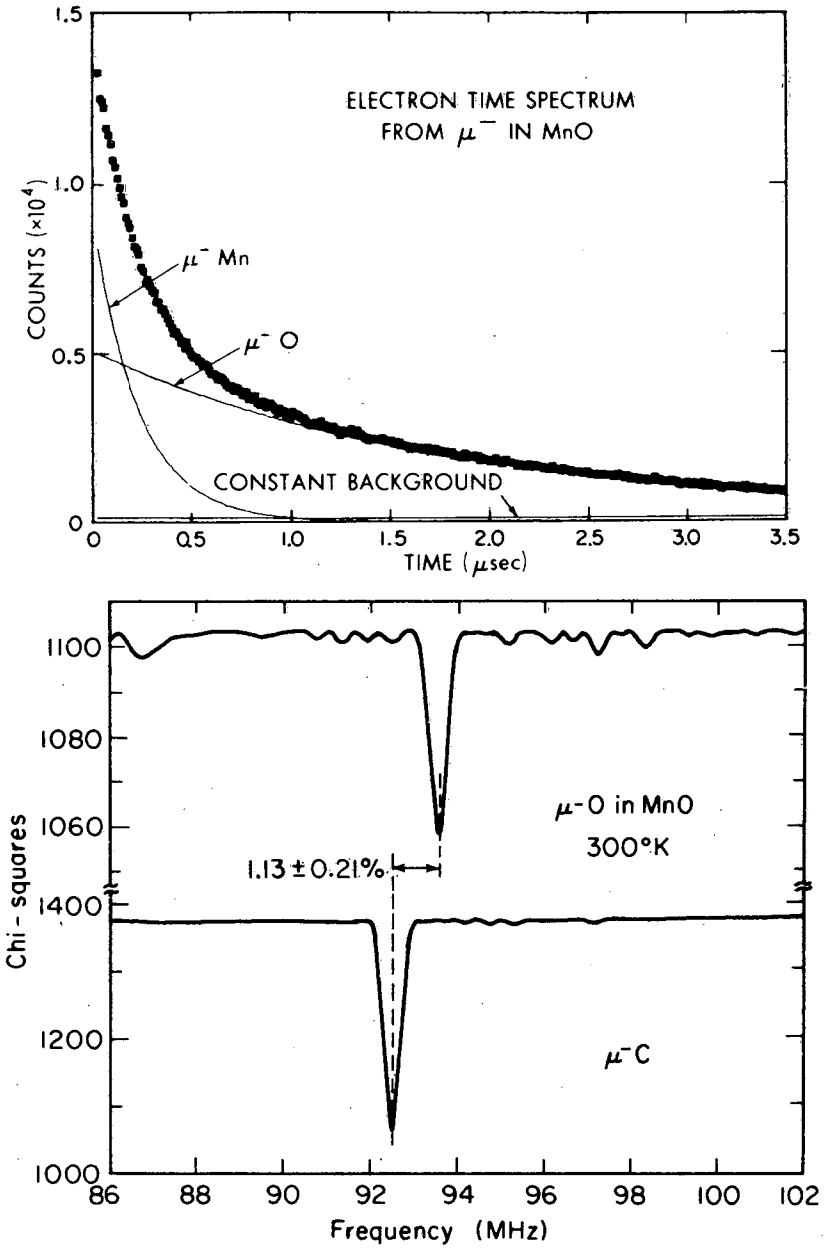

Figure 15 (*Upper*) μ^-SR time spectrum in MnO, showing the different lifetimes for μ^- bound to Mn and O. (*Lower*) μ^-SR frequency spectra in C and MnO at 6.9 kG showing a shift in the frequency of μ^-O relative to μ^-C.

new information from such data. However, in magnetic crystals the local fields at the nuclei can be huge, and the difference due to the spatial distribution of the muon may be significant.

An experiment of this sort was performed by Yamazaki et al (5) on the antiferromagnetic crystal MnO, where precession of the μ^-O component was compared with that of the μ^-C in a carbon target. Because of the weak signals in these experiments, a Fourier transform was taken of the time spectra after removal of background and correction for the exponential decay of the muon. The results are shown in Figure 15. The measured shift, $1.16 = 0.21\%$, is about a third of the O^{17} NMR shift (3.21%). Assuming a $N^{3-}(Mn^{2+})_6$ electronic configuration, the paramagnetic shift is lowered only $\sim 30\%$.

H. Kamimura and Y. Natsume (1978, private communication) have shown that if the μ^-O system forms an antisymmetrical ion configuration $N^{3-}(Mn^{2+})_5\ Mn^{3+}$ as the ground state, where the Mn^{2+} has lost an electron to a defect, then the observed shift can be explained.

2.5 μ^+SR Spectroscopy and Muonium in Semiconductors

In pure inert nonmetals, the μ^+ usually captures a single electron to form a stable neutral atom of muonium. As long as nuclear moments are small or absent and/or the Mu atom diffuses rapidly, this entity can be detected via its characteristic precession frequency, 103 times as fast as the free μ^+. The first such muonium spin rotation (MSR) measurement in solids was performed in fused quartz, which remains a reference standard (40). In moderate magnetic fields (20–150 G) the simple Mu precession described above gives way to the more general two-frequency Mu precession of Equation 12, first observed in 1971 by Gurevich et al (14). As mentioned in the introduction, the splitting of the Mu precession frequencies is inversely proportional to the hyperfine coupling strength. Thus a measurement of this splitting provides an imprecise (good to about 1% usually) but unambiguous value for the hyperfine coupling of the Mu atom in the lattice, which is in turn related to the physical size of the Mu atom.

Gurevich et al (41) were the first to study this phenomenon in semiconductor crystals, where the μ^+ also forms Mu atoms. They found a reduction in the Mu hyperfine frequency ω_0 of nearly a factor of two in germanium, as can be seen from the two-frequency precession signals in Figure 16. In fused quartz, muonium has essentially the vacuum value of ω_0, which indicates a Mu atom virtually undisturbed by the presence of the surrounding lattice. However, in Ge at 77°K the Mu atom appears to have been expanded significantly. At about the same time, Andrianov et al (44) performed a longitudinal-field "Paschen-Bach effect" experiment on Mu in Si that indicated an even more pronounced effect. This result

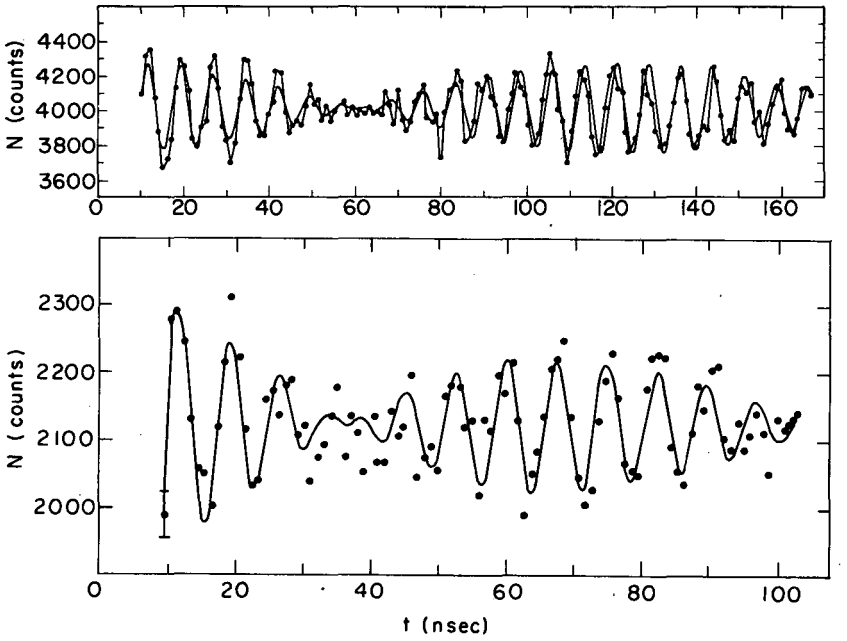

Figure 16 "Two-frequency precession" of the muon in fused quartz with a transverse field of 95 G (*upper graph*) and in cold (77°K) germanium at 98 G (*lower graph*). The smooth curves represent the best fits of the theoretical dependence to the data, which is corrected for the muon decay exponential $\exp(-t\tau)$.

was soon confirmed by the two-frequency MSR method (42). These observations stimulated theoretical interest in the electronic structure of the Mu impurity state in Si and Ge (45), where the analogous H atom impurity state, though sure to be present, has never been observed. In view of the practical importance of impurity electronic states in semiconductors, this simplest of all interstitial impurity systems provides a valuable experimental testing ground.

2.5.1 FOURIER SPECTROSCOPY AND ANOMALOUS μ^+ PRECESSION When more than one precession frequency is present in a single μ^+SR time spectrum, least-squares fitting becomes rather tedious and extremely model dependent. In these cases, and in general when systems with potential magnetic structure are being studied, it is wise to begin analysis with a Fourier transform of the time distribution (corrected for the background term and the muon decay factor). Figure 17 shows two such frequency spectra for μ^+ in fused quartz at room temperature and Si

at 77°K, both at 100 G. Both spectra show the free μ^+ signal at low frequency and the two muonium signals at about 103-times higher frequency, corresponding to the two-frequency precession as in Figure 16. Also evident in Figure 17 are at least two distinct signals at intermediate frequencies in Si, corresponding to the "anomalous μ^+ precession" reported in 1973 (42). These frequencies, representing a distinct coherent impurity state of μ^+ in Si, can be described as muonium transition frequencies ω_{12} and ω_{34} (see Figure 5 and Equation 9) as a function of applied field. This is illustrated in Figure 18a, but they will behave like this only if the hyperfine coupling is taken to be only about 2% of that in vacuum *and* the effective g factor of the electron is allowed to take a value of 13 instead of 2. Furthermore, in this model the hyperfine frequency is about 4% anisotropic with respect to the orientation of the Si crystal in

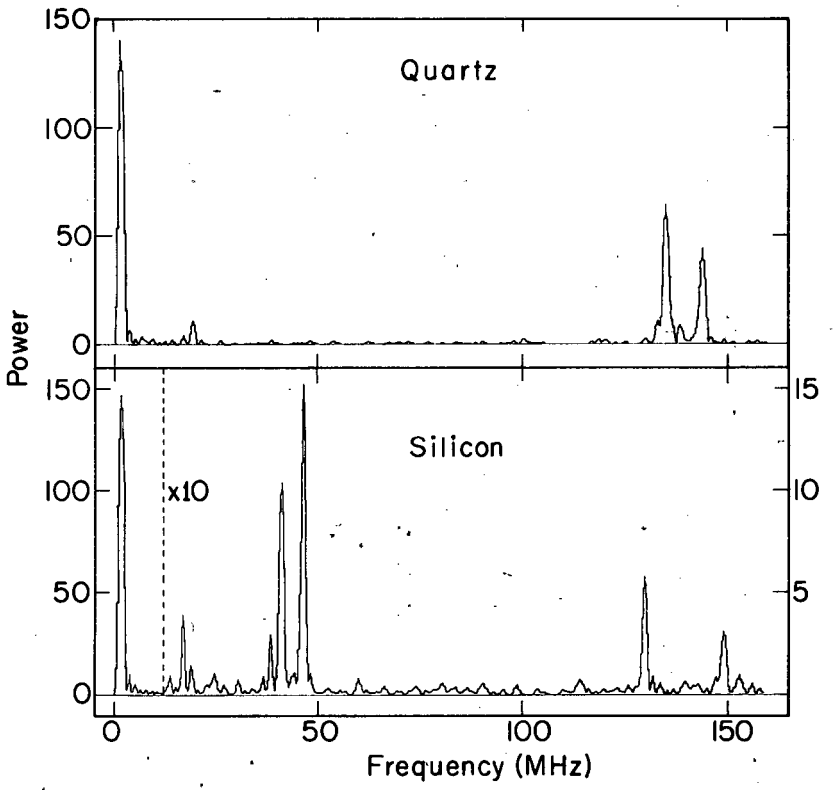

Figure 17 The μ^+SR Fourier power spectra (amplitude^2 vs frequency) for μ^+ in fused SiO_2 at room temperature and 100 G (*upper plot*) and in Si at 77°K and 100 G (*lower plot*).

experimental or a theoretical point of view. The last few years, far from clearing up the questions raised in early experiments, have mainly exposed more structure and raised new questions. Soviet work on Ge crystals has followed different lines (49, 50) but seems no less perplexing.

3 RECENT ADVANCES IN μSR

3.1 *Technology: The Surface Muon Beam*

Perhaps the most important new aid to μ^+SR in the past few years has been the "surface muon beam," also called the "Arizona beam" after the group that designed and built the beamline at Berkeley (51). This 4.1-MeV μ^+ beam, collected from the decay of positive pions at rest in the surface of the production target, is nearly 100% polarized, has a range of only about 150 mg cm^{-2} in air, and can be stopped completely in about 30 mg cm^{-2} of air. This can be seen in Figure 19, which shows the residual beam intensity following various thicknesses of Mylar degrader for surface muons produced at the Tri-University Meson Facility (TRIUMF).

While the very short range of surface muons creates problems in extraction of the beam from a vacuum pipe, passing it through a scintillator to form a μ-stop pulse, and injecting it into a target, the same effect permits a mass-stopping density orders of magnitude higher than

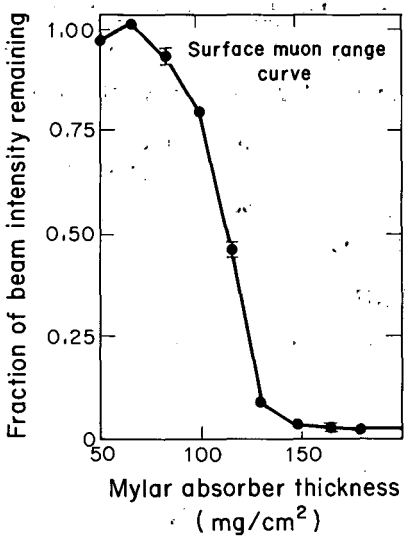

Figure 19 Range curve for surface muons at TRIUMF: Intensity of μ^+ beam as a function of Mylar degrader traversed.

previously possible. These beams have thus opened up the field of muonium chemistry by allowing convenient gas-phase studies at atmospheric pressure. They also show promise for solid state applications, providing potentially superior luminosities and offering incomparable stop rates per total mass of target. Several new facilities are being developed to exploit these possibilities, and these will give μ^+SR experimenters a chance to efficiently study targets a few millimeters in size for the first time.

3.2 *Muonium Chemistry*

3.2.1 THE MUONIUM SPIN ROTATION METHOD While the first studies of muonium chemistry were primarily dependent upon the indirect, residual polarization method described in the introduction (and discussed again below), the recent progress in this branch of μ^+SR research has developed around the more direct and less ambiguous technique of precessing the triplet state of muonium in a weak magnetic field and observing the amplitude and relaxation of that MSR signal. We begin by discussing some applications of this technique.

3.2.1.1 *Muonium formation in gases* It is believed that muonium atoms are formed as positive muons come to rest in almost all materials (11). There is adequate justification for this expectation in that Mu has a higher ionization potential than most other atoms or molecules, and can thus capture an electron even after it comes to rest. However, there are exceptions to this rule. In metals, the μ^+ is screened by conduction electrons collectively. In the lighter noble gases, the ionization potential is too high for the muon to capture an electron once it thermalizes, so any muonium must be formed as it slows down. What is the probability that this will occur? In what energy region is it most likely? These questions are not only central to the related topic of muonium hot atom chemistry, but also very relevant to the atomic physics of charge-changing collisions. Only recently has there been any experimental evidence brought to bear on this problem.

In order to study muonium formation, one has to be able to "see" muonium; that is, there must be an observable that relates directly to the fraction of Mu formed. The triplet-Mu precession signal described above is an obvious candidate. However, in solids and liquids, where most early MSR studies were made (because of stopping densities), Mu precession is generally difficult to observe. Most solids have depolarizing fields or conduction electrons that disrupt Mu precession, and all but the purest liquids have enough dissolved impurities to scavenge or depolarize muonium before it can be observed directly (11, 52). Gases, on the other

positronium formation is less important for Mu formation than the details of the charge-changing collision cross sections in the many-eV region. How can more be learned about those cross sections?

One approach has been to investigate the effect of impurity gases on Mu formation in helium and neon. To avoid "chemical" effects, this was done first with xenon, the only inert gas in Table 2 for which Mu formation is exothermic. The results of a recent study at TRIUMF are shown in Figure 21, in which the muon and muonium asymmetries are plotted as a function of Xe concentration (55). As can be seen from Figure 21, 100 ppm of Xe were sufficient to cause significant Mu formation in Ne. It was at first difficult to explain how so little xenon could affect the Mu formation probability. At 100-ppm Xe in Ne at 1 atm, assuming a cross section of $\sim 10^{-15}$ cm^2, thermal collisions between free muons and Xe atoms should occur only about every 0.5 μsec at room temperature. If Mu is formed in a thermal collision with Xe (as was first proposed), then the μ^+ precession signal should be observed to decay on this time scale as free muons are "lost" to the fast-precessing Mu state over a period of time. Figure 22 shows the relaxation rate of the muon signal as a function of Xe concentration, and in fact shows some evidence for such a thermal reaction

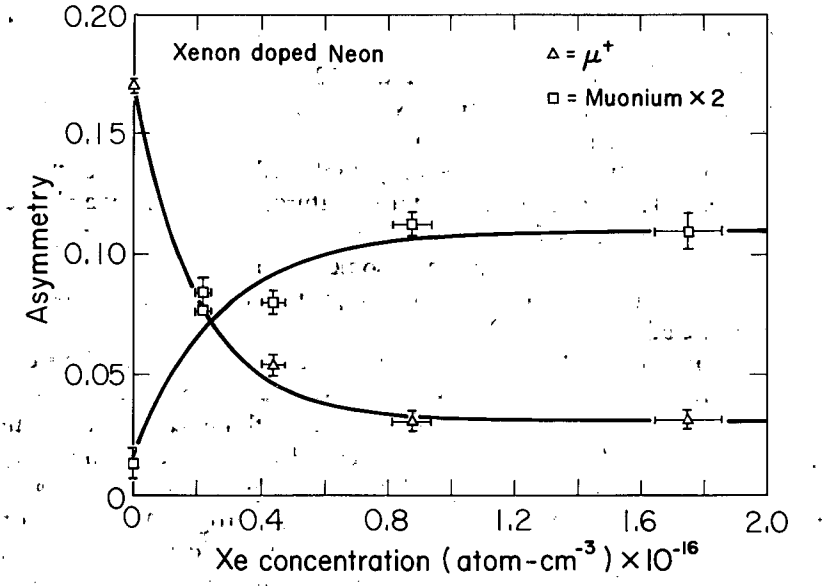

Figure 21. Muon and muonium $\times 2$ asymmetries in neon doped with xenon as a function of xenon concentration. The nonzero asymptotic muon asymmetry at high xenon concentration may be due to muons that have scattered into the walls of the aluminum gas target vessel.

(55). However, the rate is too slow to account for the muonium formation: Because of the dephasing of Mu atoms starting to precess at different times, no observable muonium signal could result from such a process.

Contrary to these expectations, both μ^+ and Mu precession signals were observed simultaneously in Ne with minute Xe impurities, as can be seen from Figure 21. This indicates that the process

$$\mu^+ + \mathrm{Xe} \rightarrow \mathrm{Mu} + \mathrm{Xe}^+ \qquad 15.$$

responsible for Mu formation in this mixture must be an epithermal charge-changing collision, and that the rate for any thermal analog of reaction (15) must be comparatively slow. This is not surprising until one considers the "collision budget" for a μ^+ slowing down in Ne. In a simple "hard sphere" elastic scattering model, it should take the muon only about 700 elastic collisions with Ne atoms to slow down through the energy region where Reaction 15 is apt to be important. With a 100-ppm Xe impurity, the number of collisions with Xe atoms over the same range

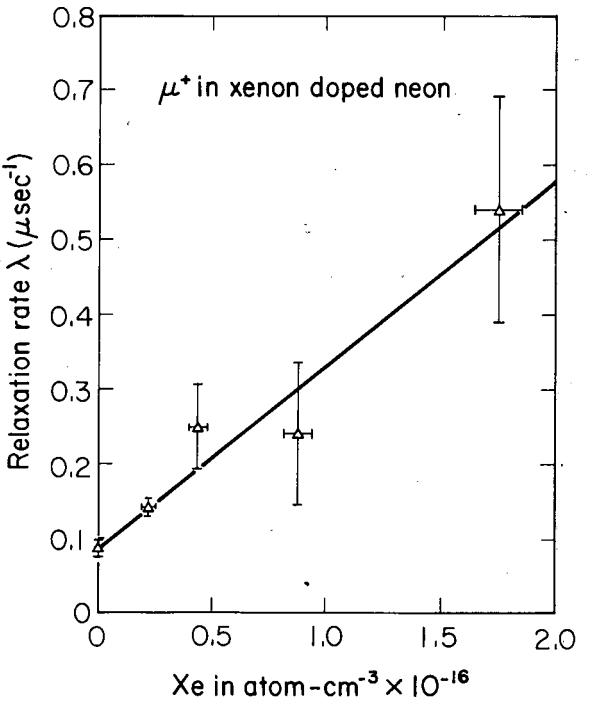

Figure 22 The rate of free muon relaxation in xenon doped neon as a function of xenon concentration at 295°K. This corresponds to the thermal production of muonium with a bimolecular rate constant $k = (2.4 \pm 0.3) \times 10^{-11}$ cm^3 atom^{-1} sec^{-1}.

should be only 0.08 times the ratio of cross sections for Mu on Xe and Ne. The muon indeed captures an electron from Xe a large fraction of the time in this situation. Thus we must conclude that the cross section for Reaction 15 is at least 10 times that for elastic hard-sphere scattering of muons with Ne, even assuming a constant cross section over the entire energy range of interest. This is plausible, since the electron is most likely to be captured from the attractive tails of the Lennard-Jones potential, which extend far beyond the repulsive core responsible for the hard-sphere scattering.

Further support for the conclusion that Mu is formed in epithermal collisions with Xe comes from the data for He with Xe impurities. While 100-ppm Xe causes significant Mu formation in Ne, it has no measurable effect in He. This would be unlikely for a thermal process; but since the μ^+ is moderated about 5 times faster by scattering from He than from Ne atoms, such a result is expected for an epithermal formation process.

Since charge-changing cross sections are generally assumed to be functions only of the velocity of the impinging light species (56), a μ^+ or

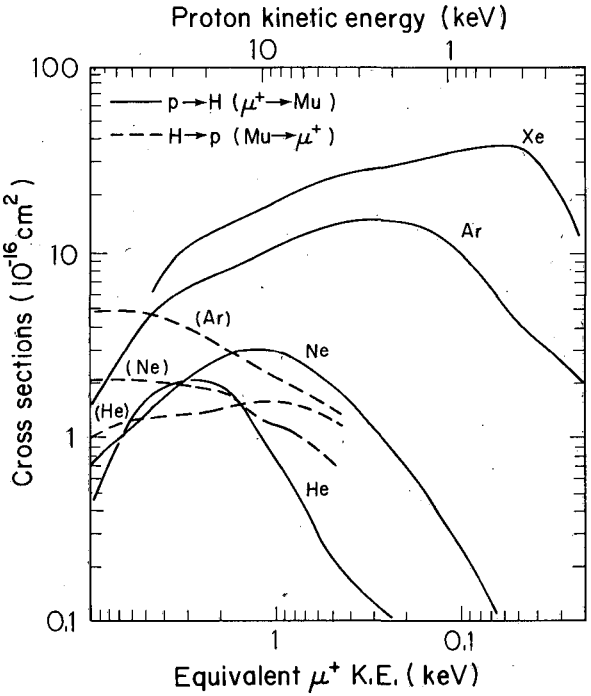

Figure 23 Charge-exchange total cross sections for H (and Mu) in various gases. Energy decreases from left to right; proton kinetic energy is plotted at the top, with the equivalent muon energy at the bottom. Solid lines are electron-capture cross sections, and dashed lines are electron-loss cross sections. From Reference 56.

Mu atom with kinetic energy T_μ may be expected to experience the same such interactions as a proton or H atom with $T_H = (M/m)\ T_\mu$, where $(M/m) = 8.85$, the ratio of proton to muon masses, assuming that positive muons behave exactly like light protons in the realm of atomic physics. Thus the extensive literature on H atom collision processes can be consulted for predictions of the detailed behavior of positive muons stopping in gases. In Figure 23, for instance, the charge-changing cross sections of interest here are plotted vs proton (upper ordinate) and/or muon (lower ordinate) kinetic energy. (The data are taken from H atom measurements reviewed in Reference 56.)

The curves in Figure 23 suggest that there are probably very few neutral atoms left in a μ^+ beam slowing down in He once the energy drops below about 200 eV; in Ne the same appears likely to be the case for $T_\mu < 50$ eV. This prediction corresponds nicely to the observed behavior. The Mu formation data in Ar and N_2 further suggest that the neutral fraction continues to rise with decreasing T_μ in N_2 but declines again below about 200 eV in Ar.

The conclusion that the electron capture cross section for μ^+ on Xe must be large compared to that on Ne or He in the many-eV energy range also agrees with the measured H atom cross sections shown in Figure 23.

The apparent slowness of the thermal Reaction 15, even though it would be exothermic by 1.4 eV, is surprising. One possible explanation is that μ^+Ne molecular ions are formed as the μ^+ comes to rest (54). Such diamagnetic ions would give a "free" μ^+ signal, as observed, but would be slow to form Mu in collisions with Xe atoms. From the measured and calculated properties of the H^+Ne molecular ion (57, 58), the binding energy of μ^+Ne can be estimated to be about 1.8 eV; the first excited state should also be bound by about 1 eV. This is just enough to reverse the energy budget for Mu formation, so that the reaction

$$\mu^+\text{Ne} + \text{Xe} \rightarrow \text{Ne} + \text{Mu} + \text{Xe}^+ \qquad 16.$$

from the ground state is endothermic by 0.4 eV, but the same reaction from the excited state will be exothermic by about the same amount. If this is indeed the explanation for the comparative stability of the "free" μ^+ signal in the presence of Xe, then some very interesting studies of the μ^+Ne ion, its ionization potential, reactivity, excited states, etc, may prove feasible.

As a tool for probing the details of atomic physics, the muon offers little competition for existing atomic beam techniques, as a glance at the literature shows (59). However, the μ^+SR technique is particularly sensitive to one parameter of general practical interest: When high energy hydrogen isotopes thermalize in various gases, what fraction comes to

equilibrium as neutral atoms? By answering this question, the μ^+SR technique may prove useful to atomic physicists.

3.2.2 MUONIUM CHEMISTRY IN GASES A very favorable consequence of the propensity of positive muons to form Mu atoms in most inert gases is the convenience with which thermal chemical reactions of Mu can be quantitatively studied. This fact was recognized early in the history of μ^+SR studies (15), but only recently did gas-phase muonium chemistry begin in earnest. New techniques developed in the last three years make such studies straightforward. The resultant data on reaction rates of Mu are of interest in the theory of isotope effects in elementary chemical reactions by virtue of the direct analogy with H atom reactions (60). This is primarily because of the unambiguous interpretation of the experimental observables and the tractability of theoretical calculations in the gas phase. Earlier results in liquids demonstrated the potential of μ^+SR techniques for measuring rate constants of Mu, but relied upon the indirect, residual polarization technique and produced rate constants in the liquid phase, for which no absolute calculations have been attempted.

These first experiments, then, demonstrated the applicability of MSR methods to physical chemistry, not as a qualitative or esoteric test, but as a precise and widely useful tool for studying isotope effects in absolute reaction rate theory.

3.2.2.1 *Experimental techniques* The apparatus for the study of muonium chemistry in gases is the same as for Mu formation studies (see Figure 20): 4.1-MeV surface muons are stopped in argon or nitrogen gas at approximately 1 atm, where they form muonium almost without exception. The Mu atoms precess in a weak applied magnetic field (typically a few gauss) at an amplitude half the maximum for free muon precession. In the absence of field inhomogeneity (less than about 0.1 gauss) or impurities (less than about 5 ppm) this precession is long lived. However, as measured contaminants are added, the Mu precession signal decays exponentially as Mu atoms react to place the muon in diamagnetic molecules (or are depolarized by spin exchange as in the case of Mu + O_2). This relaxation rate λ can be fitted from the experimental time spectrum, and the dependence of the relaxation rate on the impurity concentration [X] can be fitted to a linear dependence whose constant of proportionality is the rate constant k for the reaction: $\lambda = k[X]$.

3.2.2.2 *Measured reaction rates of muonium in gases* A typical MSR spectrum is shown in Figure 24*a* for Mu precession in pure Ar, with the constant background and exponential muon decay removed. Figure 24*b* shows the MSR signal in Ar to which 19×10^{-4} moles liter^{-1} Cl_2 was

added; the resultant relaxation of the Mu signal is evident (52). Figure 25 shows the dependence of the relaxation rate so observed upon the HBr concentration in Ar (61). The rate constant extracted from this fit is listed in Table 3 along with several others measured in the same manner (61). The corresponding rate constants for H atoms are listed for comparison.

The recent results of Garner et al (62) on the temperature dependence of $k(\mathrm{Mu} + \mathrm{Cl_2})$ and $k(\mathrm{Mu} + \mathrm{F_2})$ are shown in Figure 26. These data can be tentatively fitted to the form $k = A \exp(E_a/kT)$, with activation energies E_a shown in Table 3. At room temperature, both $k(\mathrm{Mu})/k(\mathrm{H})$ and the apparent Arrhenius activation energy E_a for the F_2 reaction are in agreement with the recent theoretical calculation of Connor et al (60). The

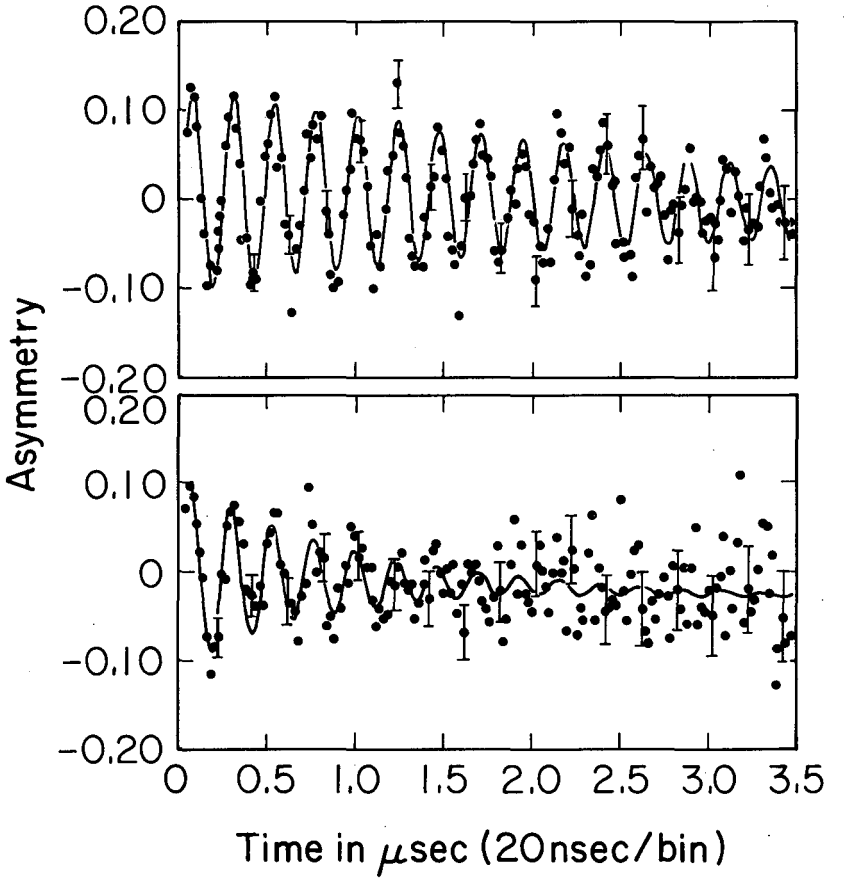

Figure 24 MSR signals in argon at 3.0 gauss, 1 atm, room temperature: (*top*) pure Ar; (*bottom*) Ar + 19 × 10^{-4} *M* Cl_2.

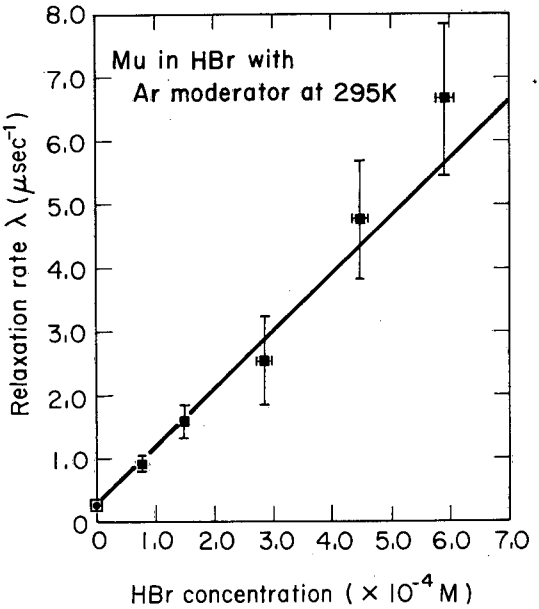

Figure 25 Muonium relaxation due to chemical reaction with HBr in Ar at room temperature corresponding to a bimolecular rate constant of $(9.1 \pm 1.0) \times 10^9$ (mole-sec)$^{-1}$.

lower activation energy for Mu + F_2 compared with H + F_2 is striking evidence for quantum tunneling in the chemical reaction of H isotopes.

3.2.2.3 *Comparison with H atom reaction rates* The similarity between Mu and H atomic physics in the energy region below a few keV (see previous section) supports the expectation that Mu can be properly and precisely treated as a light isotope of hydrogen. In this light, a comparison between Mu and H reaction rates in analogous processes is possible, because in the gas phase it is feasible to calculate absolute reaction rates almost *ab initio*, predicting dynamic isotope effects such as quantum mechanical tunneling, which can be tested by experiment (60). Previously, these tests relied upon the naturally occurring isotopic differences (H, D, and sometimes T) for experimental data. The Mu atom offers a mass difference nine times larger, without loss of generality.

In a naive hard-sphere kinetic theory, one can treat the cross section σ for reaction of Mu (or H) with reagent X as a constant independent of thermal velocity v, which allows the conceptual separation of kinetics from dynamics in writing $k = \sigma\langle v\rangle$ for the rate constant, where $\langle v\rangle$ is the mean thermal velocity of the light atom (Mu or H). (For Mu, $\langle v\rangle = 0.75 \times 10^6$ cm sec^{-1} at room temperature.) While such a model wrongly ignores the

fact that reaction cross sections are generally very strong functions of energy, it serves to emphasize the qualitative expectation that Mu reaction rates will be faster by about a factor of three faster than those of H, just because the mean thermal velocity, which varies as $m^{-\frac{1}{2}}$, is faster by a factor of three. This approximation is not as arbitrary as it sounds, since the energy distribution of Mu and H are the same at the same temperature. The muonium atom just gets there faster. Thus it is even rigorously true that the ratio between Mu and H rate constants will be 3 unless there is a genuine dynamic isotope effect—that is, unless the detailed cross sections are different for Mu and H. In general, a proper theoretical treatment requires rather difficult trajectory calculations, in effect the calculation of the orientation-averaged energy dependence of the reaction cross section for Mu and H with X; but in perusing Table 3 one should first look for $k(\mathrm{Mu})/k(\mathrm{H})$ ratios significantly different from 3.

The first muonium chemistry measurements in the gas phase included a measurement of the rate of Mu depolarization in the presence of minute

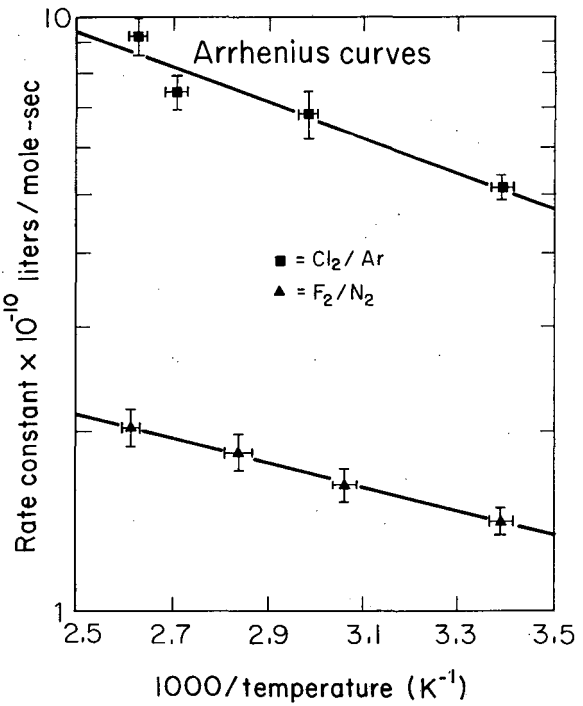

Figure 26 Rate constants for muonium reacting with halogens as a function of inverse temperature, showing Arrhenius Law dependence. (*Solid squares*) $\mathrm{Mu} + \mathrm{Cl_2} \rightarrow \mathrm{MuCl} + \mathrm{Cl}$. (*Solid triangles*) $\mathrm{Mu} + \mathrm{F_2} \rightarrow \mathrm{MuF} + \mathrm{F}$.

Table 3 Reaction rate parameters for Mu and H in the gas phase

Reaction	Muonium		Hydrogen		k_{Mu}/k_H (295°K)	H atom ref.
	k (295°K)[a]	E_a (kcal mole^{-1})	k (295°K)[a]	E_a (kcal mole^{-1})		
F_2	1.4±0.1	0.92±0.23	0.20±0.05	2.4 ±0.2	5.2–10	124, 125
			0.09±0.01	2.2 ±0.1	13–19	126
Cl_2	5.1±0.2	1.36±0.21	1.7 ±0.6	1.8 ±0.3	2.1–4.8	124
			0.41±0.04	1.4 ±0.2	11–14	127
			1.15±0.15	1.15±0.1	3.8–5.3	128
Br_2	24 ±3	—	2.2 ±1.5	1.0 ±0.5	5.7–38	129
HCl	≦0.000034[b] ±0.000005	[f]	2(0.0021[c] ±0.0002)	3.1 ±0.3	½(0.013–0.020)[c]	130, 131
		[g]	0.000018[d] ±0.000018	≧4.0	~1.9	132
HBr	0.9 ±0.10	[f]	0.21±0.02	2.6 ±0.1	3.5–5.3	133
		[g]	≦0.0023	5–6	350–440	133
HI	2.53±0.13	[f]	0.86±0.39	1.2 ±0.4	1.9–5.7	134
O_2	16.0±0.7[e]					

[a] K ($\times 10^{10}$ l/mole-sec).
[b] Upper limit only.
[c] There exists a stoichiometric ambiguity of a factor of 2 (see Reference 53).
[d] Upper limit (i.e. $< 3.6 \times 10^5$ l/mole-sec).
[e] Probably spin exchange, not chemical reaction.
[f] H atom reaction type is abstraction.
[g] H atom reaction type is exchange.

O_2 impurities in Ar (15). In that study it was not clear whether a significant role was played by the actual chemical combination of Mu and O_2, or if the spin-exchange interaction was completely dominant (11). It is now believed that the chemical reaction is relatively slow, so that the rate constant in Table 3 can be compared directly with the spin-exchange rate for H. Following References 15 and 11, the rate constant can be reduced to a spin-exchange cross section σ_{SE} by the following formula: $k = (\frac{32}{54})\sigma_{SE}\langle v\rangle$, which gives $\sigma_{SE} = (5.72 \pm 0.3) \times 10^{-16}$ cm^2 for Mu + O_2, as opposed to $(21 \pm 2.1) \times 10^{-16}$ cm^2 for H + O_2 (15). The smaller cross section for Mu is surprising; since only a spin-exchange interaction is expected, there should be little "dynamics" involved, and the hard-sphere approximation should hold reasonably well.

3.2.2.4 *Muonium in vacuum and Mu chemistry in powders* In the last several years, many experimenters have demonstrated that positronium

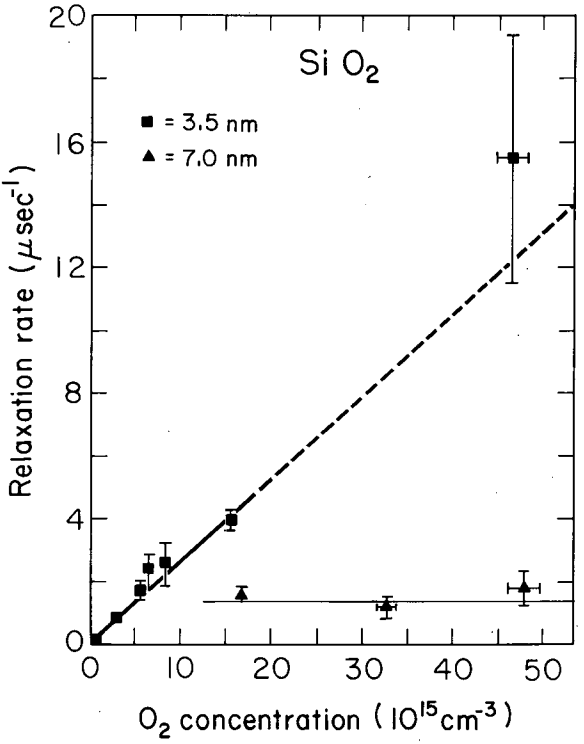

Figure 27 Rate of relaxation of MSR signal in SiO_2 powders as a function of the concentration of O_2 added to previously evacuated sample container. Square points: SiO_2 powder grain, nominal radius $r = 3.5$ nm; triangular points: nominal grain radius $r = 7.0$ nm.

atoms ($Ps = e^+e^-$) formed in very small grains of powdered SiO_2, MgO, and Al_2O_3 will very quickly diffuse out of the grains into vacuum, where they remain, affected only by gas molecules and collisions with the powder grains (63, 64). A recent study at TRIUMF has shown that the same thing happens to muonium atoms (65).

This was verified by stopping a beam of surface muons in a fine silica powder, where a long-lived Mu precession signal could be seen at low field, but only if the powder sample had been pumped to a hard vacuum. The addition of as little as 10 Torr of O_2 gas pressure resulted in the destruction of the Mu signal, as shown in Figure 27. In fact, the disappearance rate of the Mu signal had exactly the same dependence upon O_2 partial pressure in the quartz powder as it did in Ar moderator gas. It was concluded that the powder grains played essentially the same role as the molecules or atoms of the inert moderator gas—that the powder was more or less a special moderator gas with very large molecules (65).

The Mu atoms diffuse rapidly to the surface of the SiO_2 grains. In order to add some quantitative precision to this observation, a coarse-grained powder (140Å diameter) was run with high O_2 pressure (12 Torr). Whereas the 70-Å grains gave up their Mu to the depolarizing effects of the O_2 within a few nanoseconds, the coarse grains held on to it long enough for a Mu precession signal to be observed experimentally, as indicated in Figure 27. A calculation of the probability that a Mu atom formed at a random volume element inside a spherical grain will still be within that grain at time t gives the following formula which should match the precession envelope:

$$2P(t) = \mathrm{erf}(\beta t)^{\frac{1}{2}} - \frac{3(\beta t)^{\frac{1}{2}}}{\pi^{\frac{1}{2}}}\left\{1 - \frac{\exp(-1/\beta t)}{3} + \frac{2\beta t}{3}[\exp(-1/\beta t)]\right\} \qquad 17.$$

where $\beta = D/R^2$, D is the diffusion constant, and R is the grain radius.

From this the diffusion constant can be obtained by fitting the experimental data. A preliminary measurement gives $D = (2.9 \pm 0.7) \times 10^{-7}$ cm^2 sec; further experiments with more uniform grain size should allow this number to be determined with better accuracy.

3.2.3 MUONIUM CHEMISTRY IN LIQUIDS The gas-phase work described above has shown the advantage of measuring reaction rates via the relaxation of the muonium precession signal itself. However, the liquid phase presents some obstacles absent in gases.

3.2.3.1 *The direct MSR technique* The prime impediment to direct observation of Mu in liquids is the presence of dissolved O_2. At STP, the partial pressure of O_2 over a liquid is about 0.2 atm; in water, this

leads to a dissolved oxygen concentration of about 2.5×10^{-4} M at 25°C. Assuming the same bimolecular rate constant for Mu + O_2 spin exchange as measured in gases [1.5×10^{11} liter/(mole sec)$^{-1}$] we thus expect Mu to relax within about 20 nsec in water exposed to air—too fast to observe any MSR signal directly. However, techniques for removal of this dissolved O_2 are known, and it is possible to obtain pure enough water samples to permit the study of long-lived MSR signals.

Percival et al (66) were the first to observe Mu precession in a liquid, ultrapure water in a sealed glass bulb. They found a long-lived (more than a muon lifetime) MSR signal, which was positively identified as muonium by a measurement of the splitting of the precession into two frequencies at high field (recall Equation 12). The extracted hyperfine frequency was the same as that of Mu in vacuum. Muonium precession in water has since been observed at TRIUMF as well.

Even with the purification challenge met, there is a serious obstacle to direct MSR studies in most liquids, in the form of the "hot fraction"—those muons (usually a substantial percentage) that react epithermally at essentially $t = 0$. In water, about 60% of the muons are thus prevented from ever contributing to the MSR signal. Since the amplitude of a fully polarized Mu signal is only half that of an equivalent μ^+ signal anyway, this leaves only 30% of A_0 for a muonium amplitude, requiring at least 10 times as many events as a gas-phase measurement for an MSR signal of the same statistical significance.

Worse luck, Percival et al (66) found a muonium signal in water that was reduced by yet another factor of two. Taking CCl_4 and Al as asymmetry standards and correcting for the factor of two lost in the original differentiation of Mu into singlet and triplet states, they extracted the fractional populations of (magnetically) free μ^+ and free Mu in several liquids, listed in Table 4, and in water as a function of temperature, shown

Table 4 Muon polarizations in pure substances

Sample	P_D[a]	P_M[a]
H_2O, liquid	0.622 ± 0.006	0.196 ± 0.003
H_2O, ice ($T > 160$°K)	0.480 ± 0.004	0.52 ± 0.02
D_2O, liquid	0.57 ± 0.03	0.18 ± 0.01
D_2O, ice ($T > 160$°K)	0.393 ± 0.005	0.63 ± 0.01
CH_3OH	0.61 ± 0.01	0.19 ± 0.02
CD_3OD	0.51 ± 0.02	0.31 ± 0.05
C_2H_5OH	0.59 ± 0.03	0.20 ± 0.04
Al, granular	0.990 ± 0.007	—

[a] Relative to $P_D = 1.0$ for CCl_4.

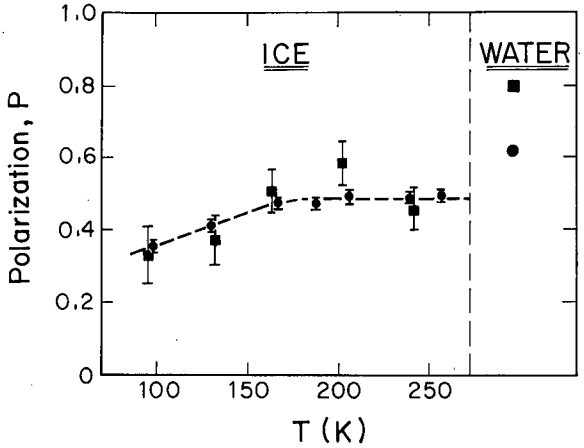

Figure 28 Fraction P_D of μ^+ in diamagnetic environments (*circles*) and fraction $(1-P_{Mu})$ not accounted for in Mu signals (*squares*) as a function of temperature for μ^+ in H_2O. Unless $P_D = (1-P_{Mu})$, part of the original μ^+ ensemble is unaccounted for (67).

in Figure 28. In each case a substantial fraction (18% for H_2O at room temperature) of the polarization is unaccounted for (except in ice, where all the polarization is accounted for). These unexpected "missing muons" may be in the form of epithermally formed radicals, which relax too rapidly to observe directly. In any case their discovery has important consequences for the interpretation of earlier residual polarization studies.

Table 5A Comparison of $k_{(Mu)}$ with $k_{(H)}$, $k_{(e_{aq}^-)}$, and $k_{(Ps)}$ (in $m^{-1}\ sec^{-1}$)

Solute	$k_{(Mu)}$[a]	$k_{(H)}$[b]	k_{Mu}/k_H	$k_{(e_{aq}^-)}$[c]	$k_{(Ps)}$[d]
Phenol	7×10^9	2×10^9	3.5	1.8×10^7	$<10^8$
p-Nitrophenol	8×10^9	$(3\pm1) \times 10^{9e}$	2.7	3.5×10^{10}	9×10^{9h}
Tl^+	8×10^8	$[1.2 \times 10^8]^f$	~7	3×10^{10}	$<10^8$
CNS^-	6×10^7	$[2 \times 10^8]^f$	~0.3	$<10^6$	$<10^8$
Zn^{2+}	$<10^7$	$<10^5$	—	1.5×10^9	$<10^7$
$Na^+/SO_4^=$	$<10^7$	very small[g]	—	$<10^6$	$<10^7$

[a] Jean, Y. C., Brewer, J., Fleming, D. G., Garner, D. M., Mikula, R. J., Vaz, L. C., Walker, D. C. Private communication (1978).

[b] Data from NSRDS-NBS 51 by Anbar, M., Farhatziz, and Ross, A. B. (Pulse data used when available).

[c] Data from NSRDS-NBS 43 by Anbar, M., Bambenek, M., Ross, A. B.

[d] Data estimated from *At. Energy Rev.* 6:(1968) by Goldanskii, V. I.

[e] Estimated from: K(H + nitrobenzene) = 3×10^9 and k(H + phenol) = 2×10^9.

[f] Obtained from only one source, and that (unpublished) is based on the rate relative to 2-propanol, which has been shown to be a poor basis for comparison in the case of some other solutes.

[g] Not recorded but most probably $<10^7$.

[h] Data from Jean, Y. C., Ache, H., *J. Phys. Chem.* 81:2093 (1977).

Table 5B Muonium and hydrogen atom rate constants in aqueous solutions[a]

Substrate	k_{Mu} (m^{-1} sec^{-1})	k_H[b] (m^{-1} sec^{-1})	k_{Mu}/k_H
Methanol	$<3 \times 10^4$	2.5×10^6	0.01
Ethanol	$<3 \times 10^5$	2.1×10^7	<0.015
2-Propanol[c]	$\approx 3 \times 10^6$	6.8×10^7	~0.04
2-Butanol[c]	$\approx 2 \times 10^6$	1.3×10^8	~0.02
Formate ion (pH >7)	7.8×10^6	1.2×10^8	0.07
Maleic acid (pH 1)	1.1×10^{10}	8×10^9	1.4
Fumaric acid (pH 1)	1.4×10^{10}	7×10^9	2
MnO_4^-	2.5×10^{10}	2.4×10^{10}	1
Ag^+	1.6×10^{10}	$(1–3) \times 10^{10}$	~1
NO_3^-	1.5×10^9	9×10^6	~170
	$[1.2 \times 10^{11}]$[d]		
	$[1.7 \times 10^{10}]$[e]		
Acetone	8.7×10^7	2.8×10^6	30
Ascorbic acid (pH 1)	1.8×10^9	1.7×10^8	10
OH^-	1.7×10^7	1.8×10^7	1
	$[1.8 \times 10^9]$[e]		
ClO_4^-	$<10^7$	—	—
	$[3.8 \times 10^{10}]$[d]		
	$[1.2 \times 10^9]$[e]		
H^+, Na^+, Cl^-	$<2 \times 10^5$	$<10^5$	—

[a] Ref. 56; Percival, P., Private communication; and Percival, P. W., Roduner, E., Fischer, H., Camani, M., Gygax, F. N., Schenck, A. 1977. *Chem. Phys. Lett.* 47:11.
[b] Anbar, M., Farhataziz, Ross, A. B. 1975. NSRDS-NBS 50.
[c] Muonium values are preliminary.
[d] Rate constants were obtained from Reference 18 and P_{res}, which may involve radical reactions etc.
[e] Minaichev, E. V., Myasischeva, G. G., Obukhov, Yu. V., Rogonov, V. S., Savel'ev, G. I., Smilga, V. P., Firsov, V. G. 1974. *Sov. Phys. JETP* 66:1926.

These effects reduce the maximum available MSR signal in water to one fifth that in N_2 gas. Although this has no effect on the principles of measurement of reaction rates as used in the gas phase, the practical effect is serious: One must measure 25 times as many events to obtain the same statistical precision. Without the high muon fluxes available at new facilities such as SIN and TRIUMF, this disadvantage would be insurmountable. However, Percival et al succeeded in measuring several rate constants in this way, clarifying the reaction mechanisms at work in aqueous results. Table 5B lists some of their recent results. Figure 29 shows the dependence of the rate of disappearance of the MSR signal upon the concentration of fumaric acid in water (from Reference 66). The rate constant k_{Mu} corresponding to the straight line fit to λ as a function of reagent concentration is listed in Table 5A along with rate constants for

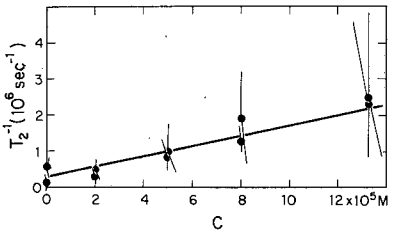

Figure 29 Muonium relaxation rate as a function of fumaric acid concentration in water (67).

analogous reactions of H, e_{aq}^-, and Ps. These results indicate that Mu is indeed best characterized as a light isotope of the H atom, even in aqueous solutions. In this context, a comparison of Mu and H rate constants in aqueous solution, shown in Table 5B, illuminates several qualitative features of the reaction mechanisms in water: H reacts with the first five substrates by abstracting another H atom from a C–H bond; apparently Mu is much less efficient for such abstraction reactions; for the next four substrates, both H and Mu apparently react at the expected diffusion-controlled rate limit; reactions with nitrate, acetone, and ascorbic acid are more efficient for Mu than for H; and the similarity of the Mu and H rates with OH^- suggest that the reaction is an interconversion of Mu (H) into its conjugate base, e_{aq}^-:

$$Mu + OH^- \rightarrow e_{aq}^- + MuOH.$$

3.2.3.2 *The residual polarization method* It is preferable to measure reaction rates of Mu by the direct MSR method described above, when feasible; for one thing, only by this method can slow ($< 10^8\,sec^{-1}$) reaction rates be studied. However, even under optimal conditions the MSR method is tedious in liquids, and in many situations of interest no Mu signal may be seen. Therefore this technique will be most useful in cooperation, rather than competition, with the residual polarization μ^+SR method developed earlier. Indeed, there are phenomena, such as hot atom reactions of Mu*, that can only be studied by this method.

Although longitudinal-field measurements (11) can provide valuable information to supplement that obtained in the transverse-field technique described here (and a thorough experimental approach should utilize both methods), we restrict our discussion to the latter because it contains the most information. In this arrangement the positron counters and the muon spin are in a plane perpendicular to the applied field, and the amplitude of the sinusoidal precession signal is proportional to the magnitude of the residual muon polarization. The initial phase of the precession depends

upon the geometry and the initial polarization direction of the beam, of course, but this part of the phase is usually removed by subtraction of the value measured when there is no depolarization. It is the deviation $\Delta\phi$ from this reference phase that provides information about the depolarization mechanism. Similarly the amplitude of the μ^+SR signal is the product of P_{res} and a maximum amplitude A_0 corresponding to no depolarization. However, an unambiguous establishment of A_0 is a more delicate matter.

There are problems associated with thick-target measurements. Some materials such as Cu metal are not thought to have any depolarizing effect on the muons at early times, and can therefore be used to establish an asymmetry standard. In liquid-phase studies, CCl_4 is often used for the same purpose, although with less confidence that P_{res} is exactly 1.0. In any case, great care must be taken in such normalizations because of the effect of density upon the experimental asymmetry for a fixed polarization.

There are two sources of this density effect. The first and lesser part of the effect is the consequence of the correlation of the polarization with the momentum of muons in the beam. Whether conventional muons are derived from "backward" or "forward" decay-in-flight of pion beams, the angle of the decay in the c.m. frame is translated into a momentum increment in the lab frame. Thus (for instance), higher momentum "forward" muons have higher polarization. Since a denser target of fixed thickness will stop more high momentum muons, it will produce a slightly larger asymmetry, even though its depolarizing properties are identical.

There is an even larger density effect due to the absorption of decay positrons. The decay asymmetry is a function of the positron energy, because of the dynamics of the weak interaction (11). To contribute to the μ^+SR signal, the positrons must escape from the target and penetrate several counters. Thus many low energy positrons are lost by absorption, raising the average experimental asymmetry. This is advantageous in the sense that the higher energy positrons have the larger asymmetries, but if the target density increases, then still more positrons are lost, which influences the experimental asymmetry.

These effects can be calculated and a correction applied to the residual polarization results; more commonly an empirical survey is made of the dependence of the asymmetry upon target thickness (40). Such corrections are less important with smaller targets. However, much older data (see for instance the asymmetry table in Reference 11) are subject to systematic fluctuations of up to 25% as a result of density effects and variations in beam polarization. Thus it would be advantageous to use a technique that makes density an unimportant parameter in residual polarization measurements. This is now available.

As a result of the low energy (4.1 MeV) and concomitant short range

(less than 1 mm of water) of "surface muons," liquid targets can be built that are of negligible thickness in the direction of positron detection and yet they will stop the entire surface muon beam in the solution of interest. The apparatus used at TRIUMF is shown in Figure 30. Preliminary studies with this technique indicate its reliability for residual polarization studies. A few such measurements are shown in Table 6.

Residual μ^+ polarizations measured in various liquids by several techniques are summarized in Table 7. Care must be taken in the interpretation of these values of P_{res}, since it is generally possible for both thermal and hot atom reactions of Mu to help prevent the complete destruction of the μSR signal (17). In addition, there is some indication

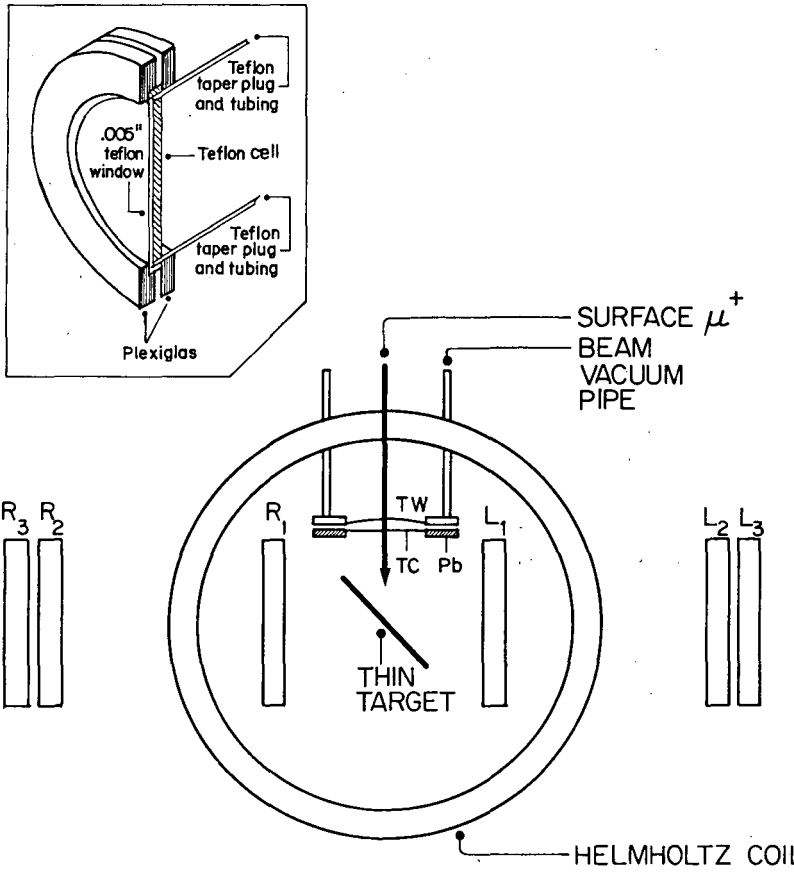

Figure 30 Sketch of the thin teflon cell used with "surface" muons and its arrangement with respect to the counters. TC is the thin counter that defined the μ^+ beam; L1, L2, L3 are the left-hand-side counters; and R1, R2, and R3 the right-hand-side counters.

Table 6 Comparison of data obtained on P_{res} from TRIUMF using surface muons with density-corrected data from LBL, JINR,[a] and SIN, using conventional muons[b]

Target liquid	TRIUMF	LBL	JINR	SIN
CCl_4	1	1	1	1
$CHCl_3$	0.86 ± 0.04	0.85 ± 0.04	0.80 ± 0.06	—
H_2O	0.61 ± 0.02	0.59 ± 0.02[c]	0.62 ± 0.04	0.62 ± 0.01
D_2O	0.57 ± 0.04	0.59 ± 0.02	—	0.58 ± 0.03
CH_3OH	0.56 ± 0.04	0.54 ± 0.02[c]	0.58 ± 0.05	0.61 ± 0.01
$(CH_3)_2CHOH$	0.61 ± 0.04	0.64 ± 0.01	—	—
C-C_6H_{12}	0.68 ± 0.04	0.67 ± 0.02	0.68 ± 0.05	—
C-C_6H_{10}	0.47 ± 0.03	—	0.48 ± 0.05	—
C_6H_6	0.12 ± 0.02	0.13 ± 0.01[c]	0.15 ± 0.03	—
CS_2	0.16 ± 0.03	0.11 ± 0.01	—	—
$(CH_3)_2CO$	0.54 ± 0.05	—	—	—
$Si(CH_3)_4$	0.54 ± 0.03	—	—	—
C_5H_{12}	0.64 ± 0.04	—	—	—
C_7H_{16}	0.65 ± 0.04	—	—	—
$C_{10}H_{22}$	0.67 ± 0.05	—	—	—
2,2,4 Trimethyl-pentane	0.61 ± 0.05	—	—	—

[a] JINR is the Joint Institute for Nuclear Research, Dubna, USSR; LBL is the Lawrence Berkeley Laboratory.

[b] The errors quoted arise from the uncertainty due to the statistics of the experiment and do not take into account other possible sources of error.

[c] These data were obtained as limiting values in titration curves and therefore required no density corrections.

that "spur" reactions in the region ionized by the passage of the incoming μ^+ may play an important role (67). However, in most inert solvents the thermal reaction rate of Mu can be expected to be too small ($\lesssim 10^8$ sec^{-1}) to save the μ^+SR signal, and the residual polarization can be tentatively equated to the hot fraction h; that is, the fraction of Mu* atoms reacting epithermally to place the μ^+ in a diamagnetic molecule before Mu* thermalizes in $\sim 10^{-12}$ sec (11). In some cases, magnetic field independence of P_{res} provides direct experimental support for the assumption that $P_{res} = h$, since destruction of more than 50% of the μ^+SR signal is the result of Mu precession, the period of which decreases with field (11).

Treating the P_{res} values listed in Table 7 as pure hot atom fractions, we notice several trends. First, even the qualitative expectation that homologous compounds such as the group IV tetrachlorides will show a systematic trend in P_{res} as a function of mass or bond energy is not verified. Evidently the behavior of Mu* in these media cannot be characterized even parametrically in these terms. However, there is a consistent tendency for compounds with a higher degree of π bonding to have smaller values

Table 7 Collection of P_{res} data from the various sources referred to in the text

Target substance	P_{res}	Reference and comments
CCl_4	1.0	By definition, Bond Energy (BE) = 78 kcal/mole
$SiCl_4$	0.48	TRIUMF (conventional muons) BE = 91 kcal/mole
$SnCl_4$	0.99	TRIUMF (conventional muons) BE = 76 kcal/mole
$TiCl_4$	1.00	TRIUMF (conventional muons) BE = 102 kcal/mole
Cyclohexane	0.68	See table 6
Cyclohexene	0.55	JINR normalized with respect to $CHBr_3$
1,4 Cyclohexadiene	0.47	JINR normalized with respect to $CHBr_3$
1,3 Cyclohexadiene	0.38	JINR normalized with respect to $CHBr_3$
Benzene	0.18	JINR normalized with respect to $CHBr_3$
Hexane	0.62	LBL
Hexene	0.50	LBL
Hexyne	0.43	LBL
2-Propanol	0.62	Table 6
Acetone	0.54	Table 6
C_6H_6	0.18	JINR
C_6H_5Cl	0.27	JINR
C_6H_5Br	0.45	JINR
C_6H_5I	0.59	JINR
$C_6H_5CH_2Cl$	0.42	JINR
$C_6H_5CHCl_2$	0.55	JINR
$C_6H_5CCl_3$	0.68	JINR
$CHCl_3$	0.85	See table 6
CH_2Cl_2	0.70	LBL
C_6H_5OH	0.38	LBL
Glycerol	0.75	LBL

of P_{res} (42). This may be related to the higher efficiency of these compounds for slowing down the Mu* by excitation of low lying electronic levels, or it may support the view that spur reactions are important, since the thermal Mu atom may be more likely to combine with such molecules to form radicals rather than diamagnetic species.

The state of theoretical interpretation of these data can only be described as preliminary and confusing; perhaps new experimental tests will lead to further progress in the next few years. Certainly gas-phase experiments should help to determine if spurs (virtually absent in gases) really play an important role in the liquid-phase hot atom effects.

3.2.4 μ^+ SR FOURIER SPECTROSCOPY OF MUONIC RADICALS As early as 1972, residual polarization studies (18, 42) indicated the role of muonic radicals (paramagnetic molecules incorporating the μ^+) in the μ^+ depolarization mechanism (see Section 2.1.1). In the following five years,

efforts were made to observe these radicals directly via their expected muonium-like precession in low fields; the beat frequency Ω (see Equations 11 and 12) would, if observed, give a direct measurement of the isotropic average hyperfine coupling of the μ^+ to the unpaired electron, $h\omega_r$. These efforts were frustrated by the fact that the large unsaturated organic molecules most convenient for radical formation by addition of Mu (e.g. benzene) contain proton spins with which the unpaired electron is $\sim\frac{1}{3}$ as strongly coupled as with the μ^+, which results in a complicated spin Hamiltonian and a spread over many precession frequencies in low field—effectively a fast relaxation of the unpaired electron.

Attempts to avoid this complication by using unsaturated molecules with no nuclear moments (CS_2, CO_2, SO_2) were unsuccessful in the liquid phase, perhaps because of the effective magnetic fields produced by the more rapid rotations of these light molecules, again splitting the precession frequencies.

By a new approach the recent experiment at SIN (67a) has demonstrated the existence of muon radicals in the Paschen-Bach limit of high magnetic fields.

Recalling the general equation (9) for muonium precession, we can write the high field ($x \gg 1$) form:

$$P(t) = \tfrac{1}{2}(e^{i\omega_{12}t} + e^{i\omega_{34}t})$$

with

$$\left|\begin{matrix}\omega_{12}\\34\end{matrix}\right| = \omega_\mu \mp \frac{\omega_0}{2};$$

that is, precession at two frequencies split by ω_0 about the normal μ^+ Larmor frequency. For most radicals, ω_r can be expected to be a small fraction of ω_0 for free muonium, so that the critical field becomes much less than $B_0 = 1592$ G, e.g. $B_r \lesssim 100$ G, and the splitting is reduced from $\omega_0/2\pi = 4463$ MHz to $\omega_r/2\pi \sim 200$ MHz. More important, for fields $B \gg B_r$, the electron is essentially decoupled from the various nuclear spins, in the sense that there is no longer any appreciable mixing of hyperfine states; thus only the frequencies appear in the time dependence to first order, and the signals are long lived. This behavior is familiar in the ENDOR spectra of free radicals with single spin $\frac{1}{2}$ nuclei at high fields (67b), and is qualitatively similar to the high field precession of the "anomalous muonium" state in silicon (see Section 2.5.1).

Using this high field technique, Roduner et al (67a) were able to identify and measure couplings of several radicals listed in Table 7A. The frequency spectrum which they observe for muons in tetramethylethylene is shown

Table 7A Hyperfine coupling constants of muonium-substituted radicals and comparison with hydrogen analogues

Compound	Radical	A_μ[MHz][a]	$A_\mu \frac{\mu_p}{\mu_\mu}$ [MHz]	A_p[MHz][b]	Reference
2,3-Dimethyl-2-butene	$(CH_3)_2CMu\dot{C}(CH_3)_2$	160.9	50.5	30.18 (298)	135
2-Methyl-butadiene	$CH_2 = C(CH_3)\dot{C}HCH_2Mu$	180.7 or 199.5	56.8 or 62.7	37.8[c] (300)	136
	$CH_2Mu\dot{C}(CH_3)CH = CH_2$	199.5 or 180.7	62.7 or 56.8	42.91[d] (363)	137
1,3-Pentadiene	$CH_2 = CH\dot{C}HCHMuCH_3$	182.7 or 169.0	57.4 or 53.1	39.74 (140)	138
	$CH_2Mu\dot{C}HCH = CHCH_3$	169.0 or 182.7	53.1 or 57.4	[e]	
Benzene	Cyclohexadienyl	514.6[f]	161.6	133.71 (288)	139
Acetone	$(CH_3)_2\dot{C}OMu$	26.0	8.2	0.90 (300)	140

[a] Values at ambient temperature, ± 0.2 MHz if not specified otherwise.
[b] Temperature (°K) indicated in parentheses.
[c] Tentative. [d] exo-CH_3 group. [e] Not determined. [f] ± 0.6 MHz.

in Figure 30*a*. There is no reason to doubt that the technique will be applicable to a wide variety of radicals, and that impacts on the physics and chemistry of these species should be far reaching.

3.3 *The Muon as a Magnetic Probe*

3.3.1 FERROMAGNETIC MATERIALS The major advance in the technique for μSR in ferromagnetic samples is the observation of μSR in zero external fields. The internal field of an unmagnetized sample will point in a random

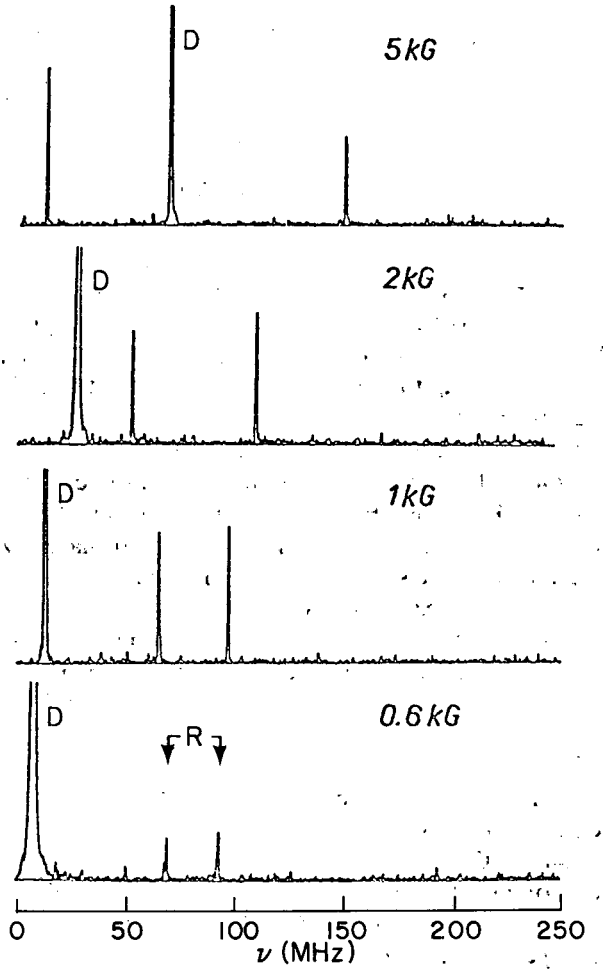

Figure 30a Muon precession frequencies for tetramethylethylene at various magnetic fields. D = muons in diamagnetic environments. R = muonium substituted radical.

dipolar contribution for the octahedral assignment vs a reduction in the tetrahedral assignment. If the hyperfine field is obtained by subtraction, the result is given in the lower curve. One would expect that the hyperfine field would be independent of the magnetization direction, since it involves only the conduction electron-spin density at the muon site in this simplified view. Therefore, there is a clear preference for the octahedral interstitial site assignment. There is a small step in $\mathbf{B}_{hf}$ at the crystal phase transition, as shown.

This qualitative analysis has been applied to another example of hcp structure, ferromagnetic gadolinium (71, 73, 74) and a comparison with the measurements gives again a good fit with the octahedral site assignment. In these analyses it is not determined whether the muon is localized at a particular octahedral site or diffuses among various 0-sites.

Iron has a bcc structure, but apparently the motion of the muon between sites averages out the differences in dipolar fields in the temperature ranges that have been studied. We shall return to iron in connection with the muon diffusion in the following section.

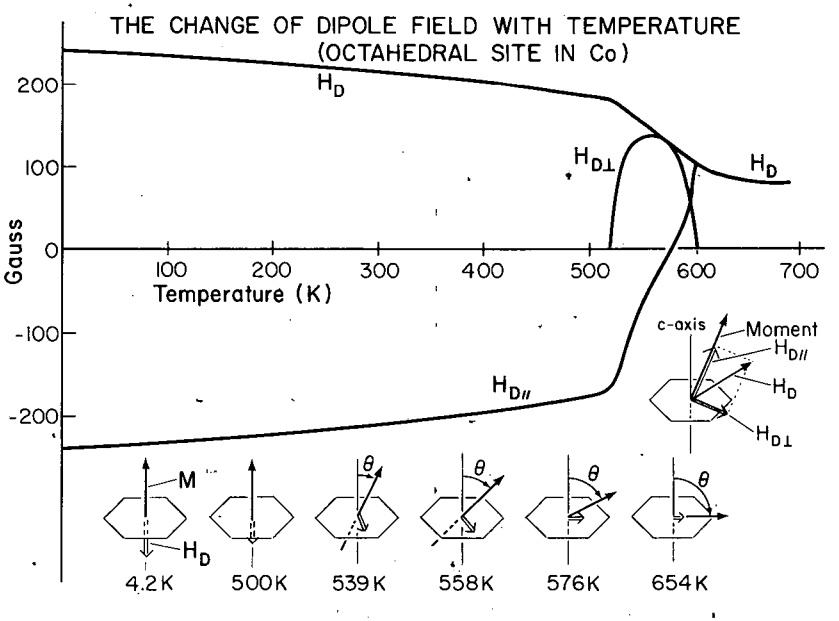

Figure 33 The variation with temperature of the dipolar field at the octahedral site in cobalt. The easy axis of magnetization is rotated by an angle θ with respect to the $\hat{c}$ axis. At 0°K, **M** is parallel to the $\hat{c}$ axis and the dipole field is antiparallel. As the temperature is elevated above 520°K, **M** tips into the basal plane, and H_{dip} lies along **M**, both lying in the basal plane.

3.3.1.1 *Hyperfine fields* The hyperfine field that arises from the polarization of the conduction electrons has been the subject of a number of experimental and theoretical studies, which are in progress at this writing. It will suffice to summarize the status experimentally and indicate briefly the difficulties various quantitative interpretations have experienced. The values of the hyperfine field at $T = 0$ have been collected (76) in Table 8 for nickel, iron, cobalt, and gadolinium, together with the results of the neutron diffraction measurements for the magnetic field present at the octahedral site due to the polarized electron-spin density. The ratios of the observed muonic hyperfine field to the unperturbed interstitial magnetization vary from 1.04 in nickel to 8.41 in iron. The models have attempted to explain this enhancement factor in terms of a distortion of the electron density distribution due to the muon's positive charge. The results can be summarized as follows: (*a*) The hyperfine field is negative in agreement with the reversal of magnetization at the

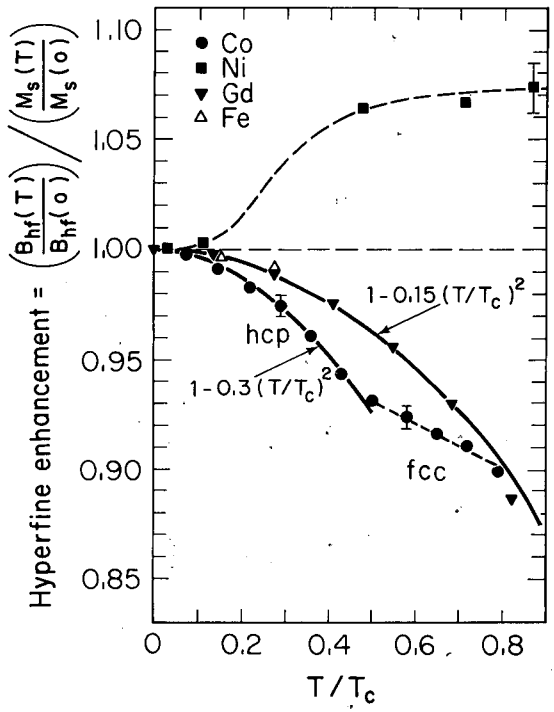

Figure 34 The variation with temperature of the normalized hyperfine enhancement for μ^+ in ferromagnetic metals. $\mathbf{B}_c$ is the hyperfine field at the μ^+ while M_s is the saturation magnetization. Nickel shows an increase of $\mathbf{B}_c$ compared to M_s whereas for cobalt, iron, and gadolinium there is a reduction.

Table 9 Knight shift enhancement data

Element	Valence state	Crystal structure	Electron density (r_s)	Susceptibility		Knight shifts		Enhancement factor
				$\chi_p^F \times 10^6$ Calculated	$\chi_p \times 10^6$ Observed	K_{μ^+} (ppm)[a]	K_p (ppm)	E[b]
Li	+	bcc	3.25	—	2.0	-9.5 ± 19	—	~ 1
Na	—	bcc	3.93	0.66	1.1	55 ± 11	—	~ 6
K	—	bcc	4.86	0.53	0.84	64 ± 11	—	~ 9.1
Cu	—	fcc	2.67	0.97	0.96	55 ± 11		~ 6
						58 ± 6	—	
						48 ± 5		—
Mg	2+	hcp	2.65	0.97	—	63 ± 11	—	~ 7.8[a]
Ca	—	fcc	3.27	0.79	—	400 ± 15	—	~ 60.4[a]
Al	3+	fcc	2.07	1.25	1.8	15 ± 15	—	~ 1
Pb	4+	fcc	2.30	1.13	1.4	110 ± 13	—	~ 9.4
Pd	2+	fcc	—	—	—	-400 ± 20	-350 ± 10	—

[a] The diamagnetic shielding correction for the μ^+ in the standard, H_2O, was applied and a demagnetizing field = $-4\pi M_s(0.5\pm0.5)$ was assumed.
[b] The enhancement of the observed Knight shift due to the response of the metal. E is given in Equation 28.

is an enhancement

$$E(k) = \frac{|\Psi_k(0)|^2}{|\Psi_k^0(0)|^2}, \qquad 24.$$

where the super zero indicates the undisturbed electron density. Table 9, taken from Schenck's review (85), gives a survey of the metals for which Knight shifts have been measured together with the corresponding enhancement observed for the μ^+.

To calculate the enhancement due to the presence of the μ^+ impurity, one must make numerous assumptions about the response of the crystal, the shielding due to screening of the conduction electrons, which depends on their density ρ_s.

Figure 35 gives the dependence of the enhancement on the electron spacing $r_s \propto (\frac{4}{3}\pi\rho_s)^{-\frac{1}{3}}$ as calculated by several authors (86, 87, 89–92) using a nonlinear approach to include the possible bound states. The more detailed calculations use the Hohenberg-Kohn-Sham (88) or HKS density

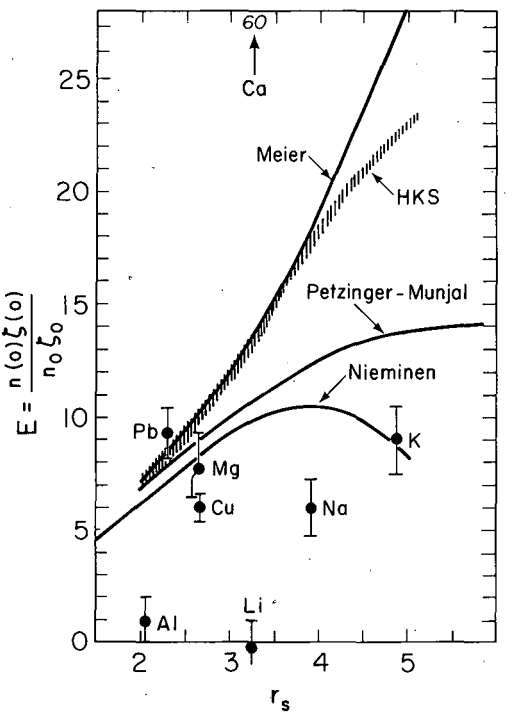

Figure 35 Comparison of theoretical predictions for the spin-density enhancement factor with experimental results from Knight shift measurements. The parameter r_s is a measure of the electron density n: $r_s = (3/4\pi n)^{\frac{1}{3}} a_B$.

functional formalism and attempt to include exchange and correlation effects. The situation can be described as confusing at this time. Clearly there is a need for improving many of the measurements to indicate whether there are real discrepancies with these screening estimates. One can also expect rapid progress in the theoretical predictions as more complete calculations are made.

3.3.2.1 *Knight shifts in ferromagnetic metals* The behavior of the local field, $\mathbf{B}_\mu$, above saturation is shown in Figure 14. The slope can be used to find the Knight shift as follows: The magnetization within a domain with an internal field $\mathbf{B}_{\text{int}} = \mathbf{B}_{\text{ext}} - \mathbf{B}_{\text{DM}}$ is increased proportional to the total magnetic susceptibility χ_T

$$M = M(0) + \chi_t \mathbf{B}_{\text{int}}. \tag{25.}$$

χ_t can be measured independently (93). The hyperfine field is increased by the Knight shift K,

$$\mathbf{B}_{\text{hf}} = \mathbf{B}_{\text{hf}}(0) + K\mathbf{B}_{\text{int}}. \tag{26.}$$

Using Equation 13 and taking $\mathbf{B}_{\text{dip}} = 0$, the field at the muon will become

$$\mathbf{B}_\mu(\mathbf{B}_{\text{ext}}) = \mathbf{B}_{\text{hf}}(0) + \frac{M_{\text{d}}(0)[\frac{4}{3}\pi - N(1+K)]}{1+\chi_t N} + \frac{1+\frac{4}{3}\pi\chi_t + K}{1+\chi_t N}\mathbf{B}_{\text{ext}}. \tag{27.}$$

The change in field $\Delta\mathbf{B}_\mu$ with applied field $\mathbf{B}_{\text{ext}}$ will be

$$\frac{\Delta\mathbf{B}_\mu}{\mathbf{B}_{\text{ext}}} = \left(1 + \frac{4\pi}{3}\chi_t + K\right)(1+\chi_t N)^{-1}. \tag{28.}$$

For a spherical nickel single crystal the results obtained by Camani et al (94) give a positive shift $K = +0.0025$ (3). Preliminary results reported by Schenck (85) indicate that this Knight shift is temperature dependent going to zero at $\sim 400°\text{K}$ and even becoming negative above T_c.

3.3.3 μ^+ RELAXATION IN MAGNETIC METALS The μ^+ depolarization rate has been measured in a number of samples of iron. Figure 36 shows a compilation of the results obtained by different groups (33, 35, 95–97).

Given a local dipolar field of about ± 10 kG, these data imply a μ^+ hopping rate of $\gtrsim 10^{11}$ sec^{-1} in the purest Fe crystals at room temperature. The temperature dependence of Λ is approximately exponential in the regions $T > 100°\text{K}$ and $50°\text{K} < T < 100°\text{K}$ but depends upon the sample quality. The observation of a short-lived signal at 23°K is taken to be strong evidence for an onset of quantum diffusion at low temperature. This result is discussed in the context of the motion of muons in pure crystals in the following section.

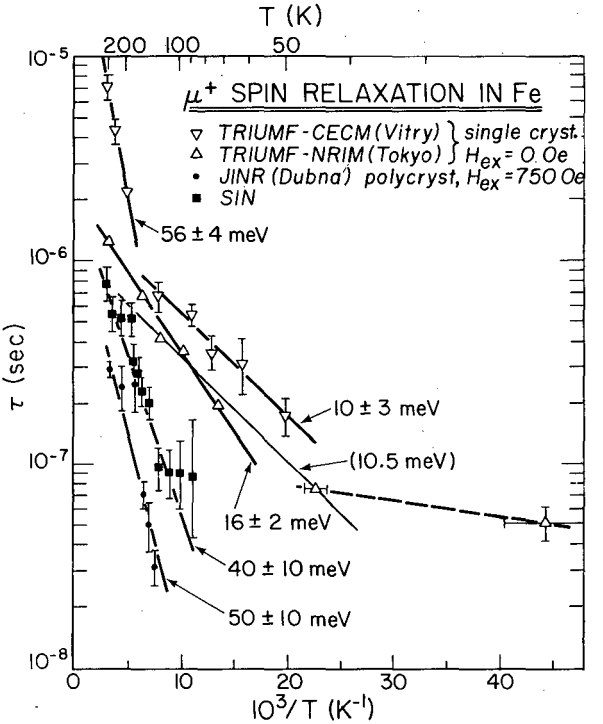

Figure 36 Positive muon spin depolarization time constant vs inverse temperature for different purity iron samples. CECM: Vitry iron ~99.995%; NRIM: Tokyo iron ~99.98%; JINR: Dubna iron ~99%.

3.4 μ^+ *Relaxation and Motion in Metals*

3.4.1 COPPER The interpretation of the anisotropic behavior of μ^+ relaxation in a single crystal of metallic copper has provided evidence for a unique assignment of the site for the muon in that crystal lattice.

The temperature dependence of the depolarization rate of muons in a Cu single crystal was measured by Gurevich (31, 98). Copper forms a fcc structure. The lattice constant is 3.6 Å. (By chance, the orientation chosen reproduced the result obtained in the polycrystal material.) The two isotopes present in copper have the same spin and approximately the same magnetic moment and electric quadrupole moments.

The motion of the μ^+ together with the action of random magnetic field fluctuations on the μ^+ spin discussed previously, leads to a time dependence for the μ^+ asymmetry

$$A(t) = \exp\left[2\sigma^2\tau^2(e^{-t/\tau} - 1 + t/\tau)\right], \qquad 29.$$

where σ^2 is proportional to the second moment of the host nuclear dipole field $\langle M_2 \rangle$ and τ is the correlation time associated with the muon diffusion:

$$\frac{1}{\tau} = \frac{\langle v \rangle}{a} = \frac{D}{a^2} \quad \text{and} \quad \sigma^2 = \tfrac{1}{2}\gamma_\mu^2 \left[\langle M^2 \rangle = \langle \Delta \mathbf{B}_{\text{dip}}^2 \rangle\right]. \tag{30.}$$

Figure 12 shows that at temperatures below 100°K the depolarization of the μ^+ appears to be consistent with that due to the fields produced by the nuclear magnetic moments of the host copper nuclei.

The line broadening is proportional to the square of the dipolar field:

$$\Delta \mathbf{B}_{\text{dip}}^2 = \tfrac{1}{3}\gamma_s^2 \hbar^2 (S)(S+1) \sum_i (3 \cos^2 \theta_i - 1)^2 r_i^{-6}, \tag{31.}$$

where the sum is over all the host nuclei at distances $|\mathbf{r}_i|$ from the muon with moments inclined at angles θ_i with respect to $\mathbf{r}_i$. This was seen in the case of gypsum (30), where the sum of nearest neighbors produced several fields, depending on the orientation. As the temperature is raised, the muon begins to diffuse and the motional narrowing (32) averages out the field inhomogeneity and the depolarization disappears. We discuss this diffusion in detail subsequently. Camani et al (99), recognizing that the contributions of the dipolar fields would vary with the crystal orientation when the muon was fixed in a given site, lowered the temperature and

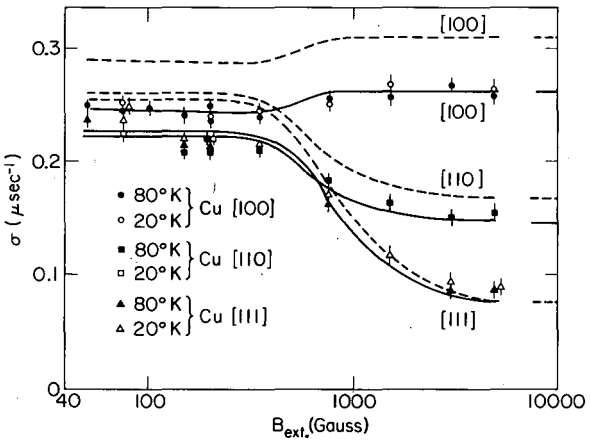

Figure 37 The field variation of the measured damping constant σ for μ^+ in a single crystal of copper oriented with the external field $\mathbf{B}_{\text{ext}}$ along different crystal axes. Assuming an interstitial octahedral site for the μ^+ the dashed curve was calculated including the quadrupole electric field gradient energy shift with no lattice distortion. The solid curve assumes a 5% dilation of the nearest neighbor separation. The pure magnetic splitting (Van Vleck values) are shown on the right.

Table 10 Damping rate (μsec^{-1}) due to nearest neighbor Cu nuclei

	External field parallel to		
Site	(100) axis	(110) axis	(111) axis
Octahedral	0.308	0.165	0.0674
Tetrahedral	0.0771	0.279	0.319

varied both the orientation of the crystal and the applied field. Figure 37 shows the resulting variation of the relaxation rate. At high fields the calculation of the Van Vleck terms (100) for the local field can be made for each assignment of muon site. The results are given in Table 10.

As the magnetic field is lowered to zero the electric field gradient (EFG) produced by the muon interacts with the quadrupole moment of the nuclei and alters the precession of the magnetic moment. Hartmann (101), recognizing that the same phenomenon occurred in Mössbauer NMR studies (102) where EFG were produced by substitutional impurities, showed that the quadrupole effect tends to alter the field broadening at low fields in agreement with the observations. The quadrupole splitting is given by

$$\frac{\omega E}{2} = \frac{eQ}{h} \cdot \frac{V_{zz}}{4S(2S-1)} = 0.16 \pm 0.02 \text{ MHz};$$

from this one obtains for the electric field gradient, V_{zz},

$$\frac{V_{zz}}{e} = 0.27 \pm 0.15 \text{ Å} \qquad 32.$$

Quantitatively the magnitude of the depolarizing magnetic field σ^2 was found to be too large if one assumed that the host lattice was undistorted. Good agreement was obtained if the lattice was allowed to expand by $\sim 5\%$. Finally it should be noted that the extraction of the EFG from the data is limited by the uncertainty of the electric quadrupole moment. Jena et al (103) calculated the EFG from first principles, using the self-consistent density formalism. The Bloch enhancement factor computed with a band structure model agrees with the measured results.

Even with all these minor uncertainties, Table 10 shows that depolarization rates are clearly interchanged for the [111] and the [100] axes for the tetrahedral interstitial site assignment as compared with the octahedral site assignment. The experimental result leads to the unambiguous conclusion that the μ^+ is trapped in the octahedral interstitial site.

3.4.2 COMPARISON OF COPPER AND OTHER PURE METALS The application of this technique to other metals with large nuclear spins and magnetic moments is clearly to be desired to determine the muon site, and at this time only a few have been tried. The time dependence of the depolarization can be used to study the diffusion of μ^+. Figure 38 shows a summary of data on the temperature dependence of the depolarization rate (98, 104). One can easily show that the expression for the motional narrowing (Equation 29) simplifies for the case where (t/τ) is large or small.

For short correlation times (fast hopping), $A(t) = \exp(-2\sigma^2\tau t)$, one has exponential decay with the damping rate $\Lambda = 2\sigma^2\tau$. For long correlation times, $A(t) = \exp(-\sigma^2 t^2)$, one has a Gaussian time dependence. In the actual situation the fits to either Gaussian or exponential are usually not sufficiently sensitive to differentiate the two different forms. If one takes the characteristic time for $1/e$ reduction, then one has either $t_{\text{relax}} = \Lambda^{-1} = (2\sigma^2\tau)^{-1}$ or σ^{-1} in the two extremes.

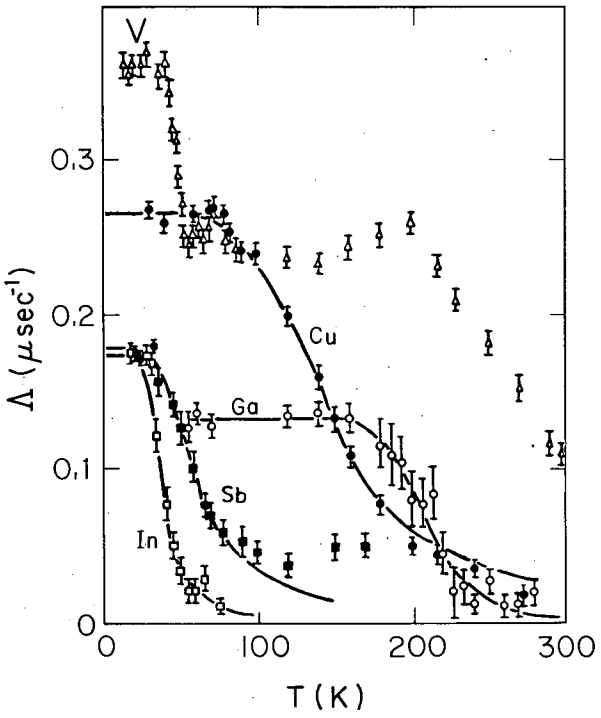

Figure 38 The temperature variation of the μ^+ depolarization rate for vanadium, copper, gallium, antimony, and indium. $\Lambda(T)$ was obtained using a Gaussian fit for the asymmetry time variation $A(t) = \exp(-\Lambda^2 t^2)$.

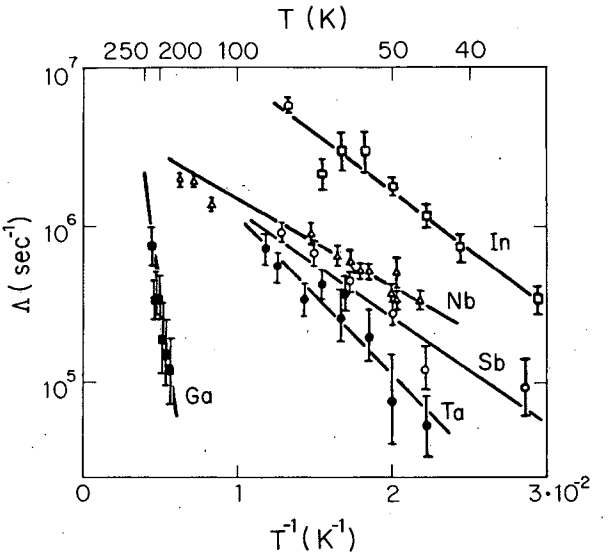

Figure 39 A summary of the Arrhenius plots for the hopping rate, inversely proportional to the correlation time τ vs reciprocal temperature.

If we characterize the data with classical Arrhenius description for the transition rate, we find $W = \tau^{-1} = Da^{-2} = \nu_0 \exp(-QkT)$, where τ is the time between collisions, D is the diffusion coefficient, a is the lattice constant, ν_0 is the "preexponential" attempt frequency, and Q is the height of the barrier or activation energy.

The frequency ν for hydrogen in copper is known (105) to be $\sim 10^{14}$ sec^{-1} at $T \sim 1000$°C. Figure 39 (104) shows the temperature dependence of Λ as an Arrhenius plot. Table 11 lists the extracted parameters. For

Table 11 The preexponential attempt frequency ν_0 and the activation energy Q obtained from the muon relaxation rates

Element	$\log_{10} \nu$	Q/k (°K)	Q (10^{-3} ev)
Cu	7.61 ± 0.04	560	48.2
Sb	6.97 ± 0.14	173	14.9
Be	9.5 ± 0.4	1200	103.4
In	6.7 ± 0.2	155	13.3
Ta	6.9 ± 0.2	200	17.2
Ga	10.1 ± 0.8	2130	183.5
Nb	6.5	100	8.61
Bi	11.2	1400	120.6

μ^+ the preexponential factor in copper is $\sim 10^{-7}$ of the hydrogen value, and the variation of ν_0^{μ} between different metals is larger than 10^5. The (highly variable) activation energies are also smaller for muons than for hydrogen.

The theoretical understanding of the diffusion of μ^+ in metals has recently become the focus of considerable activity. Schenck (106) reviewed the principal mechanisms of diffusion, which we will summarize briefly. At high temperature, the classical "hopping" behavior can be pictured as the tail of the Boltzmann μ^+ energy distribution leaking over the barrier, which corresponds in height to the saddle point in the μ^+ potential energy surface between adjacent interstitial sites.

As the temperature is lowered, the classical hopping will cease, but quantum tunneling is expected to take over. For a naive model of uncomplicated tunneling through a single barrier, one would expect the "hop" rate to be given directly by a barrier penetration factor

$$\nu \rightarrow \nu_0 \exp\left(-\frac{2l}{\hbar}\sqrt{2m\,U}\right),$$

where ν_0 is taken as the zero point frequency, typically $\sim 10^{12}$ sec^{-1}. Using this value of ν_0 and assuming a tunneling barrier-height $U \sim 0.5$ ev and a width $l \sim 1$ Å, one obtains $\nu \sim 10^6$ sec^{-1}. Even in this simple picture, complications enter as soon as one asks whether the μ^+ tunnels from ground state to ground state of its approximate rigid-lattice harmonic potential or rather between excited states. In the latter case, the μ^+ must first be thermally excited to the state that acts as a "tunneling channel" (Orbach-type process), and an Arrhenius behavior with classically unreasonable parameters can easily result (106). No doubt the results on μ^+ diffusion in Cu can be consistently treated with this picture. The assumption of "weak coupling" between μ^+ and phonons necessary for such a model is probably too naive, but the notion of a quantum tunneling process which requires assistance from lattice vibrations is widespread in current theory.

It is also naive to picture all tunneling processes as penetrations of single barriers, since the lattice consists of a periodic array of approximately identical barriers and wells; if they were perfectly identical, the tunneling process would eventually leave the μ^+ wave function spread out over many lattice sites, giving a true "muon band" in the "coherent quantum tunneling" picture of Kagan & Klinger (109). However, dislocations, impurities, single-phonon scattering, and multiphonon processes (e.g. "self-trapping") will all disrupt the coherent tunneling ("broaden the band") and slow down the diffusion. The μ^+ then relies again on "phonon-

assisted incoherent tunneling" for its motion. We now examine some of the specific predictions of such models.

If the temperature is large compared to the Debye temperature, Flynn & Stoneham (107) have shown that incoherent phonon-assisted tunneling exhibits the classical Arrhenius temperature dependence if one includes in the exponential the energy E_a associated with the distortion of the lattice, due to the presence of the μ^+ (proton) impurity, and the energy E_s due to the phonon excitations involved in the transition from site to site.

As the temperature is lowered there is a region where the pre-exponential factor has a slow temperature dependence $T^{-\frac{1}{2}}$:

$$W = \left(\frac{\pi}{4\hbar^2 E_a kT}\right)^{\frac{1}{2}} |J|^2 \exp(-E_a/kT).$$

Here J is the muon transfer matrix element.

At still lower temperature this incoherent process decreases as T^7

$$W^p = 5.76 \times 10^4 \pi \omega_D (\hbar\omega_D)^{-4} |J|^2 E_a^2 \left(\frac{T}{\theta_D}\right)^7 \exp(-5E_{a/\hbar\omega_D}),$$

where $\hbar\omega_D = k\theta_D$, and the typical energy characteristic of the phonon θ_D is the Debye temperature.

These calculations are in many ways similar to the polaron description for an electron and its strain field moving in the crystal lattice. Teichler (108) has applied an analysis of this type to the μ^+ quantum diffusion in copper. The analysis assumes phonon-assisted μ^+ tunneling between

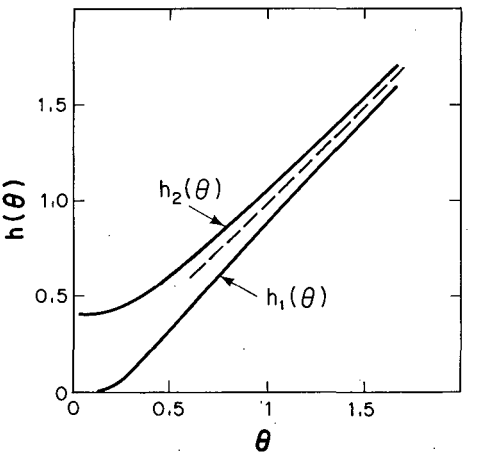

Figure 40 The auxillary functions used by Teichler (108) to calculate the quantum diffusion of muons in fcc metals when σ becomes small. For large σ, the classical (over the barrier hopping) result is the limit when $h_1 = h_2 = \theta = T/T_0 \approx 2T/\theta_D$. θ_D is the Debye temperature.

adjacent octahedral sites in the fcc lattice with suitable forces introduced to describe the lattice interaction and the muon-lattice interaction.

The universal functions $h_1(T/T_0)$ and $h_2(T/T_0)$ shown in Figure 40 are introduced to include the phonon excitations

$$h_1(T/T_0) = \frac{1}{8E_a kT_0}\frac{1}{N}\sum_q |\gamma_q|^2 (\hbar\omega_q)^2 \operatorname{csch}\left(\frac{\hbar\omega_q}{2kT_0}\frac{T_0}{T}\right),$$

and

$$\frac{1}{h_2(T/T_0)} = \frac{kT_0}{E_a}\frac{1}{N}\sum_q |\gamma_q|^2 \tanh\left(\frac{\hbar\omega_q}{4kT_0}\frac{T_0}{T}\right).$$

Here $kT_0 \simeq \frac{1}{2}k\theta_D$, and γ_q is the μ^+-phonon coupling energy. The resultant diffusion constant depends on temperature as

$$D = \frac{a^2}{\hbar}|J^2|\sqrt{\pi/4E_a kT_0}\,[h_1(T/T_0)]^{-\frac{1}{2}} \exp\left[-\frac{E_a}{kT_0 h_2(T/T_0)}\right].$$

In the calculations Teichler has included 768 points in the Brillouin zone for his q-space summation.

The results of this calculation are shown in Figure 41, together with the data of Gurevich (98). The parameters of the theory for this fit are $E_a = 75.2 \times 10^{-3}$ eV and $J = 18.4 \times 10^{-6}$ eV. The low temperature region is especially interesting as it has been predicted that the coherent quantum tunneling may be observable. Kagan & Klinger (109) investigated this problem and showed the coherent diffusion constant for protons to be

$$D_c = \frac{Za^2J^2}{3\mathbf{B}\hbar^2\omega_D}\left(\frac{\hbar\omega_D}{T}\right)^9 e^{-2\phi^s(T)}.$$

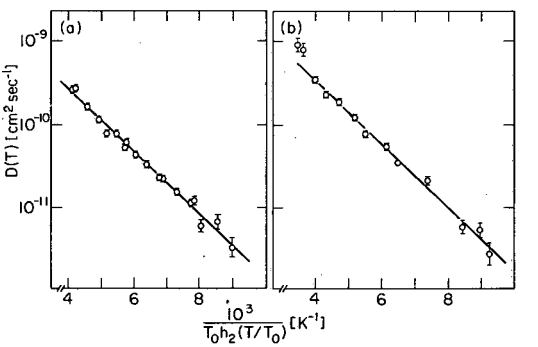

Figure 41 Teichler's calculation (108) for the diffusion of muons in copper by phonon-assisted incoherent quantum tunneling compared with the data (*a*) polycrystal and (*b*) monocrystal from Grebinnik (98).

The essential difference between the coherent and noncoherent diffusion is that for coherent diffusion the occupation numbers of the phonon states do not change with the transition. The rapid coherent process is analogous to the tunneling transition for the ammonia molecule. It will occur when the energy levels in adjacent wells coincide, i.e. the coherent process will be destroyed if (*a*) the energy levels are shifted by impurities or other

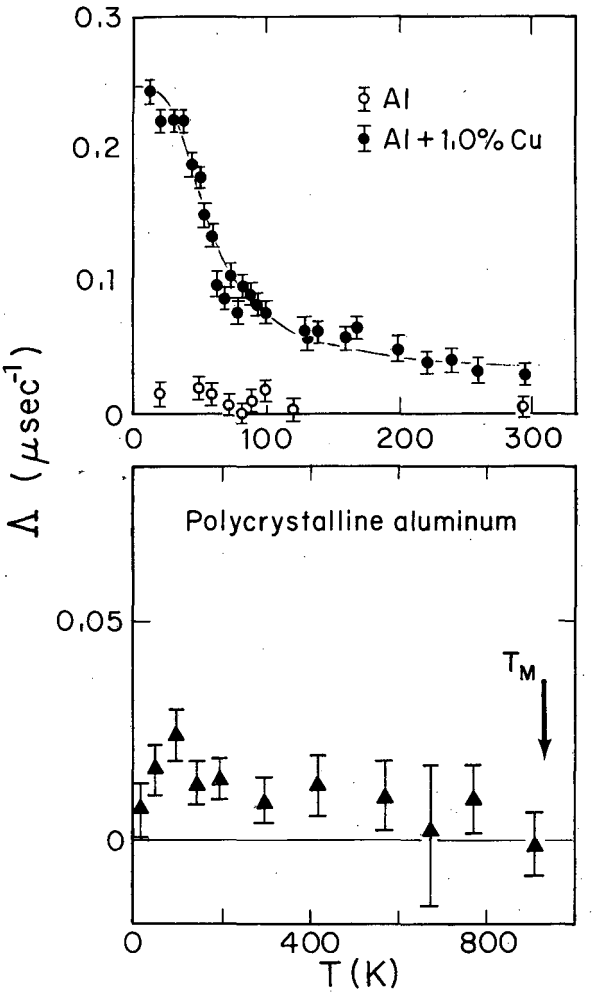

Figure 42 Temperature dependence of the depolarization for polycrystalline aluminum and aluminum alloyed with copper. The muon in pure aluminum diffuses rapidly at the lowest temperature measured. In the alloy, the muon presumably depolarizes as it is trapped by the impurity.

defects, destroying the symmetry of the crystal site; or if (*b*) the phonons are so numerous as to broaden the band until the density of states at exact resonance required by energy conservation is suppressed. In the context of (*a*) it is noteworthy that very fast diffusion has so far been observed only in metals (Al, Au, Fe, Bi,...) with monoisotopic nuclei. Self-trapping, it is asserted (109), does not enter the calculations, since the states on each side of the barrier have the same E_a. This argument would seem to depend upon the responsiveness of the lattice—i.e. the frequency spectrum of the virtual phonons responsible for the self-trapping.

The prediction of a T^{-9} dependent coherent tunneling at low temperatures with near perfect crystals is clearly an exciting prospect, and although there are possible anomalies in the hydrogen diffusion, to our knowledge no evidence has appeared in support of this prediction from hydrogen diffusion measurements. However, this phenomenon may be out of reach experimentally for muons as well.

As is clear from the above discussion, the application of the μ^+, which has a longer wavelength than the proton, to the study of quantum diffusion is an obvious challenge to μSR experimentalists; at this writing much effort is being concentrated along these lines.

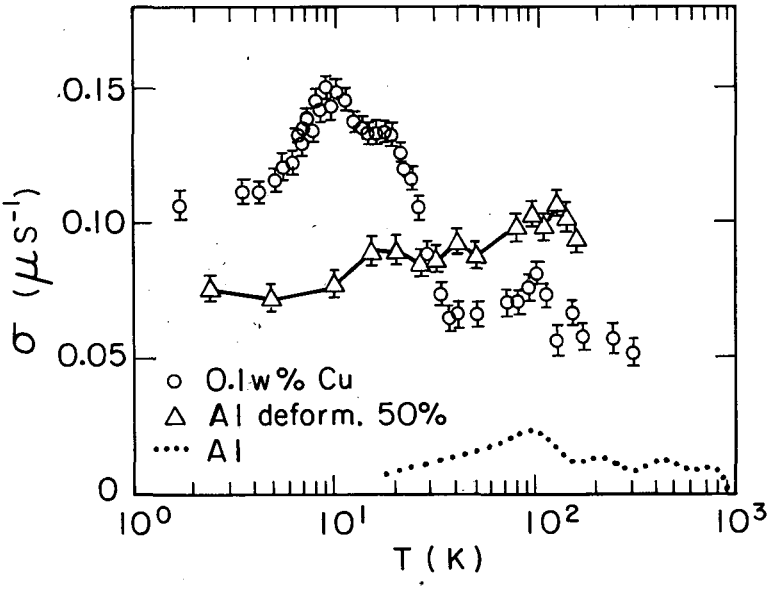

Figure 43 Preliminary data from SREL shows temperature dependence of the μ^+ diffusion in aluminum, deformed aluminum, and alloyed with copper.

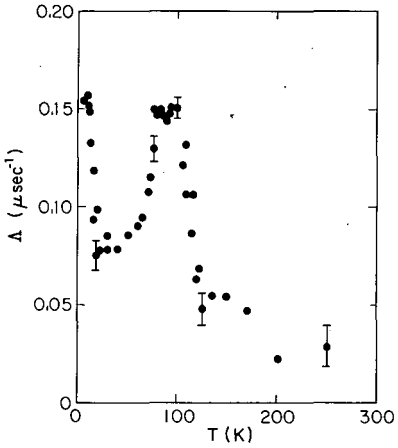

Figure 44 The depolarization rate for muons in polycrystalline bismuth has a minimum near 50°K, which implies an increased diffusion rate. The authors suggest that these data indicate a coherent quantum diffusion process. See Reference 110.

3.4.3 IMPURITY EFECTS In the studies of μ^+ diffusion in metals, aluminum seems to give anomalous results. In the Flynn-Stoneham model (107), the activation energy is dominated by the self-trapping energy if there is no neighbor host to block the transition. For example, octahedral sites

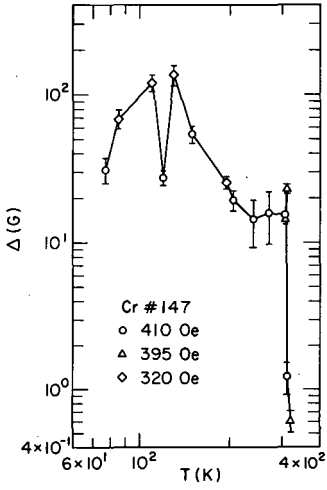

Figure 45 The muon depolarization line width from fits to an exponentially damped sine wave are plotted against temperature for polycrystalline chromium. Between the spin flip temperature 122°K and the Neel temperature 308°K, the antiferromagnetic crystal has a high local field at most interstitial sites. To fit the data in this region, a hopping frequency $\sim 0.5 \times 10^{11}$ sec^{-1} is required (110).

in bcc lattices have small hindrances compared with the octahedral site in fcc crystals. The tunneling between octahedral site in copper (fcc) will therefore (in this model) involve the lattice phonon energy E_s.

Another fcc crystal is aluminum; the magnetic moment of 3.64 μ_B and spin = $\frac{5}{2}$ assure that the magnetic interaction is ~ 3 times that of copper. The Debye temperature of aluminum is higher than copper (428°K vs 343°K). However, the data of Figures 42 and 43 show that Λ is less than 0.02 μsec^{-1} in pure Al at temperatures as low as 20°K (110–112). Apparently the muon continues to diffuse rapidly. Very slight amounts of impurities have a profound effect on this diffusion. With the addition of only 0.1% copper, the μ^+ becomes depolarized with a $Q \sim 100$°K (8 meV). Figure 44 shows the first clear evidence for trapping of μ^+ at dislocations in an otherwise pure sample of Al (111).

There are a number of other irregularities, which are illustrated in Figures 44–47. The data indicate that there are several cases where structure in the relaxation rate is observed. The interpretation of these data is uncertain at this writing. However, it is instructive to look at the different postulated mechanisms to understand what may be happening.

The high temperature line narrowing is presumably phonon activated diffusion. As the temperature is lowered, the μ^+ becomes trapped in a site connected with either defects, impurities, or vacancies; or it becomes self-trapped because of the distortion of the lattice connected with the interaction of the μ^+ with the core electrons of the host.

As the temperature is raised the last effective trapping site will be the

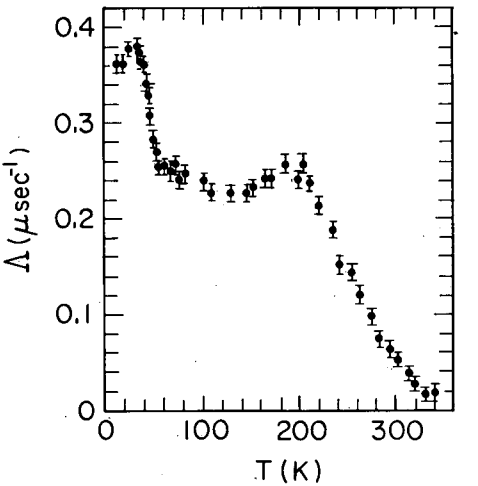

Figure 46 The depolarization rate for μ^+ in vanadium is plotted against temperature. The plateau at 200°K has a lower effective depolarizing field than at the muon site at ~40°K. Either a different type of site or higher μ^+ mobility can explain this behavior (113).

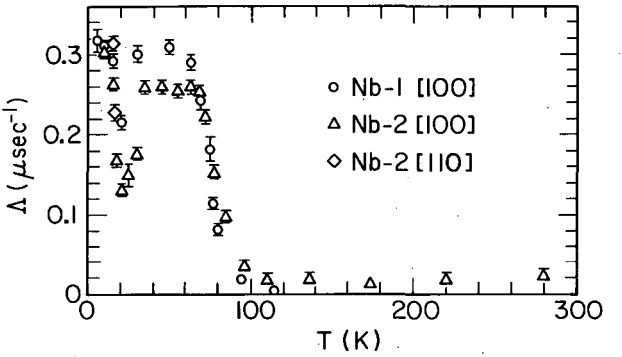

Figure 47 The μ^+ depolarization in a single crystal of niobium is plotted against temperature for different orientations relative to the external field of 102 Oe. The sharp dip at 20°K indicates a rapid increase in diffusion rate in a limited temperature region (114).

lowest or deepest trap. If the coherent diffusion becomes important the μ^+ may begin to tunnel as the temperature is lowered, and this may be responsible for the dips in the relaxation. For the case of bismuth it is speculated (110) that as the rate of coherent diffusion increases the μ^+ is captured on defects, and the μ^+ remains caught as soon as the diffusion rate is high enough for the μ^+ to find the defect within the time scale of the experiment. Note that either σ^2 or τ_c (cf Equation 29 and following) may independently undergo temperature variation. If the muon wave function is spread over a small number of sites, there will be a reduction of the average field.

Figure 47 shows the diffusion rate vs temperature in niobium. Birnbaum et al (116) rotated the crystal axes to show that the tetrahedral site is preferred. This tentative assignment is less definite than the octahedral assignment for copper. The magnitude of the σ^2 damping at low temperatures is lower than predicted by the dipolar sum (117). If quantum tunneling occurs between four interstitial sites (115), there is approximate agreement with the line broadening—only a 3% expansion of the lattice is necessary rather than the 15% expansion required if the μ^+ is trapped at a single site. The correlation time can be extracted assuming that σ^2 is fixed with the low temperature points. Figure 48 shows the diffusion rate, $1/\tau_c$ vs temperature.

The authors speculate that at low temperature the μ^+ is self-trapped in a cyclic tunneling configuration between four sites, the T_4 state, and as the temperature is elevated, jumping between these rings increases until the diffusion is sufficient to find impurity states. In corroboration of this description the addition of N_2 in small quantities ($\sim$100 ppm) was seen to gradually eliminate the notch at 20°K (118, 119). This is seen in Figure 49. These phenomena may have been clarified since this writing, and

perhaps other mechanisms may be involved to explain these interesting results. There is a hint that the μ^+ may diffuse coherently either within a ring or in a translational mode at low temperatures in the highest purity crystal. The confirmation and elucidation of these hints will be a challenging task.

3.5 *Knight Shifts*

3.5.1 μ^+ IN ANTIMONY Recently the study of μ^+ frequency shifts in semimetal crystals (120) has resulted in an observation of a very large Knight shift that is anisotropic. Figure 50 shows the shift in a

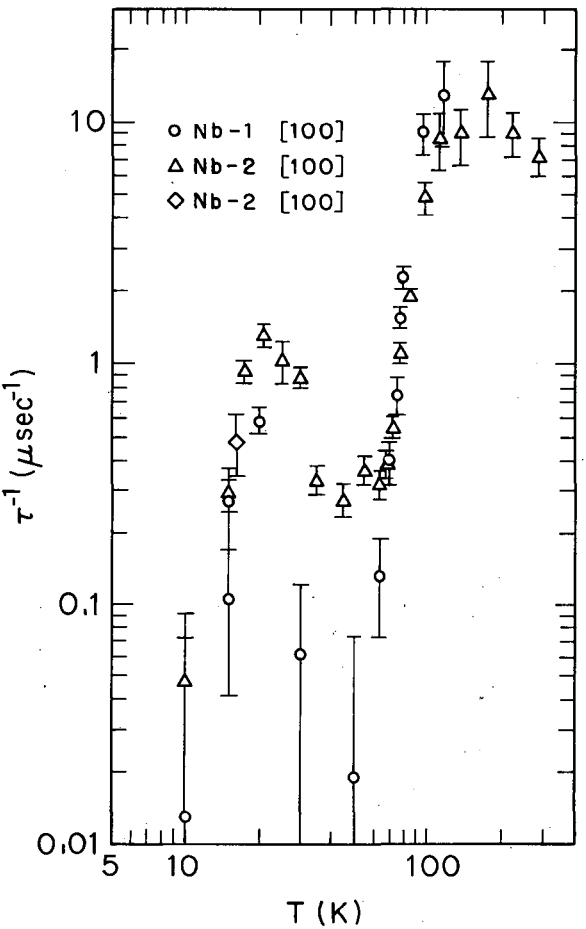

Figure 48 The correlation time for μ^+ in niobium can be extracted if one fixes the mean square field parameter $\sigma_s = 0.321$ sec^{-1} from the low temperature plateau in the previous figure (115).

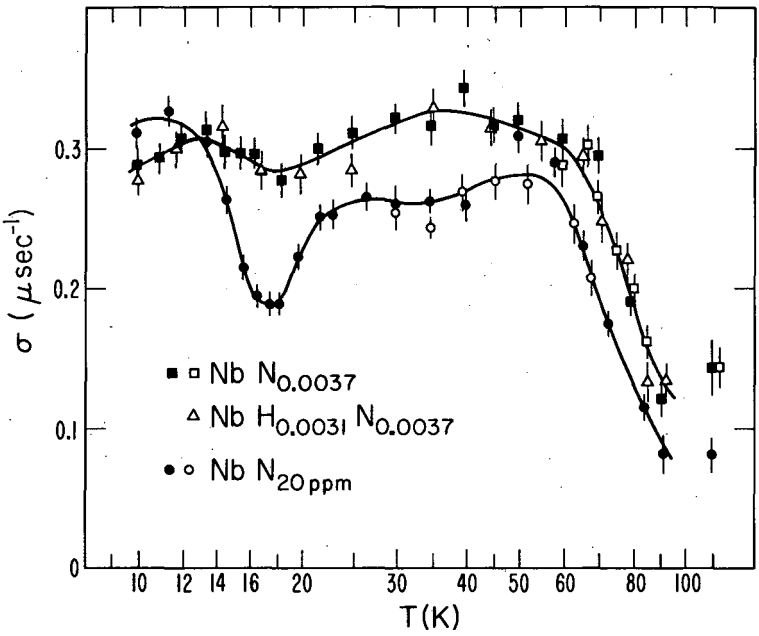

Figure 49 The relaxation rate for μ^+ in niobium with varying impurity concentrations is plotted against temperature. The presence of nitrogen of 0.37% seems to quench the muons diffusion at ~18°K. Preliminary data obtained at CERN (119).

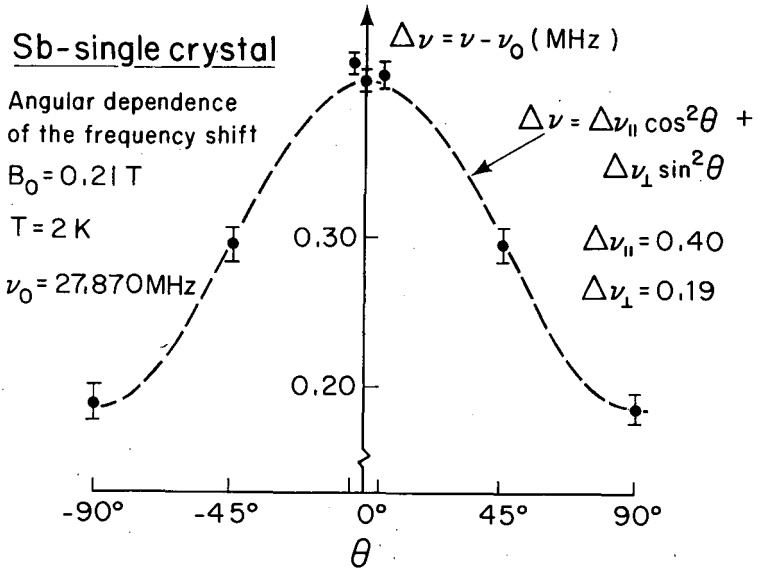

Figure 50 Dependence of the frequency shift of μ^+ in antimony single crystal on the angle between $\mathbf{B}_0$ and the $\hat{c}$-axis.

rhombohedral single crystal of antimony, which is positive amounting to 0.40 MHz and varies with angle as shown. The variation with angle fits an equation $\Delta\nu = \Delta\nu_{\parallel} \cos^2\theta + \Delta\nu_{\perp} \sin^2\theta$, with $\Delta\nu = 0.4$ MHz, and $\Delta\nu_{\perp} =$ 0.19 MHz at $\mathbf{B}_{ext} = 2100$ G and $T = 2°$K. The frequency of normal μ^+ rotation is $\sim$28 MHz. The shift decreases approximately linearly with increasing temperature and vanishes at $\sim$150°K. For a polycrystalline sample a linear decrease of the average shift with applied field as the field is dropped to 400 G was reported. It has been suggested (120) that the variations of the shifts are related to the anisotropies in the Fermi surfaces with variations of the electronic g factor (i.e., $g \simeq 15$ for the $\hat{Z}$ axis).

The existence of anisotropies in antimony like silicon suggests a p-like muonic system, which arises from the symmetry of the crystal. This implies a system with long-lived collective states extending over several lattice dimensions. The semimetal differs from the semiconductor by having a smaller gap between valence and conduction bands. A quantitative interpretation of these results has not been presented at this time.

3.5.2 μ^+ IN MANGANESE SILICIDE Another anomalously large Knight shift has been observed for a weakly helimagnet intermetallic crystal MnSi (121). Below 29°K the long period helical spin structure results from the weak polarization of itinerant d-electrons, which may produce both large static and fluctuating local fields at interstitial sites. Figure 51 shows the comparison with the μSR and NMR Knight shifts temperature dependence expressed parametrically in terms of the susceptibility.

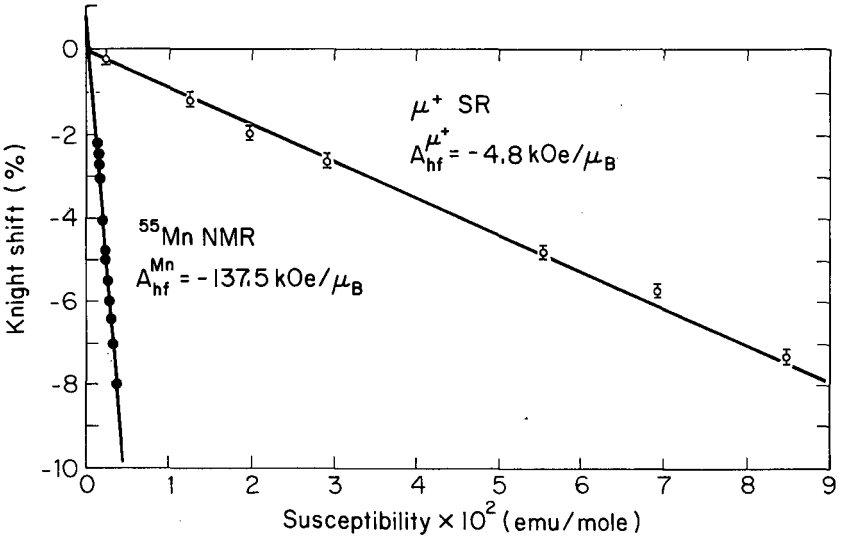

Figure 51 The Knight shift of both ^{55}Mn and μ^+ in a single crystal MnSi vs the host susceptibility with temperature as the implicit parameter.

The Knight shift is given by

$$K_\mu(T) = \frac{\mathbf{B}_{\rm hf}(T)}{\mathbf{B}_{\rm ext}} = \frac{\mathbf{B}_\mu - \mathbf{B}_{\rm ext}}{\mathbf{B}_{\rm ext}} - \left(\frac{4\pi}{3} - N_Z\right)\frac{M(T)}{\mathbf{B}_{\rm ext}} = A^\mu_{\rm hf}\chi(T).$$

The slope $A^\mu_{\rm hf}$ is -4.8 kG per μ_B. For the NMR at $\chi = 0$, the Knight shift is slightly positive because of the electron orbital susceptibility. For μSR the shift is close to zero and the hyperfine field is proportional to the d-spin magnetization and is larger than the other ferromagnets. Quantitative interpretation of this system is desired.

3.6 μ^+ *in Magnetic Insulators*

There have been two observations of μSR in antiferromagnetically aligned crystals. The crystal αFe_2O_3 (hematite/rust) is an insulator that has a corundum D^6_{3d} structure. The Fe ions lie on trigonal axes that form the hexagonal two-dimensional array shown in Figure 52. Neutron scattering analysis shows that the magnetic moment lies in the (111) plane below the Neel temperature (945°K) and rotates at the Morin temperature (263°K) so that the moments lie close to the [111] (trigonal) direction.

Figure 53 (122) shows the local field variation with temperature in the insulator αFe_2O_3. Below the Morin temperature T_M the precession frequency is shown in Figure 54, with and without external field. The maximum asymmetry is observed when the trigonal axis of the crystal is perpendicular to the initial muon polarization, and the asymmetry vanishes with this axis parallel to the initial spin. This indicates that the local field must be parallel to this axis. Its magnitude is ± 15.7 kG. If one applies a field of 1.9 kG the line splits. Above the Morin transition $\mathbf{B}_\mu$ drops

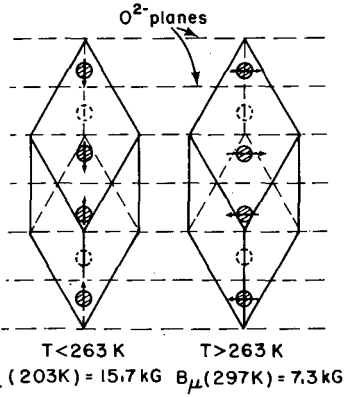

Figure 52 Spin structure of αFe_2O_3 below and above the Morin temperature. The likely muon stopping sites are indicated by the dashed circles.

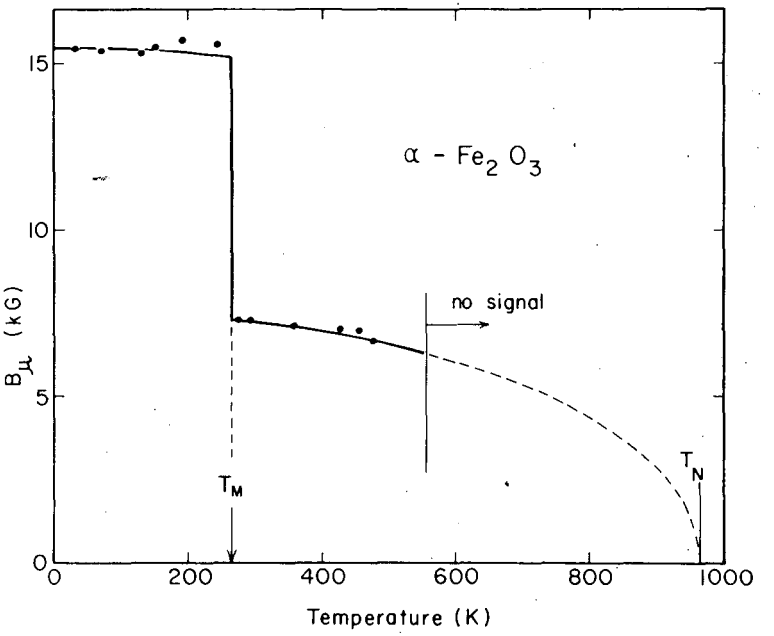

Figure 53 The measured local field **B** in single crystal αFe_2O_3 as a function of temperature. At the Morin temperature T_M, $\mathbf{B}_\mu$ changes by a factor of two. Above 500°K, diffusion causes the local field to average to zero.

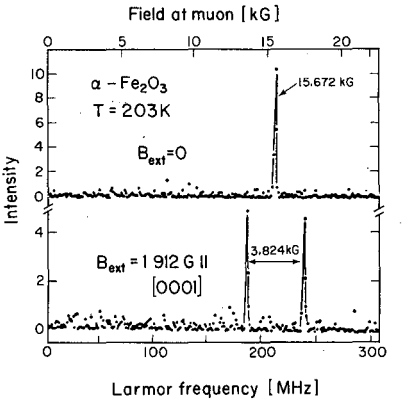

Figure 54 Below the Morin temperature the μ^+ precesses in the local fields of the antiferromagnet. At the top, frequency spectra of the muon precession are shown in zero external field. At the bottom 1.912 kG applied along the trigonal axis causes a symmetrical splitting depending on the μ^+ site.

to ~7 kG and a lower asymmetry is present at all angles. Above 430°K the signal begins to be depolarized and disappears at ~500°K. No muonium is observed in this insulator.

The interpretation of these results in terms of the muon location is as follows: Below 430°K the μ^+ is localized at distinct interstitial sites. The μ^+ diffusion above 430°K relaxes the asymmetry, and above 500°K the μ^+ asymmetry disappears. The averaging of the two sublattice fields destroys the symmetry. Below the Morin transition there is a strong indication that the muon is localized on or near the trigonal axis (Figure 53). The local field, which has dipolar symmetry, changes by a factor of two as the spins rotate by 90°. The preliminary model calculations of $\mathbf{B}_\mu$ require rapid diffusion in the cyclic orbit shown in Figure 52 to average out the perpendicular field components. The longitudinal field estimated from the dipole sum is ~23 kG. Refined calculations are in progress at the time of this review.

3.7 μ^+SR in *Antiferromagnets*

μSR has been seen in annealed polycrystalline dysprosium (123). Dysprosium is ferromagnetic below 85°K with a saturation magnetization

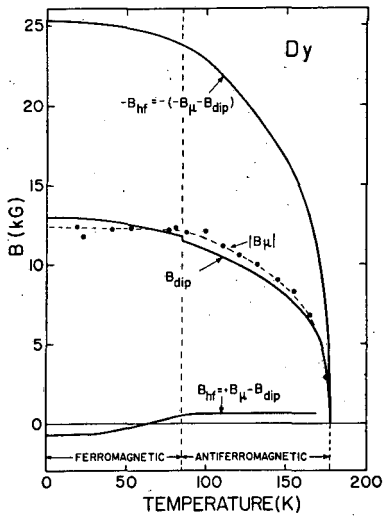

Figure 55 The measured field $\mathbf{B}_\mu$ as a function of temperature (*dots with dashed line*) for polycrystalline dysprosium. No discontinuity of $\mathbf{B}_\mu$ was observed at the Curie temperature. $\mathbf{B}_{dip}(T)$ is the calculated dipolar field for the octahedral interstitial site. (The curve for the tetrahedral site differs by less than 100 G from the one given.) From $\mathbf{B}_\mu$ and $\mathbf{B}_{dip}$ the hyperfine field $\mathbf{B}_{hf}$ is evaluated for the two possible signs of $\mathbf{B}_\mu$. Since $\mathbf{B}_{hf}$ shows no abrupt change at T_C, there is an indication that $\mathbf{B}_\mu$ is positive and $\mathbf{B}_{hf}$ is small.

of 10.2 μ_B per atom. Between 85°K and 179°K, it has a helical antiferromagnetic ordering with the helix axis parallel to the hexagonal axis $\hat{c}$. In the antiferromagnetic case, the $4f$ moments lie in the hexagonal basal plane. The crystal structure is hcp. The moment is rotated from plane to plane by an angle θ, which depends on the temperature.

In Figure 55 the local field is followed through the ordering phase transition and above. No discontinuity in $\mathbf{B}_\mu$ is observed. The amplitude of precession is small, ~ 0.03. The relaxation time, $T_2 \simeq 150$ nsec is approximately constant in the range investigated. $\mathbf{B}_{dip}$ is calculated using the known magnetization density from other data. In the interpretation of this data the authors conclude: (*a*) The μ^+ is probably located in the octahedral site. (*b*) The $\mathbf{B}_\mu$ is probably parallel to the magnetization M_{local} and the hyperfine field is small. The antiparallel choice implies a large $\mathbf{B}_{hf}$ that would change rapidly at T_c when the interlayer spin turn angle is known to shift abruptly $\sim 26°$. And (*c*) Single crystal studies would presumably resolve these ambiguities.

4 SUMMARY

The most significant recent progress in μSR has been conceptual. In each field of application, new data and new interpretations have combined to clarify our understanding of the behavior of the muon in matter, leaving a better picture of its potentials as a probe. In gases, it is clear that Mu behaves just as expected of a light isotope of the H atom, both in its formation and in its subsequent reactions. However, its mass is light enough to make quantum tunneling through reaction barriers an important process. Such an unprecedented mass difference in true chemical isotopes provides a testing ground for elementary rate theories in physical chemistry. Chemical reactions of Mu in liquids, after years of mainly qualitative study via the residual polarization technique, have now also been opened up for precise quantitative investigation by the successful observation of Mu precession in liquids. So far the results support the same characterization of Mu in solution as in the gas phase: a light isotope of H.

Our understanding of the motion of the μ^+ in metals has improved rapidly in the last three years, thanks to numerous experiments on μ^+ spin relaxation and extensive theoretical work relating the temperature dependence of the relaxation to diffusional motion of the μ^+. The familiar "motional narrowing" picture has now been refined to include detailed models of quantum tunneling, self- and defect-trapping, and other phenomena of general importance in the motion of light interstitials. One

lesson that emerges from these efforts is that the μ^+-lattice interaction, often an annoyance when one hopes to probe the intrinsic properties of the crystal, is actually a rich source of information about the coupling of impurities to their environment. This has been evident in the theoretical work on hyperfine fields at the μ^+ in magnetic metals, where attempts to understand the experimental data in terms of spin-dependent screening, etc, have led to fresh original work in the area of interstitial magnetism.

Certain experimental milestones can be expected to mark new avenues of μSR research. One example is the successful observation of muonic radicals and their hyperfine structure via Paschen-Bach (high transverse field) Fourier spectroscopy, which should permit extensive comparisons between muonic radicals and the analogous hydrogenic radicals. Another is the empirical characterization of the anisotropic spin Hamiltonian for anomalous muonium in silicon, which must still be combined with a physical model of that entity, but should then make a real contribution to our understanding of the electronic structure of impurity states in semiconductors. A third discovery whose potentials are still largely untapped is the diffusion of Mu out of fine grains of powdered insulators and into vacuum, which may make possible a study of the physiochemistry of surfaces with muons. In solids, the observation of large anisotropic Knight shifts in semimetals, large local fields in antiferromagnetic insulators, magnetic phase transitions in magnetic media and spin glasses, all lead to potential programs of investigation with unpredictable results.

We would like to conclude by reiterating what we consider to be the most urgent unanswered questions in μSR. In both gas and liquid phases, the fraction of muons that thermalize in diamagnetic states is still mysterious. In Ne and He gases, does the μ^+ precession signal come from actual "bare" muons or from molecular ions $Ne\mu^+$ and $He\mu^+$? If the slow relaxation of the μ^+ signal with added Xe is really due to thermal electron capture, temperature-dependent studies may expose the identity of this component. In liquids, does the μ^+ reach a diamagnetic state at early times primarily via hot atom reactions or through short-lived processes, in the radiation "spur" caused by its ionization? A major controversy has arisen over this issue; it should be resolved, at least in part, by studies of hot atom reactions in the gas phase, where there is no "spur." In semiconductors the physical identity of the "anomalous muonium" state must be determined. Straining the crystals may help. Will such states be observed in other crystals besides Si? These questions may be difficult to answer, but the potential rewards make the effort worthwhile. In insulators as well as semiconductors, Mu forms in some crystals but not in others. Why is this? So far there is not even a consistent

empirical rule governing this differentiation. A broader survey may be helpful. In all crystals, but especially in metals, the relative importance of quantum tunneling, polaron-type effects, and impurity trapping must be better understood before μ^+SR can have its full impact on studies of the motion of light interstitials. Various experiments determining the μ^+ site in different crystal lattices have been performed, but more are needed. When the zero-point motion of the μ^+ and the distortion of the lattice by its presence are properly combined with a correct description of spin-dependent screening, the contribution of μ^+SR hyperfine studies to magnetism theory will be more evident. These theoretical challenges have been accepted by the solid state physics community, but much remains to be explained.

ACKNOWLEDGMENTS A complete list of the people who have actively contributed to this review would be longer than the reference list. We offer our greatest appreciation to the many members of the μSR community who have lent us their ideas, data, and friendly criticisms for this work. However, certain of these people have made such important contributions that they must at least be mentioned by name.

Don Fleming (Chemistry Department, University of British Columbia) and Ken Nagamine (Physics Department, University of Tokyo) were so intimately involved with the initial stages of this review that they must be considered virtual co-authors, and would have been formal co-authors had circumstances not removed them from North America during the final writing. Their respective contributions to the discussions of muonium chemistry and μ^+ in metals cannot be over emphasized.

Numerous experimenters have allowed us to "steal" their unpublished data; the current rapid growth of μSR makes this essential for a review that will not be hopelessly outdated before it can be published. We offer special thanks to Dave Garner, Jerry Jean, Randy Mikula and David Walker of UBC (Chemistry); to Glen Marshall, Rob Kiefl, and John Warren of UBC (Physics); to Nobu Nishida, Ryu Hayano, Toshi Yamazaki, and other members of the University of Tokyo group at TRIUMF; to Paul Percival, Emil Roduner, and Hanns Fischer of the Institute of Physical Chemistry, University of Zurich; to Bruce Patterson (now at TRIUMF) and W. Kundig of the Physical Institute, University of Zurich; to Alex Schenck and Fred Gygax of ETH; to Tony Fiory of Bell Labs; to Jack Kossler of the College of William and Mary; and to Bob Heffner, Will Gauster, and Chao-Yuan Huang of LAMPF.

We are particularly indebted to the many theorists who have patiently helped us understand the problems treated herein. Special thanks to Birger Bergerson of UBC (Physics), Tom McMullen of Queens University,

Alan Portis and Leo Falicov of Berkeley, Peter Meier of Zurich, Puru Jena of Argonne National Laboratory, and Yu. V. Kagan and V. G. Smilga of Moscow.

Finally, we would like to thank Pat Schoenfield of LBL and the editorial staff of ARNPS for patience and cooperation in the assembly of this text.

Literature Cited

1. Garwin, R. L., Lederman, L. M., Weinrich, M. 1957. *Phys. Rev.* 105: 1415–17
2. Friedman, J. I., Telegdi, V. L. 1957. *Phys. Rev.* 105:1681–82
3. Yamazaki, T., Nagamiya, S., Hashimoto, O., Nagamine, K., Nakai, K., Sugimoto, K., Crowe, K. M. 1974. *Phys. Lett B* 53: 117
4. Yamazaki, T. 1977. *Phys. Scr.* 11:133; *Phys. Scr.* 86–88B: 1053
5. Nagamiya, S., Nagamine, K., Hashimoto, O., Yamazaki, T. 1975. *Phys. Rev. Lett.* 35:308
6. Deleted in proof
7. Firsov, V. G., Byakov, V. M. 1965. *Sov. Phys. JETP* 20:719
8. Crowe, K. M., Hague, J. F., Rothberg, J. E., Schenck, A., Williams, D. L., Williams, R. W., Young, K. K. 1972. *Phys. Rev. D* 5:2145
9. Combley, F., Picasso, E. 1976. *Int. Sch. Phys. Meteorol. Fundam. Constants, Varenna, Italy, July 1976*; Bailey, J., Borer, K., Combley, F., Drumm, H., Farley, F., Field, J., Flegel, W., Hattersley, P., Krienen, F., Lange, F., Picasso, E., Ruden, W. von. 1977. *Phys. Lett. B* 68:191
10. Casperson, D. E., Crane, T. W., Denison, A. B., Egan, P. O., Hughes, V. W., Mariam, F. G., Orth, H., Reist, H. W., Souder, P. A., Stambaugh, R. D., Thompson, P. A., zu Putlitz, G. 1977. *Phys. Rev. Lett.* 38:956; Hughes, V. W. 1966. *Ann. Rev. Nucl. Sci.* 16:445
11. Brewer, J. H., Crowe, K. M., Gygax, F. N., Schenck, A. 1975. *Muon Physics*, Vol. III, ed. V. W. Hughes, C. S. Wu, pp. 3–139. New York: Academic
12. Swanson, R. A. 1958. *Phys. Rev.* 112: 580
13. Hughes, V. W. 1975. *High Energy Phys. Nucl. Struct., AIP Conf. Proc.* 26:515
14. Gurevich, I. I., Ivanter, I. G., Makariyna, L. A., Mel'eshko, E. A., Nikol'skii, B. A., Roganov, V. S., Selivanov, V. I., Smilga, V. P., Sokolov, B. V., Shestakov, V. D., Yakovleva, I. V. 1969. *Phys. Lett. B* 29: 387
15. Mobley, R. M., Bailey, J. M., Cleland, W. E., Hughes, V. W., Rothberg, J. E. 1966. *J. Chem. Phys.* 44:4354; Mobley, R. M. 1967. PhD thesis, Yale Univ.
16. Ruderman, M. A. 1966. *Phys. Rev. Lett.* 17:794
17. Brewer, J. H., Gygax, F. N., Fleming, D. G. 1973. *Phys. Rev. A* 8:77
18. Brewer, J. H., Crowe, K. M., Gygax, F. N. Johnson, R. F., Fleming, D. G., Schenck, A. 1974. *Phys. Rev. A* 9:495

18a. Percival, P. W., Fischer, H. 1976. *Chem. Phys.* 16:89

18b. Minaichev, E. V., Myasishcheva, G. G., Obukhov, Yu. V., Roganov, V. S., Savel'ev, G. I., Firsov, V. G. 1970. *Sov. Phys. JETP* 30:230

19. Eisenstein, B., Prepost, R., Sachs, A. M. 1966. *Phys. Rev.* 142:217
20. Hutchinson, D. P., Menes, J., Shapiro, G., Patlach, A. M. 1963. *Phys. Rev.* 131:1351, 1362
21. Schenck, A., Crowe, K. M. 1971. *Phys. Rev. Lett.* 26:57
22. Babaev, A. I., Balats, M. Ya., Myasishceva, G. G., Obukhov, Yu. V., Roganov, V. S., Firsov, V. G. 1966. *Sov. Phys. JETP* 23:583
23. Nosov, V. G., Yakovleva, I. V. 1965. *Nucl. Phys.* 68:609
24. Ivanter, I. G., Smilga, V. P. 1968. *Sov. Phys. JETP* 27:301
25. Ivanter, I. G., Smilga, V. P. 1969. *Sov. Phys. JETP* 28:796
26. Ivanter, I. G., Smilga, V. P. 1971. *Sov. Phys. JETP* 33:1070
27. Brewer, J. H., Crowe, K. M., Johnson, R. F., Schenck, A., Williams, R. W. 1971. *Phys. Rev. Lett.* 27:297
28. Schenck, A. 1970. *Phys. Lett. A* 32:19
29. Schenck, A., Williams, D. L., Brewer, J. H., Crowe, K. M., Johnson, R. F. 1972. *Chem. Phys. Lett.* 12:544
30. Pake, G. E. 1948. *J. Chem. Phys.* 16:327
31. Gurevich, I. I., Meleshko, E. A., Muratova, I. A., Nikol'skii, B. A., Roganov, V. S., Selivanov, V. I., Sokolov, B. V. 1972. *Phys. Lett. A* 40:143
32. Abragam, A. 1961. *The Principles of Nuclear Magnetism* Oxford: Clarendon. 439 pp.
33. Foy, M. L. G., Heiman, N., Kossler,

W. J., Stronach, C. E. 1973. *Phys. Rev. Lett.* 30:1064
34. Patterson, B. D., Crowe, K. M., Gygax, F. N., Johnson, R. F., Portis, A. M., Brewer, J. H. 1974. *Phys. Lett. A* 46: 453
35. Gurevich, I. I., Klimov, A. N., Maiorov, V. N., Meleshko, E. A., Nikol'skii, B. A., Roganov, V. S., Selivanov, V. I., Suetin, V. A. 1973. *JETP Lett.* 18:332; Gurevich, I. I., Klimov, A. I., Maiorov, V. N., Meleshko, E. A., Muratova, I. A., Nikol'skii, B. A., Roganov, V. S., Selivanov, V. I., Suetin, V. A. 1974. *Zh. Eksp. Teor. Fiz.* 66:374; *Sov. Phys. JETP* 39:178
36. Patterson, B. D., Falicov, L. M., 1974. *Solid State Commun.* 15:1509
37. Deleted in proof
38. Deleted in proof
39. Favart, D., Brouillard, F., Grenacs, L., Igo Kemenes, P., Lipnik, P., Macq, P. C. 1970. *Phys. Rev. Lett.* 25:1348
40. Myasishcheva, G. G., Obukhov, Yu. V., Roganov, V. S., Firsov, V. G. 1968. *Sov. Phys. JETP* 26:298
41. Gurevich, I. I., Ivanter, I. G., Meleshko, E. A., Nikol'skii, B. A., Roganov, V. S., Selivanov, V. I., Smilga, V. P., Sokolov, B. V., Shestakov, V. D. 1971. *Sov. Phys. JETP* 33:253
42. Brewer, J. H., Crowe, K. M., Gygax, F. N., Johnson, R. F., Patterson, B. D., Fleming, D. G., Schenck, A. 1973. *Phys. Rev. Lett.* 31:143
43. Deleted in proof.
44. Andrianov, D. G., Minaichev, E. V., Myasishcheva, G. G., Obukhov, Yu. V., Roganov, V. S., Salel'ev, G. I., Firsov, V. G., Fistul', V. I. 1970. *Sov. Phys. JETP* 31:1019
45. Wang, J. Shy-Yih, Kittel, C. 1973. *Phys. Rev. B* 7:713
46. Johnson, R. F. Unpublished PhD thesis, Univ. Calif., Nov. 1976; LBL Rep. 5526
47. Kohn, W., Luttinger, J. M. 1955. *Phys. Rev.* 98:915
48. Patterson, B. D., Hintermann, A., Kundig, W., Meier, P. F., Waldner, F., Graf, H., Recknagel, E., Weidinger, A., Wichert, Th. 1978. *Phys. Rev. Lett.* 40: 1347
49. Gurevich, I. I., Nikol'skii, B. A., Selivanov, E. I., Sokolov, B. V. 1976. *Sov. Phys. JETP* 41:401
50. Kudinov, V. I., Minaichev, E. V., Myasishcheva, G. G., Obukhov, Yu. V., Roganov, V. S., Savel'ev, G. I., Samoilov, V. M., Firsov, V. G. 1975. *Sov. Phys. JETP* 21:22; 1976. *Sov. Phys. JETP* 43:1065
51. Pifer, A. E., Bower, T., Kendall, K. R. 1976. *Nucl. Instrum. Methods* 135:39
52. Percival, P. W., Fischer, H. Camani, M., Gygax, F. N., Ruegg, W., Schenck, A., Schilling, H., Graf, H. 1976. *Chem. Phys. Lett.* 39:333
53. Fleming, D. G., Brewer, J. H., Garner, D. M., Pifer, A. E., Bowen, T., DeLise, D. A., Crowe, K. M. 1976. *J. Chem. Phys.* 64:1281
54. Stambaugh, R. D., Casperson, D. E., Crane, T. W., Hughes, V. W., Kaspar, H. F., Souder, P., Thompson, P. A., Orth, H., zu Pulitz, G., Denison, A. B. 1974. *Phys. Rev. Lett.* 33:568
54a. Green, J., Lee, J. 1964. New York: Academic (and references therein); Goldanskii, V. I., Firsov, V. G. 1971. *Ann. Rev. Phys. Chem.* 22:209
55. Jean, Y. C., Brewer, J. H., Fleming, D. G., Garner, D. M., Mikula, R. A., Vaz, L. C., Walker, D. C. 1978. Private communication; Mikula, R. A. 1978. Private communication
56. Allison, S. K. 1958. *Rev. Mod. Phys.* 30: 1137; Massey, H. S. W., Burhop, E. H. S. 1969. *Electronic and Ionic Impact Phenomena.* London: Oxford Univ. Press; Tawara, H., Russek, A. 1973. *Rev. Mod. Phys.* 45:178
57. Chupka, W. A., Russel, M. E. 1968. *J. Chem. Phys.* 49:5426
58. Bondybey, V., Pearson, P. K., Schaefer, H. F. III. 1972. *J. Chem. Phys.* 57:1123
59. Tawara, H., Russek, A. 1973. *Rev. Mod. Phys.* 45:178
60. Connor, J. N. L., Jakubetz, W., Manz, J. 1977. *Chem. Phys. Lett.* 45:265
61. Garner, D. M. 1978. Private communication; Fleming, D. G., Garner, D. M., Vaz, L. C., Walker, D. C., Brewer, J. H., Crowe, K. M. 1978. In press; In *Positronium and Muonium Chemistry*, ed. H. J. Ache. ACS
62. Garner, D. M., Fleming, D. G., Brewer, J. H., Warren, J. B., Marshall, G. M., Clark, G., Pifer, A. E., Bowen, T. 1977. *Chem. Phys. Lett.* 48:393; Garner, D. M., Fleming, D. G., Brewer, J. H. 1978. *Chem. Phys. Lett.* 55:163
63. Brandt, W., Paulin, R. 1968. *Phys. Rev. Lett.* 21:193
64. Gidley, D. W., Marko, K. A., Rich, A. 1976. *Phys. Rev. Lett.* 36:395
65. Marshall, G. M., Warren, J. B., Garner, D. M., Clark, G. S., Brewer, J. H., Fleming, D. G. 1978. *Phys. Lett.* 65A:351
66. Percival, P. W., Fischer, H., Camani, M., Gygax, F. N., Ruegg, W., Schenck, A., Schilling, H., Graf, H. 1976. *Chem. Phys. Lett.* 39:333
67. Percival, P. W. Roduner, E., Fischer, H. 1978. See Ref. 61; Percival, P. W. 1977. Private communication
67a. Roduner, E., Percival, P. W., Fleming,

D. G., Hochmann, T., Fischer, H. 1978. Private communication
68. Birss, R. R., Martin, D. J. 1975. *J. Phys. C* 8:189
69. Sucksmith, W., Thompson, J. E. 1954. *Proc. R. Soc. London Ser. A* 225:362
70. Graf, H., Kundig, W., Patterson, B. D., Reichart, W., Roggwiller, P., Camani, M., Gygax, F. N., Ruegg, W., Schenck, A., Schilling, H., Meier, P. F. 1976. *Phys. Rev. Lett.* 37:1644
71. Nishida, N., Nagamine, D., Hayano, R. S., Yamazaki, T., Fleming, D. G., Duncan, R. A., Brewer, J. H., Ahktar, A., Yasuoka, H. 1978. *Jpn. J. Phys. Soc.* In press
72. Bertaut, E. F., Delapalme, A., Pauthenet, R. 1963. *Solid State Commun.* 1:31
73. Gurevich, I. I., Klimov, A. I., Maiorov, V. N., Meleshko, E. A., Nikol'skii, B. A., Purogov, A. V., Roganov, V. S., Salivanov, V. I., Suetin, V. A. 1975. *Zh. Eksp. Teor. Fiz.* 9:1453; *Sov. Phys. JETP* 42:741
74. Graf, H., Hofmann, W., Kundig, W., Meier, P. F., Patterson, B. D., Reichart, W. 1977. *Solid State Commun.* 23:653
75. Deleted in proof
76. Schenck, A. 1977. Int. Sch. Phys. Exotic Atoms, Erice, Italy
76a. Slichter, Charles P. 1963. *Principles of Magnetic Resonance.* New York: Harper & Row
77. Mook, H. A., Shull, G. G. 1966. *J. Appl. Phys.* 37:1034
78. Shull, G. G., Mook, H. A. 1966. *Phys. Rev. Lett.* 16:184
79. Moon, R. M. 1964. *Phys. Rev. A* 136:195
80. Moon, R. M. et al. 1972. *Phys. Rev. B* 5:997
81. Jena, P. 1976. *Solid State Commun.* 19:45
82. Jena, P., Singwi, K. S., Nieminen, R. M. 1978. *Phys. Rev. B* 17:301
83. Meier, P. F. 1975. *Solid State Commun.* 17:987
84. Petzinger, K. G., Munjal, R. 1977. *Phys. Rev. B* 15:1560
85. Schenck, A. 1977. *Hyperfine Interactions, 4th,* Madison, NJ, pp. 282–99
86. Meier, P. F. 1975. *Helv. Phys. Acta* 48:227
87. Nieminen, R. M. 1977. Preprint NORDITA-77/16
88. Kohn, W., Sham, L. J. 1965. *Phys. Rev. A* 140:1133
89. Petzinger, K. G., Munjal, R. 1977. *Phys. Rev. B* 15:1560
90. Popovic, Z. D., Stott, M. J. 1974. *Phys. Rev. Lett.* 33:1164
91. Almbladh, C. O., et al. 1976. *Phys. Rev. B* 14:2250
92. Jena, P., Singwi, K. S. 1978. Private communication
93. Foner, S., et al. 1969. *Phys. Rev.* 181:863
94. Camani, M., Gygax, F. N., Ruegg, W., Schenck, A., Schilling, H., 1977. *Phys. Lett. A* 60:439
95. Nishida, N., Hayano, R. S., Nagamine, K., Yamazaki, T., Brewer, J. H., Garner, D. M., Fleming, D. G., Takeuchi, T., Ishikawa, Y. 1977. *Solid State Commun.* 22:235
96. Gurevich, I. I., Klimov, A. I., Maiorov, V. N., Meleshko, E. A., Nikol'skii, B. A., Pirogov, A. V., Selivanov, V. I., Suetin, A. V. 1974. *JETP Lett.* 20:254
97. Graf, H., Kundig, W., Patterson, B. D., Reichart, W., Roggwiller, P., Camani, M., Gygax, F. N., Ruegg, W., Schenck, A., Schilling, H. 1976. *Helv. Phys. Acta* 49:730
98. Grebinnik, V. G., Gurevich, I. I., Zhukov, V. A., Manych, A. P., Meleshko, E. A., Nikol'skii, B. A., Selivanov, V. I., Suetin, V. A. 1975. *Zh. Eksp. Teor. Fiz.* 68:1548 *Sov. Phys. JETP* 41:777
99. Camani, M., Gygax, F. N., Ruegg, W., Schenck, A., Schilling, H. 1977. *Phys. Rev. Lett.* 39:836
100. Van Vleck, J. H. 1948. *Phys. Rev.* 74:1168
101. Hartmann, O. 1977. *Phys. Rev. Lett.* 39:832
102. Matthias, E., Schneider, W., Steffen, R. M. 1962. *Phys. Rev.* 125:261
103. Jena, P., Das, S. G., Singwi, K. S. 1978. *Phys. Rev. Lett.* 40:264
104. Grebinnik, V. G., et al. 1977. Proc. Int. Symp. Meson Chem. Mesomolec. Processes Matter, Dubna, USSR, June 1977, p. 266
105. Sicking, G. 1972. Int. Meet. Hydrogen Metal, Julich, Germany, 1972. 2:408
106. Schenck, A. 1976. *On the Applications of Polarized Positive Muons in Solid State Physics. Nuclear and Particle Physics at Intermediate Energy,* ed. J. B. Warren. New York: Plenum
107. Flynn, C. P., Stoneham, A. M. 1970. *Phys. Rev. B* 1:3966; Stoneham, A. M. 1972. *Ber. Bunsenges. Phys. Chem.* 76:816
108. Teichler, H. 1977. *Phys. Lett. A* 64:78
109. Kagan, Yu., Klinger, M. I. 1974. *J. Phys. C Solid State Phys.* 7:2791
110. Grebinnik, V. G., Gurevich, I. I., Zhukov, V. A., Klimov, A. I., Manych, A. P., Maiorov, V. N., Meleshko, E. A., Nikol'skii, B. A., Pirogov, A. V., Ponomarev, A. I., Selivanov, V. I., Suetin, V. A. 1977. *Proc. Int. Symp. Meson Chem. Mesomolec. Processes Matter, Dubna, USSR, June 1977.* p. 272
111. Lankford, W. F., Kossler, W. J.,

Lindemuth, J., Stronach, C. E., Fiory, A. T., Minnich, R. P., Lynn, K. G. 1978. *Bull. Am. Phys. Soc.* 23:361
112. Gauster, W. B., Heffner, R. H., Huang, C. Y., Hutson, R. L., Leon, M., Parkin, D. M., Schillaci, M. E., Triftshauser, W., Wampler, W. R. 1977. *Solid State Commun.* 24:619
113. Kossler, W. J., Fiory, A. T., Murnick, D. E., Stronach, C. E., Lankford, W. F. 1977. *Hyperfine Interactions* 3:287
114. Nikol'skii, B. A. 1977. See Ref. 104, p. 246
115. Lankford, W. F., Birnbaum, H. K., Fiory, A. T., Minnich, R. P., Lynn, K. G., Stronach, C. E., Bieman, L. H., Kossler, W. J., Lindemuth, J. 1977. See Ref. 85, pp. 833–37
116. Birnbaum, H. K., Camani, M., Fiory, A. T., Gygax, F. N., Kossler, W. J., Ruegg, W. Schenck, A., Schilling, H. 1978. *Phys. Lett. A* 65:435
117. Birnbaum, H. K., Flynn, C. P. 1976. *Phys. Rev. Lett.* 37:25
118. Hartmann, O., Karlsson, E., Norlin, L.-O., Pernestål, K., Borghini, M., Niinikoski, T. O. 1977. *Phys. Lett. A* 61:141
119. Hartmann, O., Karlsson, E., Norlin, L. O., Pernestål, K., Borghini, M., Niinikoski, T. 1977. See Ref. 85, pp. 824–27; Borghini, M., Hartmann, O., Karlsson, E., Kehr, K. W., Niinikoski, T., Norlin, L. O., Pernestål, K., Richter, D., Soulie, J. C., Walker, E. 1978. Private communication
120. Hartmann, O., Karlsson, E., Norlin, L. O., Pernestål, K., Borghini, M., Niinikoski, T. 1977. See Ref. 85, pp. 828–31
121. Yasuoka, H., Hayano, R. S., Nishida, N., Nagamine, K., Yamazaki, T., Ishikawa, Y. 1978. Pricate communication
122. Graf, H., Hofmann, W., Kundig, W., Meier, P. F., Patterson, B. D., Reichart, W. 1977. See Ref. 85, pp. 452–56
123. Hofmann, W., Kundig, W., Meier, P. F., Patterson, B. D., Ruegg, K., Echt, O., Graf, H., Recknagel, E., Weidinger, A., Wichert, T. 1978. *Phys. Lett. A* 65:343
124. Albright, R. G., Dodonov, A. F., Lavrovskaya, G. K., Morosov, I. I., Tal'roze, V. L. 1969. *J. Chem. Phys.* 50:3632
125. Rabideau, S. W., Hecht, H. G., Lewis, W. B. 1972. *J. Magn. Reson.* 6:384; Levy, J. B., Copeland, B. K. W. 1968. *J. Phys. Chem.* 72:3168
126. Homann, K. H., Schweinfurth, H., Warnatz, J. 1977. *Ber. Bunsenges. Phys. Chem.* 31:724
127. Ambidge, P. F., Bradley, J. N., Whytock, D. A. 1976. *J. Chem. Soc. Faraday Trans. 1* 72:1157
128. Bemand, P. P., Clyne, M. A. A. 1977. *J. Chem. Soc. Faraday Trans. 2* 73:394; Wagner, H. Gg., Welzbacher, U., Zellner, R. 1976. *Ber. Bunsenges. Phys. Chem.* 80:902
129. Fleming, D. G., Brewer, J. H., Garner, D. M., Pifer, A. E., Bowen, T., DeLise, D. A., Crowe, K. M. 1976. *J. Chem. Phys.* 64:1281
130. Ambidge, P. F., Bradley, J. N., Whytock, D. A. 1976. *J. Chem. Soc. Faraday Trans 1* 72:2143
131. Westenberg, A. A., deHaas, N. 1968. *J. Chem. Phys.* 48:4405; Clyne, M. A. A., Stedman, D. H. 1966. *Trans. Faraday Soc.* 62:2164
132. Endo, H., Glass, G. P. 1976. *Chem. Phys. Lett.* 44:180
133. Endo, H., Glass, G. P. 1976. *J. Chem. Phys.* 80:1519
134. Jones, W. E., MacKnight, S. D., Teng, L. 1973. *Chem. Rev.* 73:407; Sullivan, J. H. 1962. *J. Chem. Phys.* 36:1925
135. Griller, D., Ingold, K. U. 1974. *J. Am. Chem. Soc.* 96:6203
136. Linder, R. E., Winters, D. L., Ling, A. C. 1976. *Can. J. Chem.* 54:1405
137. Krusic, P. J., Meakin, P., Smart, B. E. 1974. *J. Am. Chem. Soc.* 96:6211
138. Krusic, P. J., Kochi, J. K. 1971. *J. Am. Chem. Soc.* 93:846
139. Eiben, K., Fessenden, R. W. 1971. *J. Phys. Chem.* 75:1186
140. Zeldes, H., Livingston, R. 1966. *J. Phys. Chem.* 45:1946

This report was done with support from the Department of Energy. Any conclusions or opinions expressed in this report represent solely those of the author(s) and not necessarily those of The Regents of the University of California, the Lawrence Berkeley Laboratory or the Department of Energy.

TECHNICAL INFORMATION DEPARTMENT
LAWRENCE BERKELEY LABORATORY
UNIVERSITY OF CALIFORNIA
BERKELEY, CALIFORNIA 94720